12-1-1984

Dynamic Studies of Multiterminal DC-AC Systems

Alireza Hamzei-Nejad
Purdue University

C. M. Ong
Purdue University

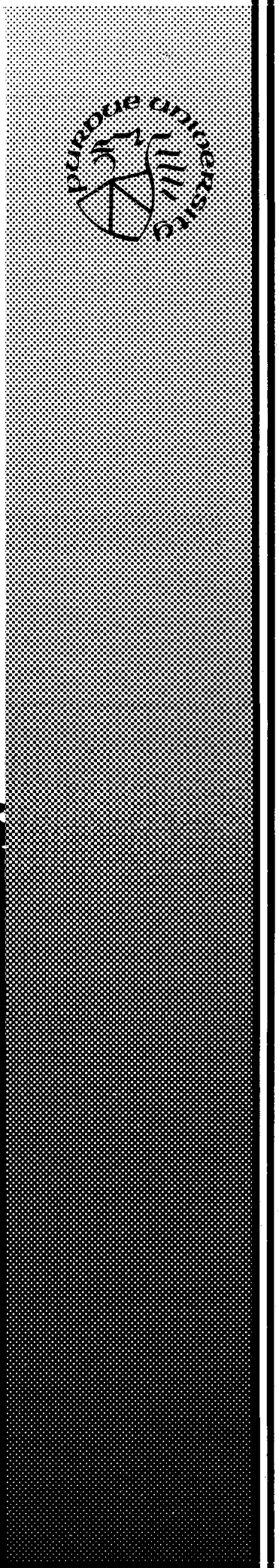

Dynamic Studies of Multiterminal DC-AC Systems

Alireza Hamzei-Nejad
C. M. Ong

TR-EE 84-45
December 1984

School of Electrical Engineering
Purdue University
West Lafayette, Indiana 47907

DYNAMIC STUDIES OF MULTITERMINAL DC-AC SYSTEMS

by

Alireza Hamzei-Nejad

C. M. Ong

TR-EE 84-45

December 1984

School of Electrical Engineering

Purdue University

West Lafayette, Indiana 47907

TABLE OF CONTENTS

Page

Page

LIST OF TABLES

LIST OF FIGURES

Figure Page

Figure Page

ABSTRACT

In transient stability programs that use a static dc network representation, the procedure to determine the control mode of operation and the solution of the multiterminal dc system is complex and time consuming. A systematic approach that is based on a linear programming formulation is presented in this thesis. The constraints incorporated in the LP formulation automatically ensure that the solution obtained is feasible. It is shown that the method is not only computationally efficient but also versatile in its ability to handle many of the common control characteristics, such as those of the constant angle (extinction and ignition), constant voltage, constant power and current controls, voltage dependent current order limiter (VDCOL), end-stops, and also simulate the dynamics of power modulation and restart.

As some applications require a three-phase detailed representation of the ac/dc system, a technique for detailed simulation of the dc converter and controls is also presented.

The developed dynamic simulation program is used to investigate the problem of on-line network flow control using converter controls of a multiterminal dc system. In view of fast response of the dc powers to converter controls, a control method is proposed that extends the application of ac network flow control to dynamic situations. Possible applications of the method are to regulate power flows in a select group of ac lines, to smoothly steer the ac/dc

system from its present state to some desired state and to enhance the dynamic performance of the ac system by controlling the transient changes in key or "backbone" ac lines.

CHAPTER 1
INTRODUCTION

In the past, two-terminal dc transmission systems (dc links) were used to transmit electric power between two ac networks whenever the use of an ac tie was not technically feasible, for reasons such as interconnecting ac networks of different operating frequency, and/or where long submarine cables were required but were too costly for ac transmission because of expensive line compensation required to balance the line charging requirements.

The commercial availability of high power solid-state valves (thyristors) in place of mercury valves since the early 70's has made the conversion process more reliable and less expensive. As a result, HVDC transmission is now competitive with ac for distances exceeding 400 miles over land, or about 20 miles for underwater transmission.

There are altogether about 26 HVDC projects operating in the world today, with eight more projects coming into operation in the next two years. Examples of some of these HVDC projects are:

1- The Pacific Northwest-Southwest intertie (Oregon - California) is 400 kV, 2000 MW, and 1362 km long.

2- The Eel River is a 80 kV, 320 MW back-to-back tie (in Canada) connecting Hydro Quebec with New Brunswick asynchronously.

3- The Square Butte tie (N. Dakota - Minnesota) is +250 kV, 500 MW and 749

km long.

4- The CPA - UPA (or CU) tie (N. Dakota - Minnesota) is +400 kV, 1000 MW and 710 km long.

The largest capacity, highest voltage HVDC system in the world today is in Brazil, taking hydroelectric power from the Itaipu Dam to Sao Paulo, some 500 miles away. In this case, the +600 kV, 6300 MW dc tie is not only less expensive, but also serves as a reliable link for power exchange with the neighboring country of Paraguay which uses 50 Hz instead of the 60 Hz in Brazil.

To date, all the HVDC systems in commercial operation are two-terminal (either point-to-point or back-to-back) schemes. However, the decreasing trend in the cost of dc converters and the benefits of their fast and flexible controls to enhance the system operation under transient conditions have created greater incentives to expand existing two-terminal systems to multiterminal systems. Currently, several multiterminal dc (MTDC) transmission projects are already in the planning stages.

1.1 Motivation

The rapid controllability of the dc power through relatively simple controls in dc transmission schemes has been recognized and applied to enhance the dynamic and transient stability of the associated ac systems. For example, small signal dc power modulation has been used in the Pacific Northwest dc intertie to raise the dynamic stability limit of the ac intertie, permitting larger amount of power to be transferred by the ac intertie than what was previously possible without the dc power modulation. Dc power modulation is also being

used to increase the damping to torsional oscillations of the generators closed to Square Butte terminal of the dc link owned by Minnesota Power.

The control of the real and reactive powers of the dc terminals, when properly coordinated, has been shown in [1,2] to alleviate line overload or overvoltage conditions in the ac network. Although the earlier works in [1,2] were for steady-state conditions, there is no reason why the concept of coordinated real and reactive power control could not be applied to dynamic situations, thus opening the door to such applications as: large-signal dc power modulation, transient stability enhancement and emergency control.

The original and main motivation of this research is to explore the technical feasibility of dynamic control of real power flows in the ac network using the dc power injections of an available multiterminal dc transmission system. Such an investigation will require computational tools not unlike those required by utility planners and operators. For determining the operating point of the ac/dc system, one would require load-flow programs with capabilities to handle the various operating control characteristics of the multiterminal dc systems. Such techniques and programs have been developed in earlier studies at Purdue [3,4]. Similarly, dynamic simulation programs are needed to evaluate the transient response of the ac/dc system to control action or to an applied disturbance.

The dynamic simulation of the dc converters is much more complex than other circuit elements because of the varying circuit topology as different thyristor valves are turned on and off. The switching operation is further complicated by the dependence of switching instant with respect to ac and dc variables. Detailed representation of the converter's switching elements is required when the harmonics and commutation characteristics are vital to the

study objectives. However, for most of the planning and new control studies that focus on the power oscillations in the ac network, such detailed characteristics may be sacrificed when the disturbance on the converter ac voltages is not so severe or distorted as to introduce any commutation failure. In which case, a simpler single-phase model of the converter, based on the average-valued relationship between ac and dc quantities is often used. The single-phase, average-valued model of the converter is of course consistent with the equivalent single-phase network representation of the ac network used in standard ac transient stability programs.

A review of the literature on simulation techniques applied to ac/dc power systems showed that there has been some work on the detailed digital simulation of multiterminal HVDC systems [5,6]. And though the Electromagnetic Transient Program (EMTP) from the Bonneville Power Administration is readily available, its suitability for simulating a HVDC system, especially a multiterminal dc system, is unclear because of the general-purpose nature of the "tacs" (acronym for transient analysis of control systems) For purposes of simulating a particular converter such as the Graetz bridges used in HVDC systems, there is reason to believe that a dedicated algorithm using the methods described in [7] and [8] can be computationally more efficient than the general-purpose EMTP tacs.

Similarly, a literature survey on simulation techniques for ac/dc systems using the simple average-valued converter model revealed a need for more efficient computational algorithm. In this respect, much can be done to reduce the computation time for the case when dc network dynamics are ignored. Instead of cycling through possible control modes of operation of the dc system, computational effort at each time step can be reduced if the mode and the dc

network solution could be determined concurrently.

1.2 Research objectives

In an integrated ac/dc system, the power injections of the dc network can be coordinated to effect within limits, the desired ac power flow distribution in the ac network. Redistribution of the power in the ac system is often required either to avoid sustained overloading of transmission lines or simply to enforce a more desired power flow pattern for security or economic reasons. The effectiveness of coordinating the dc transfer to effect real and reactive ac power flow control, under steady-state condition, has been demonstrated in [1,2]. The effectiveness of these methods depends on the extensiveness of the dc system, available control effort and the proximity of the dc terminals to those key ac lines whose powers are controlled.

Since the response of the dc powers to dc control is fast relative to the electromechanical oscillations in the ac network, extending the network flow control concept to dynamic situations is a logical development. The essential requirements of such an on-line dynamic controller are speed and adaptability.

The main objective of this research is to develop an on-line dynamic network flow controller that will provide the dc set point controller with the required changes in the dc power orders to bring about the desired control action on a select group of ac lines. Potential applications of such a dynamic network flow controller are steering and regulating the power flows in select group of ac lines and damping the power oscillations in these lines.

The development of the necessary dynamic simulation tools is an important part of this research. In particular, the development of a more versatile ac/dc transient stability technique that can handle various control

characteristics of multiterminal operation is essential to conducting the control studies. In addition, simulation capability with a detailed representation of the converter would be beneficial for considering disturbances where the proper commutation of the bridge becomes questionable. Of course, such detailed simulation capability can also be used for other types of studies such as those concerned with harmonics and commutation characteristics and unbalanced operating conditions.

1.3 Scope of the report

The main contributions of this report are the developments of dynamic simulation tools and an on-line control power control algorithm for multiterminal dc/ac power systems. These developments are described in Chapters 3 through 5.

Before going into the details of the research topics, some background on the modeling and simulation of ac/dc systems would be beneficial. Chapter 2 is a review of the converter models and the techniques used in dynamic simulation of ac/dc systems.

In chapter 3, a new formulation for representing multiterminal dc systems in transient stability programs with the capability of handling various control characteristics of the dc system is presented. Results of dynamic simulation studies demonstrating the successful handling of various kinds of dc control characteristics are included.

In chapter 4, the development of the detailed model for the converter and its controls is given. Results of simulation studies on sample two-terminal and multiterminal dc systems are included.

In chapter 5, the development on the on-line network power flow controller is presented. Results of the control performance obtained on a 3-terminal, 3-machine system are presented.

Finally, a summary of the main findings from this research, conclusions, and recommendations for possible areas of future research are given in Chapter 6.

CHAPTER 2
BACKGROUND ON MODELING AND SIMULATION TECHNIQUES

The reemergence of the HVDC transmission as an alternative to ac transmission has created a need for efficient computational tools for operational and planning purposes. The use of computer programs in planning HVDC schemes has not been popular because of their excessive computation costs and their failure to accurately represent the dc system controls. The accurate representation of the dc converters and their controls is an essential requirement in studying the overall transient behavior of ac/dc systems being planned. With dc transmission now considered as viable, technical and economical, alternative to the ac option, there are strong motivations to develop digital simulation programs which not only better portray the dc system's behavior during transient periods, but are also computationally more efficient. Similar requirements, although requiring a more detailed representation of the components, are required for operational studies involving faults and protection.

One popular method of studying dc links is the laboratory models. Though useful in some cases, such as examining valve stresses in converters, these laboratory models suffer from an inherent drawback of scaled models, that of requiring expensive and time-consuming construction and modification when evaluating different types of control. Today, the use of scaled down

models is limited to manufacturers of dc systems who have convenient access to the control hardware. For others, especially the utilities interested in considering dc systems in their future plans or already with dc system, digital simulation techniques, which offer great flexibility in representing system components and configurations, are preferred over hardwired simulators.

The manner in which the HVDC system is represented in digital simulation techniques depends on the purpose of the study. Since the representation for dc lines and filter elements are similar to those used for similar ac components, their representations need not be discussed further. The converter with its switching devices is, however, a complex component. Varying degree of simplification can be used to model the converter. The two common models of the converter are the average-valued model and the detailed model. Fig. 2.1 shows the equivalent circuit representation of the average-valued model of the converter. The converter is represented as a variable voltage source in series with a commutation resistance that accounts for the voltage drop due to the transformer reactances.

Since the standard ac transient stability study is based on single-phase rms values of the system variables, the average-value model of the converter is consistent with the ac network representation used in existing ac stability programs. With the average-valued model of converter, the dynamics of the dc control and of the dc lines may or may not be represented. When dynamics of the primary control loop are taken into account, the voltage source in Fig. 2.1 is responsive to the changes in the ac voltages as well as the dynamic changes in the control angles from one time instant to the next. The result is a better approximation of the actual dc voltage as compared to the case when the dynamics of the dc control are neglected. When the dynamics associated with

the dc lines and the smoothing reactors are also taken into account, the computed response of the dc network will have not only the dynamics but also whatever delay introduced by these network elements. It should, however, be pointed out that such improvements in the accuracy of the predicted response are achieved at a cost of increased computing time. For, in addition to the sizable increase in the number of differential equations representing the converters, controls and lines, the integration step size has to be made very much smaller because of the small time constants associated with these components.

Where higher harmonics due to the valve switching and unusual topological changes within the converter are to be simulated, a detailed model of the converter is necessary. In the detailed model (Fig. 2.2), the switching operation within the converter is represented in full detail. Since the firing and blocking of each valve are simulated, varying circuit topologies within the converter during a severe fault can be simulated. Such a detailed model of the converter requires an enhanced representation of the dc converter control. Correspondingly, the bandwidth of the ac and dc models should be extended to cover the higher harmonic components of interest.

Studies using the detailed representation require considerably more computation time because of the very small integration time step (in the order of 0.1 msec) required by the dynamic equations. Therefore, the use of detailed model is often confined to short periods before and after disturbance. Nevertheless, the detailed model is irreplaceable when it comes to studying current stresses on the valves during internal converter and line faults, transient overvoltages across the valves due to faults or switching in the ac system, asymmetrical faults, and uncharacteristic harmonics generated by the

converters; such studies are not possible with simplified models.

In many of the early studies of ac/dc system dynamics with digital computers an average-valued model was utilized to represent the dc converters [9-11]. In these studies dynamics associated with the dc network and primary control loops were taken into account. The differential equations describing the dc network and controls require a much smaller integration time step (in the order of 0.001-0.005 sec) compared to what is normally required in standard transient stability studies (0.01-0.05 sec). For a given study period, the small time step requirement increases the computational effort considerably.

Further simplification in modeling can be achieved by neglecting the dynamics of the primary control loop and the dc network, on the assumption that such dynamics are much faster than those of the electromechanical oscillations of the ac system [12,13]. With a static representation of the dc network, discontinuities in the dc currents are possible, thus creating a new problem resulting from the uncertainties about the control mode of operation of the dc system during transient conditions. Depending on the magnitudes of ac voltage and the dc variables, the control mode of a converter may change during transient condition. While there are three possible modes of operation for a two-terminal dc system, seven for a three-terminal dc system, the number of possible modes of operation increases rapidly as the number of dc terminals increases. In [13], a search through possible modes to find a feasible solution was suggested. As the solution of these ac and the dc variables is based on an a priori assumption of certain control modes for the converters, the scheme to select the control mode should preferably avoid having to cycle over all combinations of the control modes at each time step of the solution.

Attempts to minimize the computation time for studies which require the use of detailed representation have led to the idea of hybrid modeling technique [14-16]. Due to the computational efficiency associated with the use of the average-valued model, the overall computational effort can be minimized by restricting the use of detailed representation to the most disturbed part of study. As the dc system regains normal control and attains predictable behavior, the detailed representation is replaced by the simplified average-valued model.

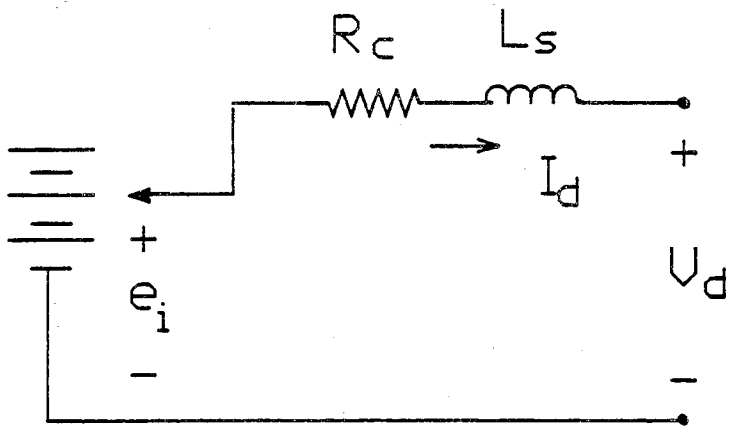

Figure 2.1 Average-valued (simplified) dc converter model

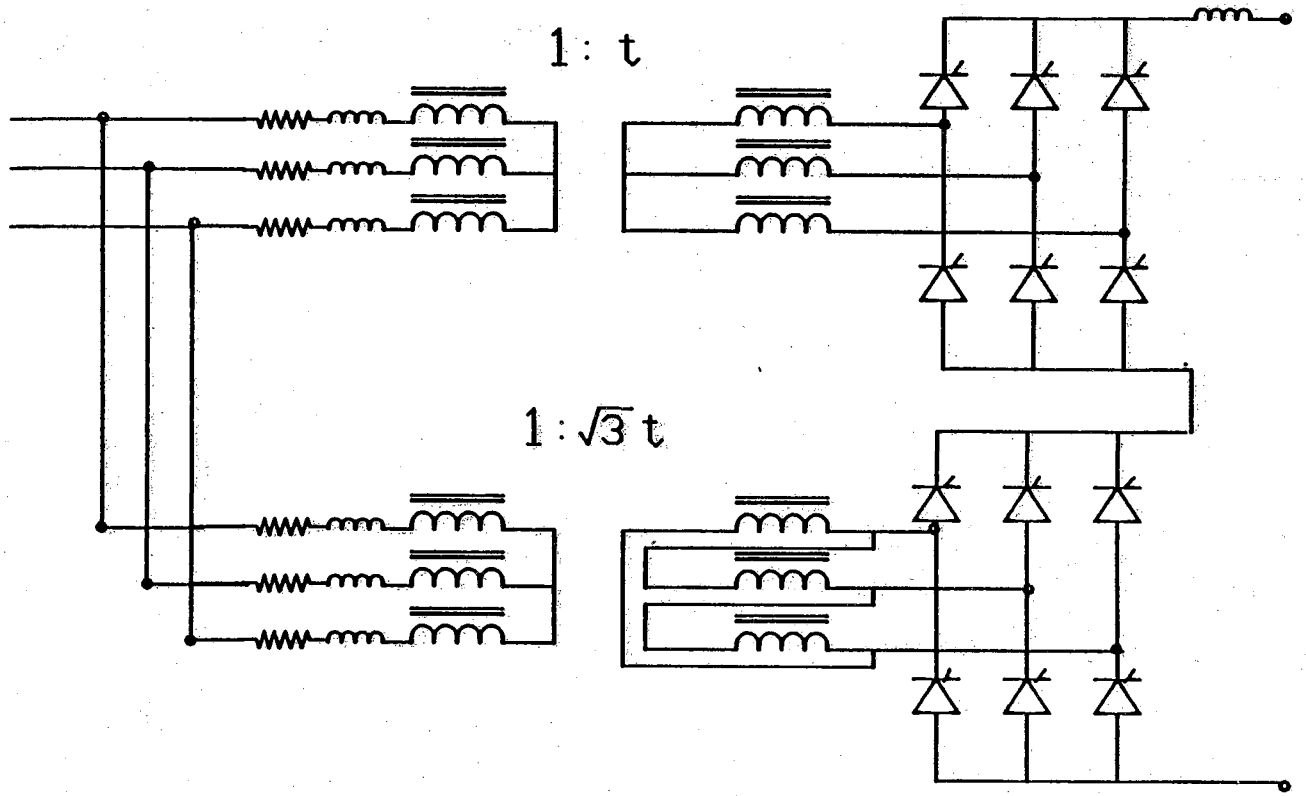

Figure 2.2 Detailed converter model with transformer connections

CHAPTER 3
TRANSIENT STABILITY STUDIES USING A SIMPLIFIED DC SYSTEM REPRESENTATION

Converter operating characteristics are highly nonlinear, especially so when the operating constraints on the firing angle, current and reactive power are taken into account. Since the control mode of operation of the dc system is variable dependent and the operating margin between neighboring modes is narrow, changes in the control mode of operation of the dc system often occur during transient conditions. The approach now used in transient stability programs that employ a static dc network representation cycles through the probable control modes until the computed values of the current operating state are consistent with the assumed mode of operation. The program logic for multiterminal dc system soon becomes complex and time-consuming, because the number of possible combinations of control modes increases rapidly with the number of converter terminals.

In this chapter, a more systematic method, based on a Linear Programming formulation is presented. The constraints incorporated in the LP formulation automatically ensure that the solution obtained is feasible.

3.1 Simplified dc system representation

The assumptions leading to a simplified dc system representation are as follows:

(i) The dynamics in the primary control loop and in the dc network are assumed to be much faster than the electromechanical transients of the ac system that they can be neglected.

(ii) The dynamics associated with dc filters are neglected and they are represented as constant admittances.

(iii) Harmonic components of both dc and ac quantities are ignored.

3.2 Problem description

When the dynamics in the primary control loop and in the dc network are neglected, the control angles and dc variables, in the simulation, respond instantaneously to changes in the ac voltages and to changes in the inputs from the secondary and supplementary controls. The discontinuities introduced by the instantaneous changes of the control angles and dc variables present computational difficulties to the task of determining which control characteristic each of the converters will be operating on, or the mode of operation of the dc system , for the next computing step. For example, Fig. 3.1 shows that there are three possible modes of operation for a two-terminal dc system with just the basic current and angle limit control characteristics. Fortunately, the mode of operation for such a simple two-terminal system can be determined simply by comparing some trial value of the line current with the current orders [17]. But then when other control and operating limits are considered, the procedure for determining the mode of operation is no longer as

straightforward.

The procedure for determining the control mode of operation for multiterminal dc systems is much more complex, because of the larger number of possible modes of operation and the variety of ways that the terminals can be interconnected by the dc network. It is not clear how the procedure described in [17] can be extended to determine the solution of a multiterminal dc system. One early approach [18] to this problem is to cycle through the modes one by one, beginning with the most probable mode and proceeding down through the less probable ones until a feasible solution is found. Thus, the procedure is one of assuming some mode of operation and then performing a dc load flow to find the dc voltages and the control angles. The computed control angles should be consistent (feasible), that is within the permissible range of the assumed mode of operation, otherwise the procedure has to be repeated with another mode of operation until a feasible solution is found. Such a procedure becomes complicated to program and time-consuming to execute as the number of terminals in the dc system grows, because the number of possible modes of control operation increases rapidly with the increase in the number of terminals. As the procedure to determine the mode of operation and the dc system solution is executed at each time step of the study, computational efficiency of the method used is of particular importance.

A systematic method, based on established linear programming techniques, that will simultaneously determine the control mode and the dc solution is presented here. It is shown that the method is not only computationally efficient but also versatile in its ability to handle many of the common control characteristics, such as those of the constant angle (extinction or ignition), constant voltage, constant power and current controls, voltage dependent

current order limiter, end-stops, and also simulate the dynamics of power modulation and restart.

3.3 Solution of the dc system

There are several control methods [19-23] to operate a parallel multiterminal dc system, but the discussion here will be limited to the widely used current-margin control method. The formulation, however, is general; it can easily be modified to deal with other control methods, such as the limiting-voltage method, the method using arbitrary V-I characteristics or the method described in [23].

With the current-margin method of control, one of the terminals operates as the voltage-controlling terminal while the other terminals operate with current or power control. The converter controls are coordinated with the tap-changers of their respective converter transformers to minimize the reactive power demands and to attain as high a dc operating voltage as possible. The tap-changers normally operate to hold the control angles of the current or power controlling terminals a few degrees above their respective minimum limits, allowing some narrow margin for rapid control of the currents. To avoid unnecessary cycling between tap positions during short transients, a time delay is introduced in the tap-changer control loop. Since the tap response is sluggish, fast transient changes in the ac voltages can cause the voltage-controlling function to be shifted from the assigned terminal to any other terminal which now has the lowest dc voltage.

The basic idea behind the proposed LP approach to determine the dc solution of a two-terminal dc system can be explained with the V-I characteristics shown in Fig. 3.2 [24]. For simplicity, the details relating to the

dc network constraints that are also incorporated in the LP formulation will be ignored. Given a set of ac voltages and current orders, the operating characteristics of the converters as shown in Fig. 3.2 can be obtained. If the inverter has the operating characteristics KCMNQRS, the dc solution is given by point C. At point C, the sum of the cosine function of the control angle of the rectifier and the inverter is minimum, subject, of course, to the control and network constraints. This is also true for the case where the inverter has a segment of voltage control characteristic M'C'C'', in which case the actual dc solution is point C'. Therefore, a LP formulation that minimizes the sum of the cosine function of the control angles of all the terminals, subject to the network and control constraints, would in these cases yield the correct dc solutions.

In the LP formulation, the operating characteristics of the converters are conveniently described by inequality constraints, but then the mathematically feasible operating region of the rectifier includes the area to the left of the operating characteristics ABCDFG, and that of the inverter includes the area to the right of the operating characteristics KCLMNQRS or KCMNQRS. A problem arises in the case where the inverter has the extinction angle characteristic KCL; the LP procedure will pick point L instead of point C as the solution, because the control angle of the rectifier at point L is even less than that of point C, the control angle of the inverter being the same for both points. Observe that at point L, the voltage-controlling inverter is operating with no current margin. Point C will be selected over point L, if the voltage-controlling terminal is forced to operate with the current margin ΔI. Computationally, this can be implemented by a second LP iteration in which the current constraint on the voltage-controlling terminal (identified by the

first LP iteration) is redefined appropriately. Fortunately, most practical systems either incorporate a current error control segment to avoid the problem of multiple operating points or use a constant voltage control.

3.4 Problem formulation

The problem of determining the dc system solution may be stated as equivalent to minimizing the control angles, subject to the various control and network constraints. This is same as finding the feasible network solution with the highest dc voltage. To formulate this as a linear programming problem, the objective function and the problem constraints must be expressed as linear functions of the problem variables and the decision variables have to satisfy the non-negativity restriction. The nonlinearity introduced by the cosine function of the control angle in the ac to dc voltage relation of a converter can be eliminated by using $\cos\theta$ instead of θ as a variable. However, when the control angle θ exceeds 90°, $\cos\theta$ will not satisfy the non-negativity restriction. This problem can be overcome by introducing a bias to $\cos\theta$, defining $g_i = 1+\cos\theta_i$, and using g_i instead of $\cos\theta$ in the LP formulation.

One suitable objective function is

$$f = \sum_{i=1}^{m} g_i \tag{3.1}$$

where $g_i = 1 + \cos\theta_i$, the control angle θ_i represents the ignition angle for rectifier operation and the extinction angle for inverter operation. The above objective function is maximized, subject to a number of equality and inequality constraints.

3.4.1 Equality constraints

The equality constraints are the dc network equations and the relations between the open circuit voltages and the ac voltages at the converter buses. The m-1 R-bus equations for an m-terminal dc system are

$$e_i - R_{ci}I_{di} = e_1 - R_{c1}I_{d1} + \sum_{j=2}^{m} r_{ij}\,(-1)^k\, I_{dj} \qquad i=2,...,m \tag{3.2}$$

where R_{ci} is the commutation resistance of i th terminal, r_{ij} is the ij th element of the bus resistance matrix of the dc network with terminal 1 arbitrarily chosen as the reference bus. I_{di} is the current flowing out of a rectifier or into an inverter, it is always positive; k=1 for an inverter and k = 2 for a rectifier. The algebraic sum of all the dc currents flowing into the network must be zero.

$$\sum_{i=1}^{m} (-1)^k I_{di} = 0 \tag{3.3}$$

The equations relating the open circuit voltages, e_i, to the ac bus voltages, V_{aci}, and the control angles, cos θ_i, can be expressed as

$$e_i = t_i\, V_{aci}\, (g_i - 1) \qquad i=1,...,m \tag{3.4}$$

3.4.2 Inequality constraints

The inequality constraints typically define the permissible operating range of the various control characteristics. For example, the permissible operating ranges of the control angles are defined by

$$\cos\,\theta_i^{max} \leq (g_i - 1) \leq \cos\,\theta_i^{min} \tag{3.5}$$

and those of the dc currents of the terminals with current orders I_{doi} are

$$I_{di} \leq I_{doi} \quad \text{for a rectifier} \tag{3.6}$$

$$I_{di} \geq I_{doi} \quad \text{for an inverter} \tag{3.7}$$

The characteristic of a constant voltage control with a voltage order V_{doi} is obtained using the following inequality constraint.

$$t_i V_{aci} (g_i - 1) - R_{ci} I_{di} \leq V_{doi} \tag{3.8}$$

In the LP procedure, slack variables are introduced in the inequality constraints, the resultant equations along with the equality constraints are assembled into the form AX=B. The unknown vector X consists of the variables g_i and I_{di}. Once these variables are determined by the LP, the dc voltages can be calculated from

$$V_{di} = t_i V_{aci}(g_i - 1) - R_{ci} I_{di} \tag{3.9}$$

The power factor, real and reactive powers, and the ac current of each converter can be determined using the following relations:

$$\phi_i = \cos^{-1}(V_{di} / t_i V_{aci}) \tag{3.10}$$

$$P_{di} = (-1)^{k+1} V_{di} I_{di} \tag{3.11}$$

$$Q_{di} = -V_{di} I_{di} \tan \phi_i \tag{3.12}$$

$$I_{aci} = \left(\frac{P_{di} + j\, Q_{di}}{V_{aci}}\right)^* \tag{3.13}$$

where the above expressions for P_{di}, Q_{di} and I_{aci} are for the powers and current injected into the ac network, and * denotes the conjugate of the phasor.

3.5 Nonlinear controls and operating limits

Nonlinear control characteristics can be simulated by modifying the limits in the inequality constraints iteratively. The techniques used to handle some of the common ones are described below.

3.5.1 Constant power control

Constant power control is usually implemented by dividing the power order by the dc voltage and using the resultant current as the current order. Constant power control characteristics can be simulated by modifying the corresponding current orders I_{doi} in Eqs. 3.6 and 3.7 after fresh estimates of the dc voltages become available, and repeating the LP calculation until convergence is obtained.

3.5.2 Voltage dependent current order limit

The Voltage Dependent Current Order Limiter (VDCOL) is used to lower the current order during a prolonged low ac voltage condition. Its function is to reduce the probability of commutation failures which could depressed the ac voltage further and to ease the recovery of the ac voltages by reducing the reactive power demands of the converters. The effect of the VDCOL is not immediate as it normally has a significant built-in delay.

Two types of the VDCOL have been considered, one modifies the current order according to the ac voltage while the other modifies the current order according to the dc voltage. The characteristics of both types of VDCOL can easily be simulated by modifying the corresponding current orders I_{doi} in Eqs. 3.6 and 3.7 according to some predefined relations of the ac or dc voltages. The delay element can be simulated separately using a first order time constant

representation. Since the ac voltages are available from the ac network solution at the previous time step, modifying the current orders according to the ac voltages is straightforward. On the other hand, modifying the current orders according to the dc voltages requires an iterative procedure as the dc voltages are only available after a LP calculation.

3.5.3 End-stop characteristics

An end-stop is usually incorporated into the control of the inverter to prevent it from crossing over to rectifier operation during fault periods. Control angle end-stops can easily be enforced by specifying the appropriate upper limits in Eq. 3.5.

3.5.4 Restart

A restart from a fault is initiated only after the ac voltages have recovered. The restart begins by first stepping the dc current to some intermediate value and then ramping it to the desired level. Such a restart current profile can easily be simulated by using preprogrammed values of the current order in Eqs. 3.6 and 3.7 at the appropriate time.

This has been a description of the basic formulation and examples of the control characteristics that can be readily handled by the formulation. The formulation could be expanded to deal with other forms of control characteristics and could be enhanced further by introducing sparsity

3.6 Algorithm

As shown in Fig. 3.3, the ac-dc transient stability program may be divided into three parts: (1) a standard ac transient stability program using dynamic machine and static ac network representations, (2) a program using the proposed algorithm to solve the dc network solution using the steady-state operating characteristics of the converters, and (3) a program to simulate the dynamic equations of the secondary or supplementary dc controllers.

At the beginning of the computation, the ac-dc solution is obtained from a standard ac-dc load flow calculation. Then at each new time step, the iterative process for the ac-dc solution begins with the dc solver using the ac voltages of the previous time step as initial estimates to determine the corresponding ac currents injected by the converters into the ac system. In the ac transient stability program the ac currents of the converters are treated in the same manner as the injected currents of the ac generators. The ac transient stability program calculates the ac network voltages based on the new estimates of the injected ac currents of the converters and generators. The new set of ac voltages at the converter buses is then used by the dc system solver in parts 2 and 3 to determine fresh estimates of the injected currents of the converters. This iterative process between the ac and dc networks solvers is repeated until the ac voltages converge within some preset tolerance.

As the number of terminals of practical dc systems in the near future is likely to remain small (under 10), there is little advantage in resorting to sparsity or constraint relaxation techniques in the LP computation, a standard LP package will be more than adequate to problems of such order. When used with a standard LP package, the programming of the LP algorithm is straightforward. All that is required is the specification of the objective

function given in Eq. 3.1, the dc network equation and current constraint given by Eqs. 3.2 and 3.3 respectively, and for each terminal the appropriate equality and inequality constraints, such as those given by Eqs. 3.5-8. A change in the dc network configuration, in the course of a study, can be handled by modifying the R-bus matrix in Eq. 3.2. The addition or removal of any terminal would require similar changes to those constraints associated with that terminal from the overall constraint set.

3.7 Numerical examples

The proposed algorithm was applied to the 3-terminal dc system shown in Fig. 3.4. The parameters of the dc network and the VDCOL characteristics of the converters are given in Appendix A. The ac system was adopted from a nine-bus system given in [25]. The computation time step used was 0.0167 sec (one period of 60 Hz). For convenience of testing the algorithm, the first four examples were obtained with programmed ac voltages to all three terminals. Each of these examples demonstrates the ability of the algorithm to simulate mode shift involving certain types of control characteristics.

Case 1: All three terminals were equipped with just the basic current and extinction angle controls. The programmed ac voltages of Fig. 3.5a caused the two inverters and the rectifier to operate under minimum extinction angle control in turn; this can easily be verified by observing that the dc system voltage, which was determined by the terminal operating under extinction angle control, tracked the lower envelope of the three ac voltages.

Case 2: Inverter 3 had a constant power control with a power order of 0.4 pu.

The ac voltages to the other two terminals were programmed so that the voltage-controlling function alternated between these two terminals. In spite of the sharp drop of the dc voltage, the power transfer of inverter 3 was held constant at 0.4 pu by the constant power control. If inverter 3 were forced to operate at its extinction angle limit, it would not be able to maintain constant power simultaneously.

Case 3: Inverter 2 had a constant voltage control with a voltage order of 0.75 pu. With the programmed ac voltages shown in Fig. 3.7a, inverter 2 was able to maintain constant voltage at 0.75 pu only part of the time, that was when it was not forced to operate at its minimum extinction angle limit. When the voltage order was lowered to 0.6 pu, inverter 2 maintained control of the voltage over the entire period as shown in Fig. 3.7g.

Case 4: Besides the basic current and extinction angle controls, time delayed voltage dependent current order limits were introduced in the rectifier terminal. The time constant of the delay loop was set to 0.5 second. The ac voltage of inverter 2 was temporarily depressed from 0.9 to 0.4 pu for a period of 1.5 seconds. The effect of the VDCOL in reducing the reactive powers of the terminals not controlling the dc voltage over the depressed ac voltage period is clearly visible from Fig. 3.8f. Without the VDCOL, the reactive powers would have remained constant during the same period. The time-delay in the VDCOL loop prevented abrupt changes in the dc current orders.

Case 5: The sequence of events simulated was that of a severe ac network fault close to inverter 2 for 12 cycles. Two cycles into the fault, the current orders

were reset to zero. This was followed by a period of waiting for the ac voltages to recover to within some prescribed range, then a further 7 cycles delay, before initiating a restart. The restart sequence consisted of stepping the current orders to 50% of the desired values and then ramping them up to the desired values over the next 5 cycles. The response of the dc system to this sequence of events is shown in Fig. 3.9. Over the short period of fault, the effect of the VDCOL with its long delay (0.5 sec.) was slight. This case has been selected to demonstrate the capability of the simulation technique and not the modeling, as it is obvious that for such a severe fault the simplified dc representation is no longer suitable.

Case 6: The sequence of events was the same as in case 5, except that power modulation signals were introduced after the restart to damp down the electromechanical oscillations of the generators. The modulation signals can be derived from centralized or decentralized schemes, and they can be applied to modulate both real and reactive powers of the converters. But for this simple example, it was sufficient to consider the modulation at the current control loop level; the modulation signals applied to the current orders of rectifier 1 and inverter 3 were just proportional to the difference in speed of the generators, $\omega_2-\omega_1$ and $\omega_3-\omega_1$, respectively. The response of the relative angles, $\delta_{21} = \delta_2-\delta_1$ and $\delta_{31} = \delta_3-\delta_1$ are shown in Figs. 3.10a and 3.10b; a noticeable improvement in the damping of the rotor oscillations of the case with modulation over that without can be seen from these figures.

3.8 Conclusion

In transient stability programs that use a static network representation of the dc network, the program logic to determine the dc solution from the large number of control modes of operation of a multiterminal dc system can be both complicated and time-consuming. Nevertheless, it is important that changes in the control mode be properly accounted for in the transient simulation of a dc system

This paper has presented a systematic method, based on a LP formulation, which can be used to determine the mode of operation as well as the dc network solution of a general multiterminal HVDC system in such transient stability programs. The constraints in the LP formulation automatically ensure that the solution obtained is feasible. Nonlinear control characteristics are simulated by modifying the appropriate limits of these constraints in an iterative loop around the main LP calculation.

The capabilities of a digital program using the proposed algorithm were demonstrated by numerical examples based on a 3-terminal, 3-machine ac-dc system. The examples illustrated the successful handling of mode shifts between various kinds of control characteristics, restart and power modulation to damp the electromechanical oscillations of the ac generators following a severe ac network fault.

Given the simplicity of the formulation with respect to the programming of various control characteristics and the fact that the LP technique is computationally efficient in sorting through the feasible solutions of the large order systems, the advantage of the proposed LP method when applied to the larger size dc systems is quite obvious.

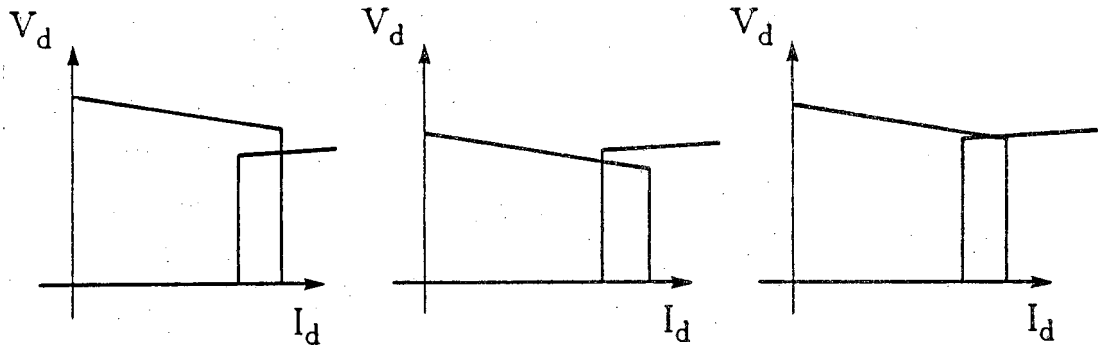

Figure 3.1 Operating modes of a two-terminal system with only current and angle limit controls

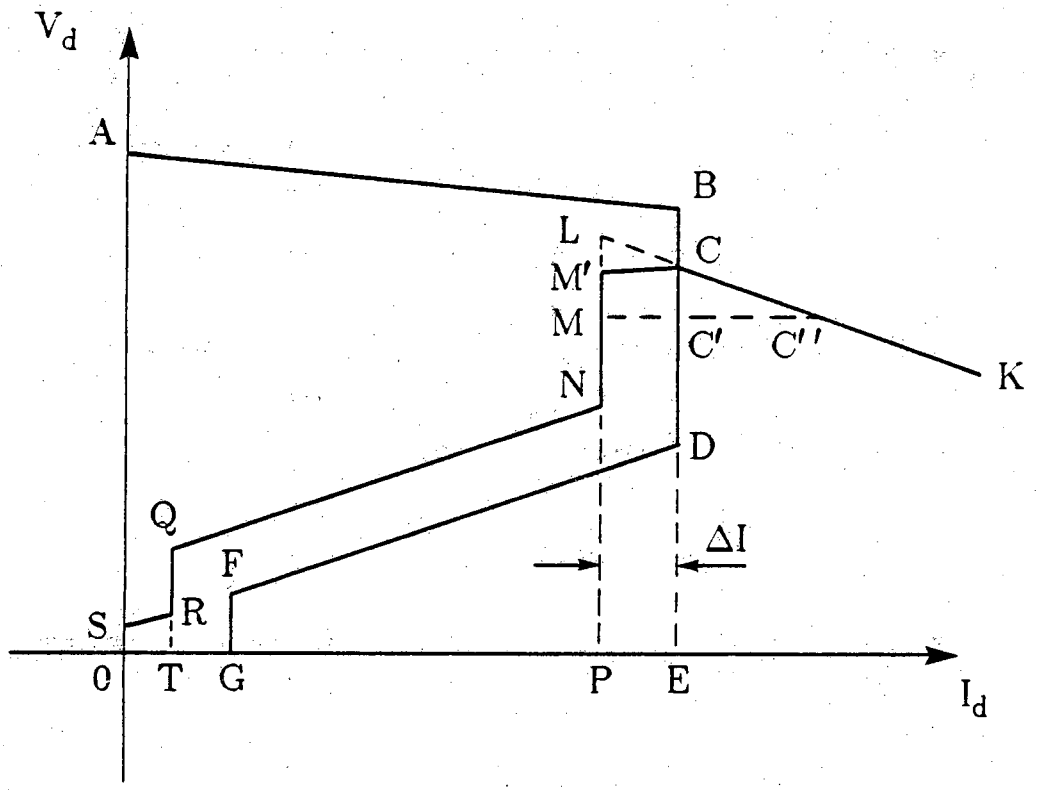

Figure 3.2 Static V-I characteristics of the converter

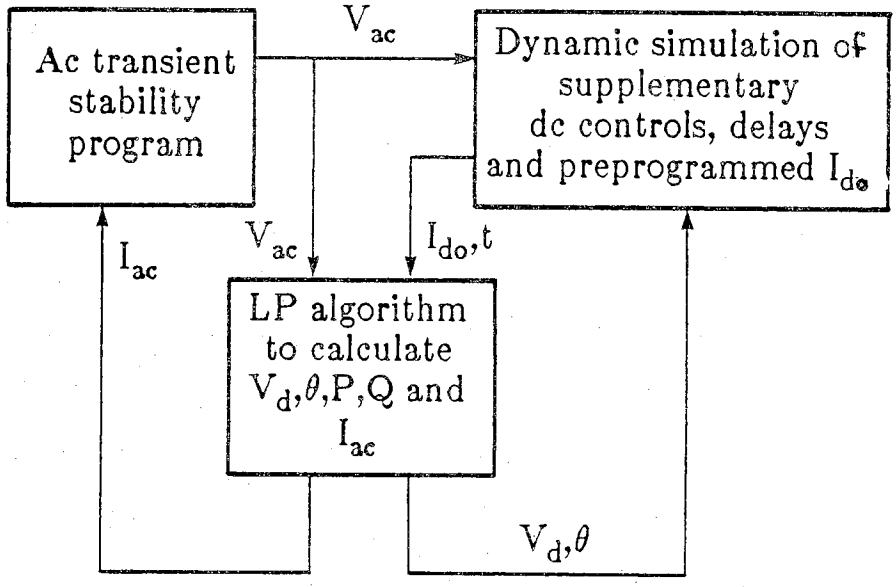

Figure 3.3 AC-DC transient stability program

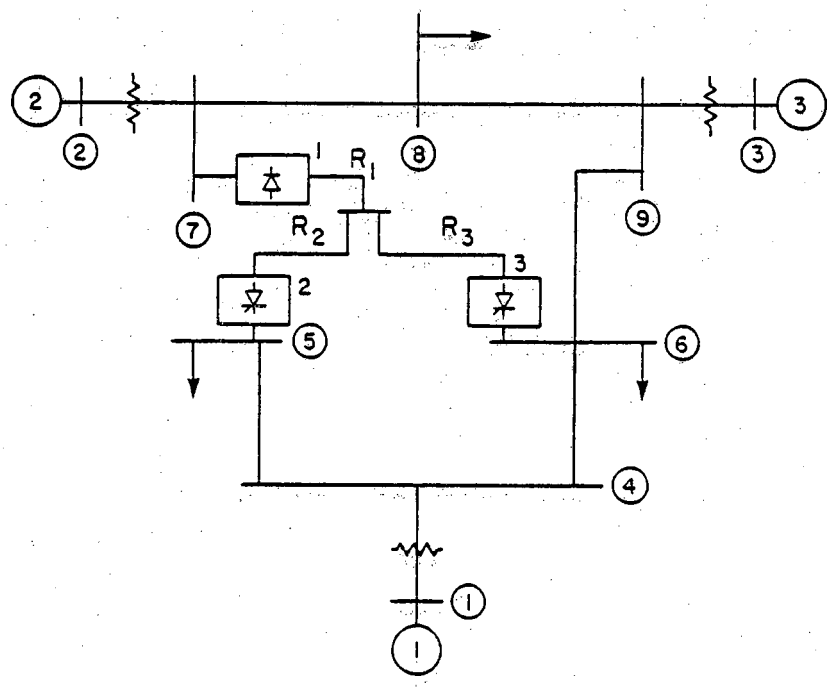

Figure 3.4 Sample 3-terminal, 3-machine system

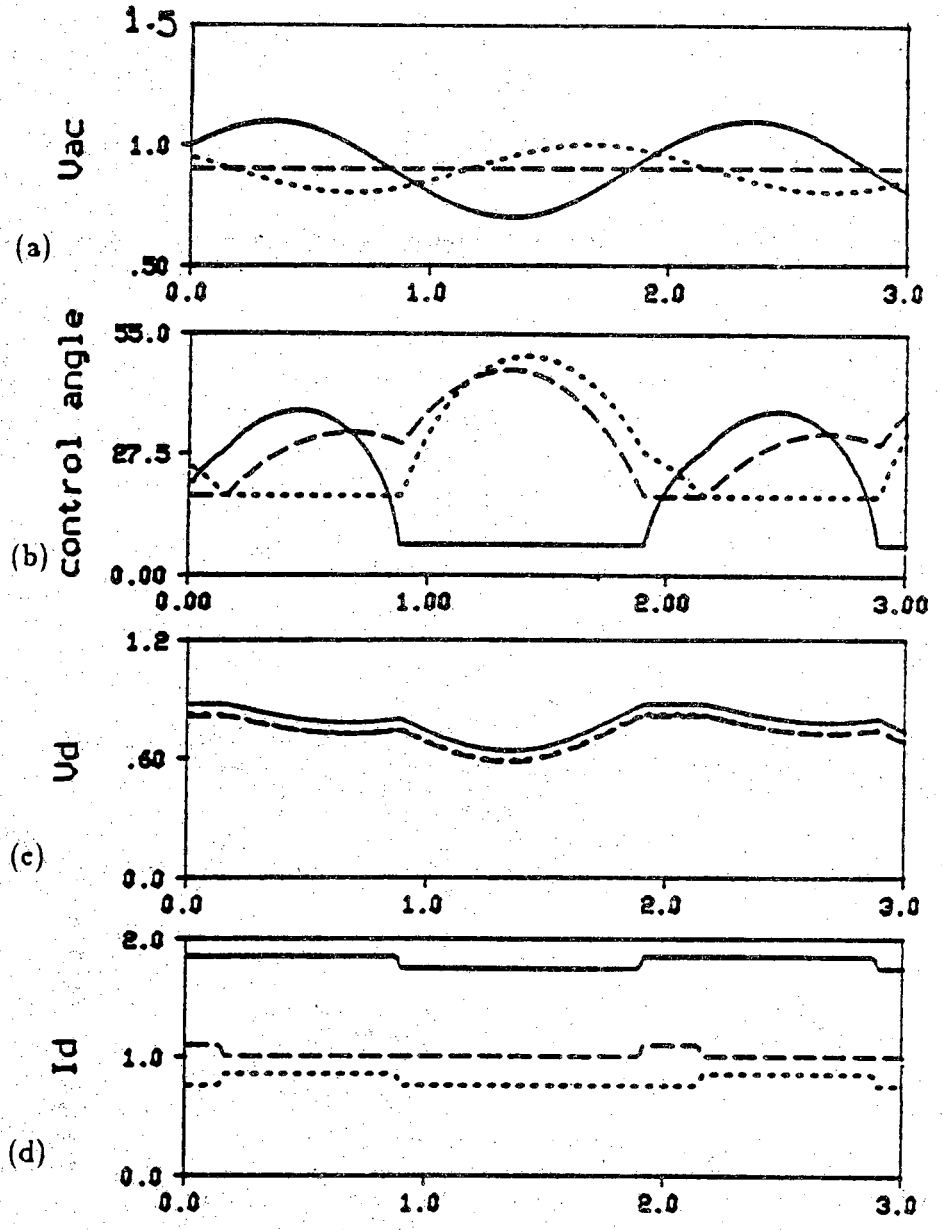

Figure 3.5 Case 1: Basic current and extinction angle controls on all terminals

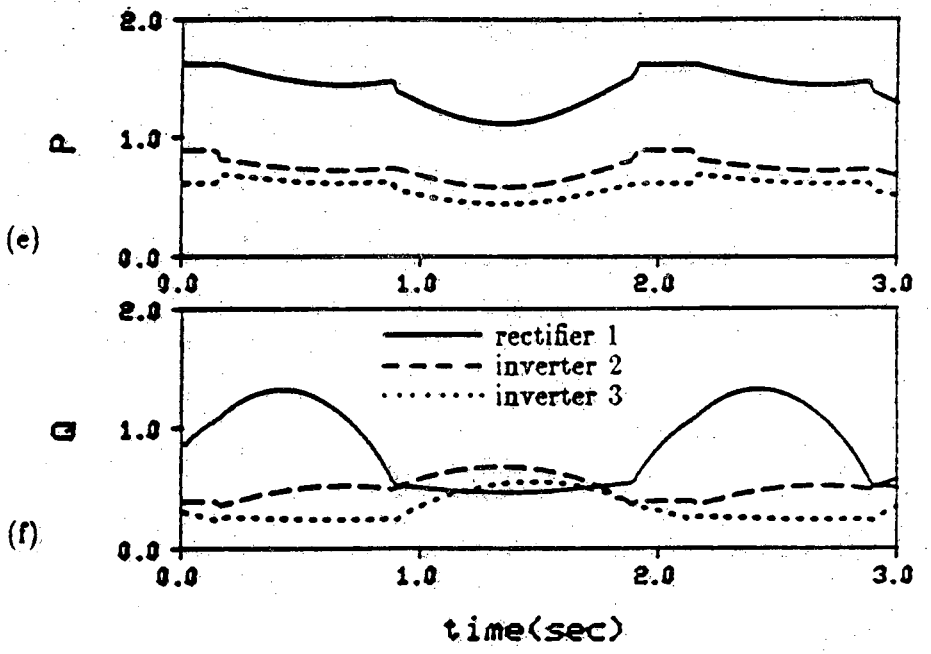

Figure 3.5 continued

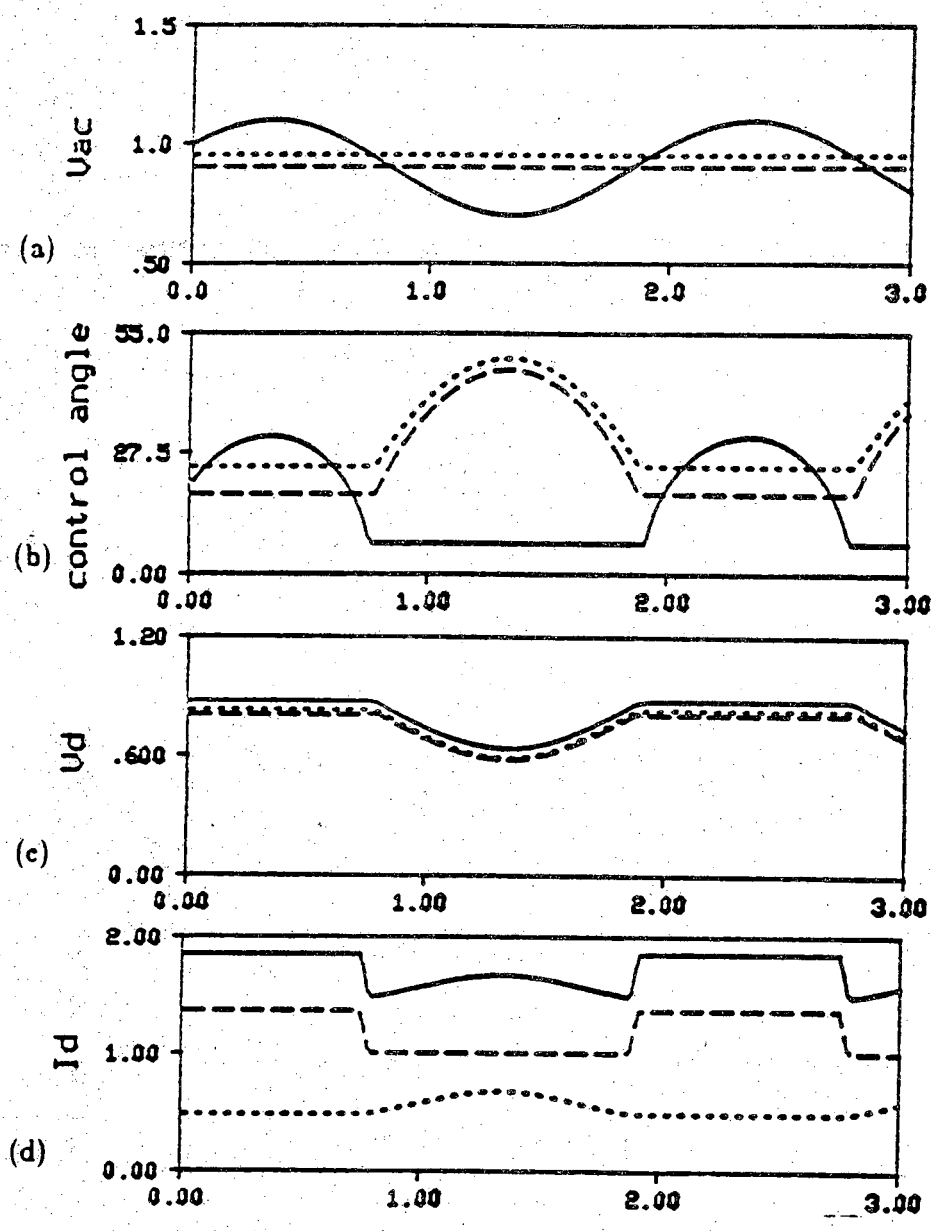

Figure 3.6 Case 2: Constant Power control on inverter 3

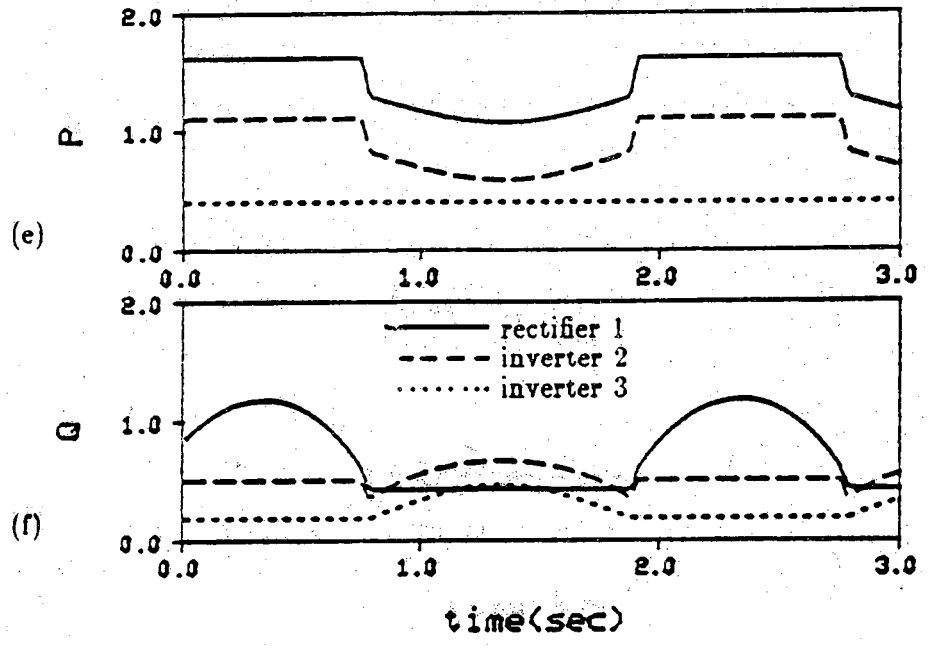

Figure 3.6 continued

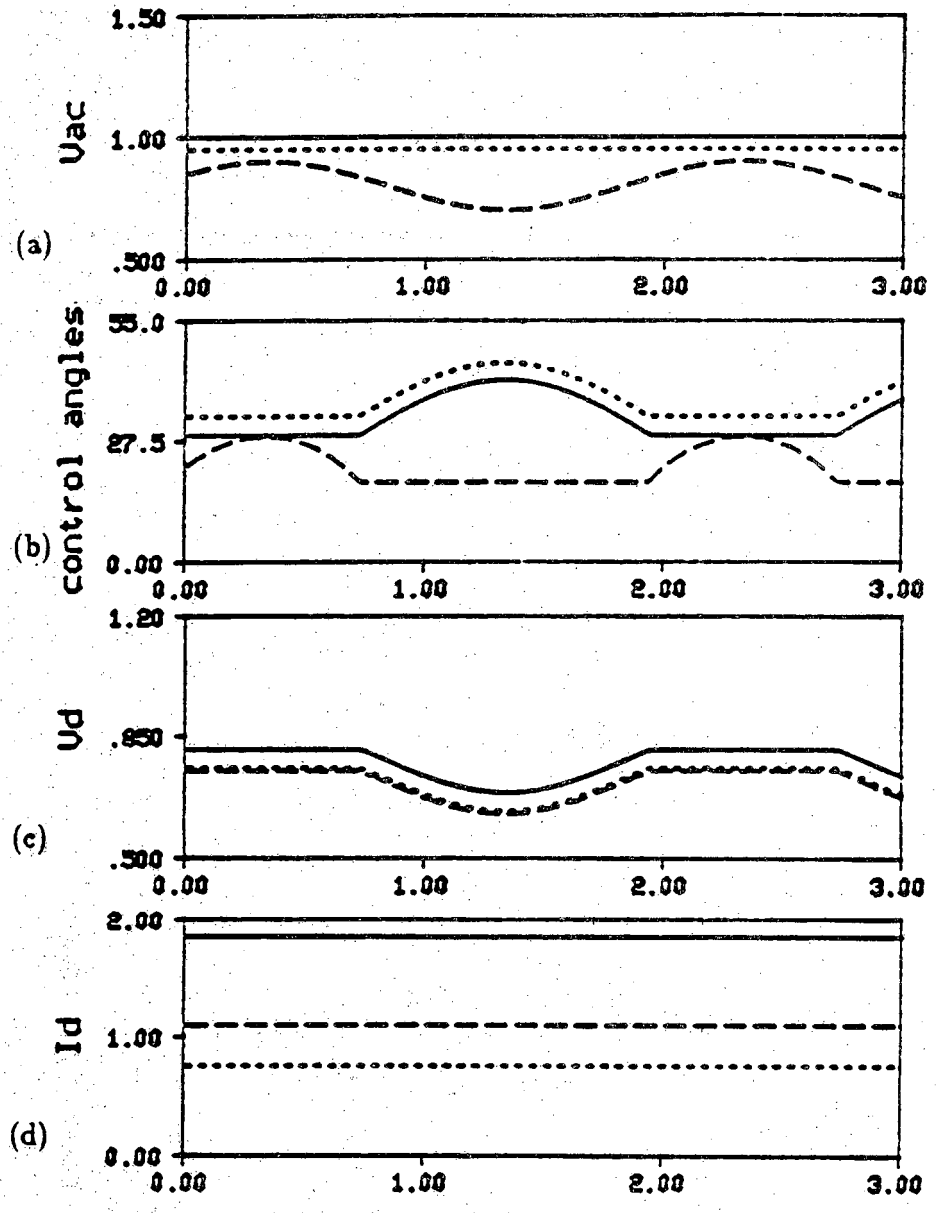

Figure 3.7 Case 3: Constant voltage control on inverter 3

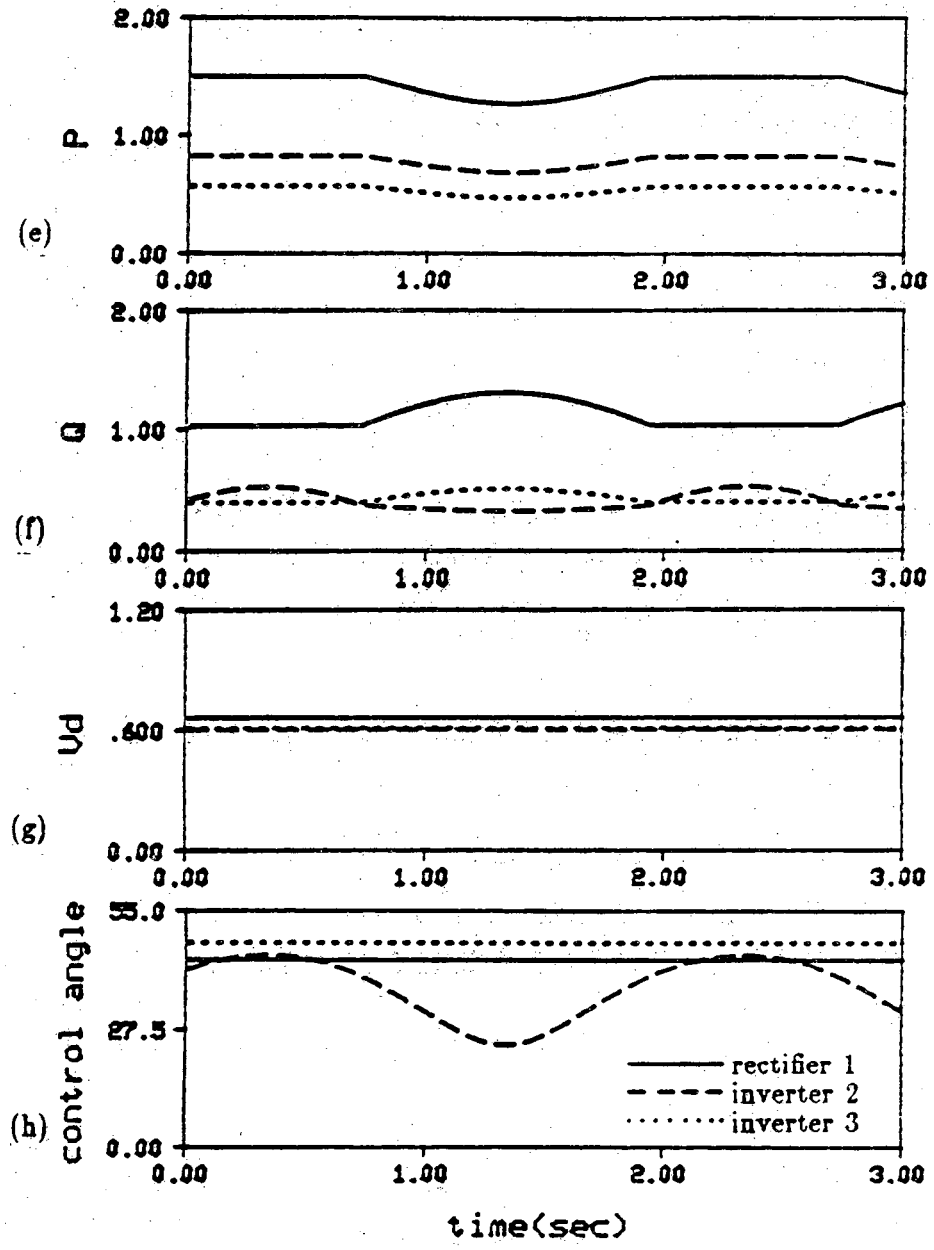

Figure 3.7 continued

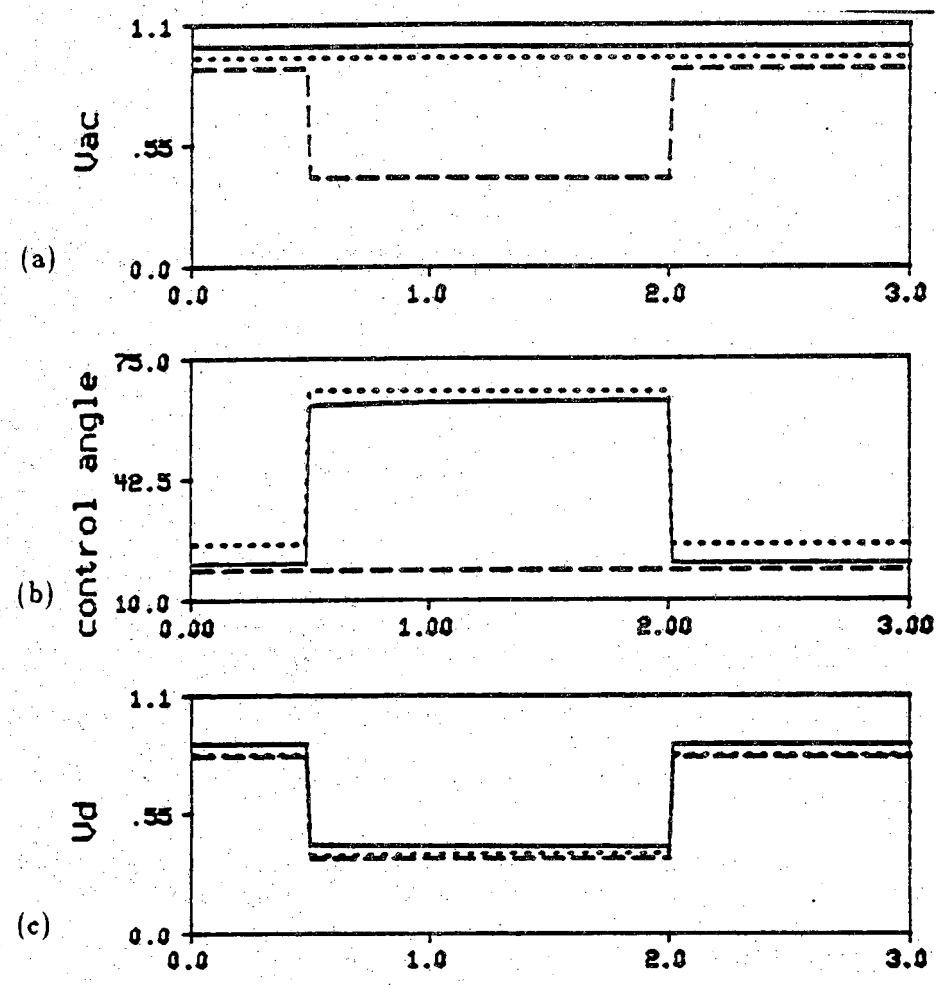

Figure 3.8 Case 4: Voltage dependent current order limiting

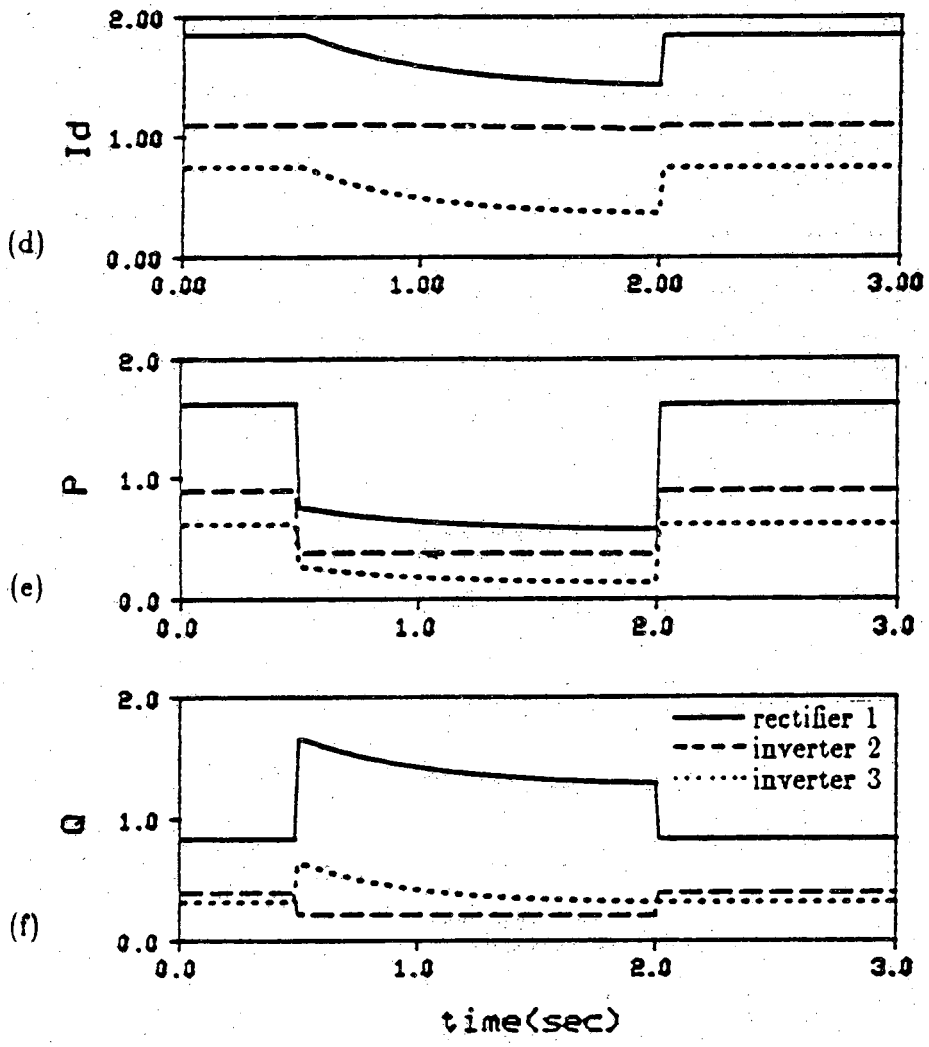

Figure 3.8 continued

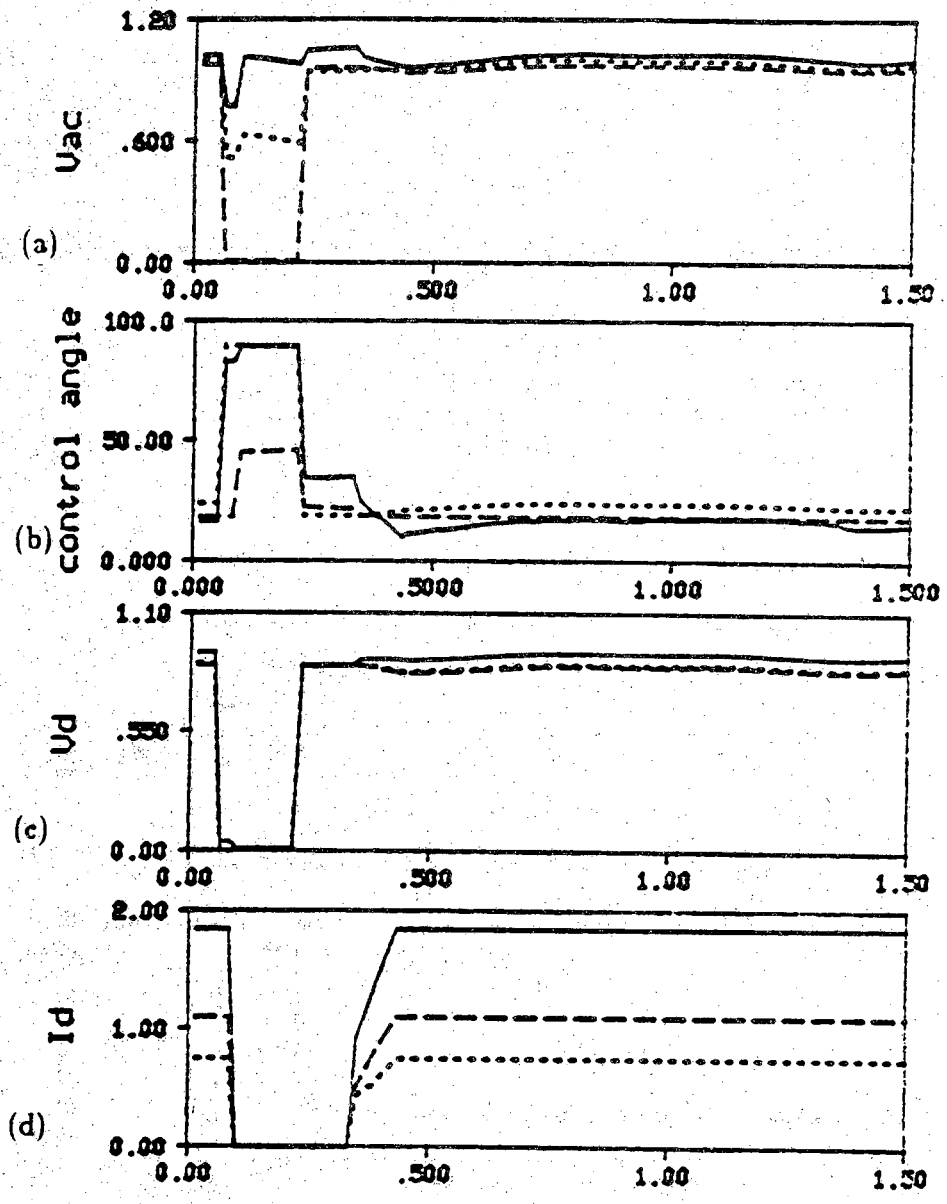

Figure 3.9 Case 5: Restart after an ac network fault

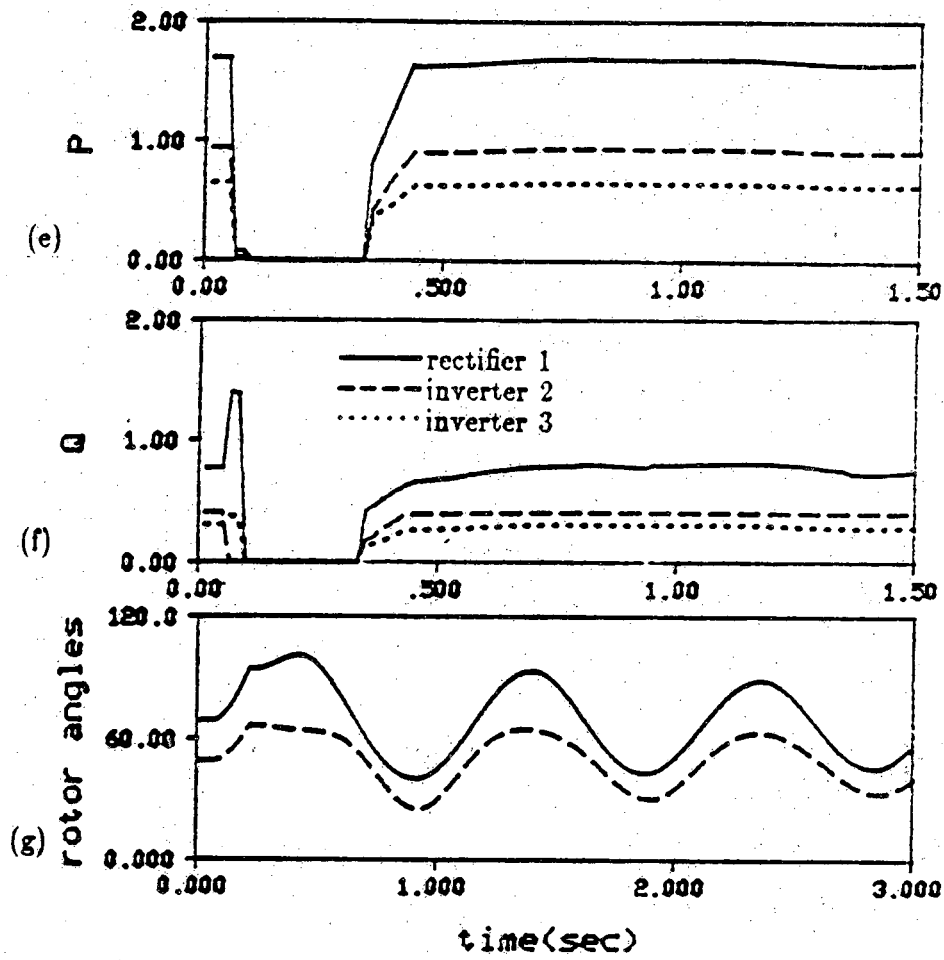

Figure 3.9 continued

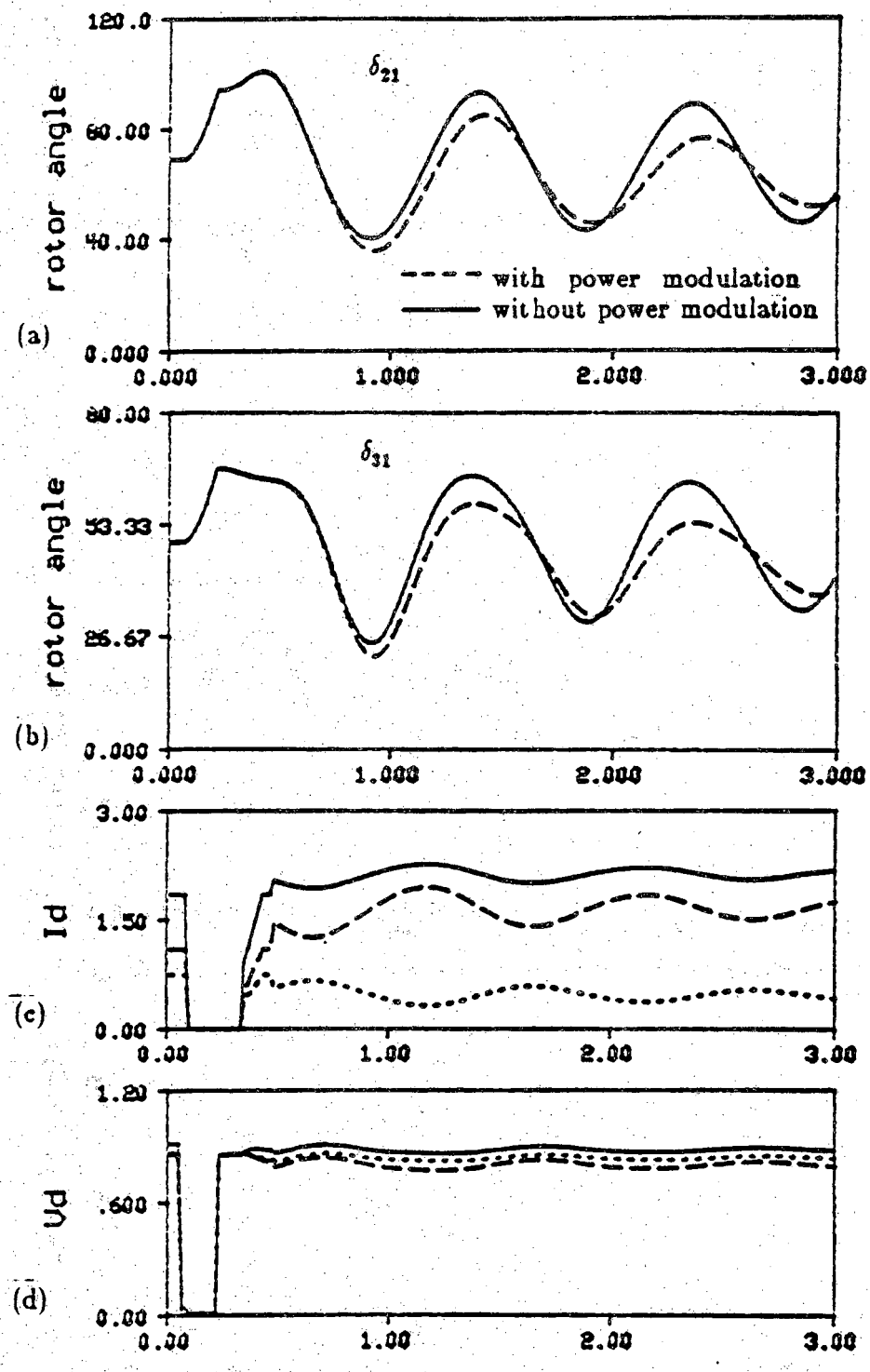

Figure 3.10 Case 6: Power modulation

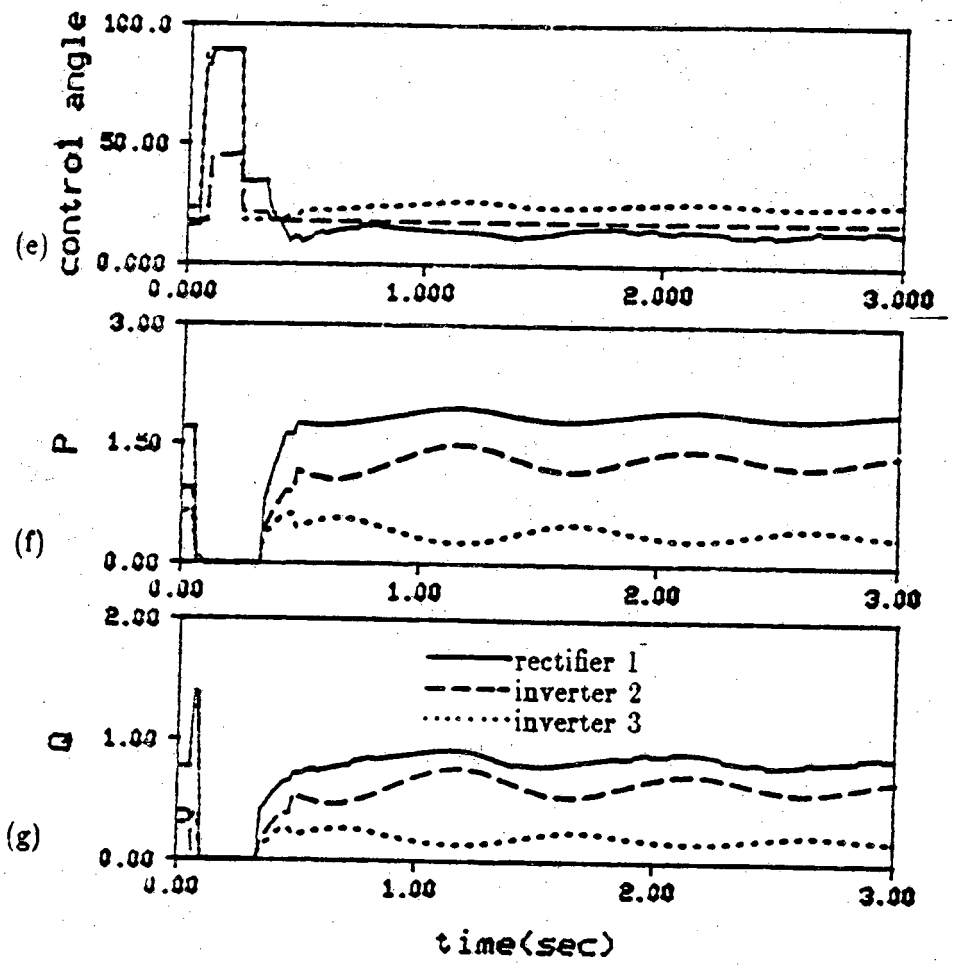

Figure 3.10 continued

CHAPTER 4
DETAILED REPRESENTATION OF HVDC SYSTEMS

In a detailed representation of the HVDC system, the converters, the dc network and the converter controls are represented in full detail. In the converter representation, the voltage across and the current through the individual valves are calculated at each instant of time with the firing and blocking of each valve simulated. The constant ignition angle and constant current controls for rectifiers and constant extinction angle control and constant current controls for inverters are also simulated in detail. The dc network is represented by a dynamic representation with RLC components.

4.1 Detailed representation of dc converters

One approach to simulate the converters is to assign separate subroutines to handle the different set of differential equations representing various circuit topologies. Since the converter circuit topology changes anytime a valve starts or ceases to conduct, the dynamic simulation of the converter is extremely difficult, especially when it is connected to a weak ac system. Furthermore, this approach is not capable of handling unusual conducting patterns during fault periods. To overcome such drawbacks, a method based on tensor analysis has been developed [7,8]. In this method, the set of equations representing the converter with all the valves conducting is reduced by matrix transformation to

represent a particular conducting pattern at each instant of time. Kron's tensor analysis is used to eliminate the branches corresponding to non-conducting valves. This avoids numerical instabilities in some of the earlier approaches which approximated non-conducting valves by very large impedances. This approach is versatile as it has the capability to handle any conduction pattern with an arbitrary number of conducting valves.

4.2 Simulation of the dc converter

To illustrate the method, let's consider the 3-phase 12-pulse converter shown in Fig. 4.1. It consists of two 6-pulse bridges connected in series. The transformer bank of one bridge is connected Y-Y and that of the other Y-Δ. This ensures that there is a 30° phase shift between the ac voltages applied across the two bridges. In a 12-pulse converter the interval between valve firings is 30° as opposed to 60° in a 6-pulse converter. Since the bridges are connected in series on the dc side, the output dc voltage of the 12-pulse converter is twice that of the 6-pulse bridge, doubling the power capacity of the converter. Under balanced conditions, the 12^{th} harmonic is the lowest one in the direct voltage and 11^{th} and 13^{th} are the lowest pair in the ac current.

The 12-pulse converter can be fully represented by a set of equations describing ten network meshes. The number of required meshes and the independent currents reduces to five for a 6-pulse converter. The general impedance matrix relating the secondary ac voltages to the set of independent currents is defined by

$$\mathbf{V}_m = \mathbf{Z}_m \mathbf{I}_m \tag{4.1}$$

where

$$\mathbf{Z}_m = \begin{bmatrix} \mathbf{Z}_m^Y & \mathbf{Z}_c \\ \mathbf{Z}_c^t & \mathbf{Z}_m^\Delta \end{bmatrix} \tag{4.2}$$

$\mathbf{Z}_m^Y$ and $\mathbf{Z}_m^\Delta$ are the impedance matrices corresponding to the Y-Y and Y-Δ bridges respectively and are defined in Appendix B. $\mathbf{Z}_c$ is the coupling matrix and $\mathbf{Z}_c^t$ is the transpose of $\mathbf{Z}_c$. The superscripts "Y" and "Δ" will be used throughout this chapter to refer to the parameters corresponding to the Y-Y and Y-Δ bridges respectively. Also, vectors and matrices are denoted by bold letters. The vectors $\mathbf{V}_m$ and $\mathbf{I}_m$ are defined as

$$\mathbf{V}_m = \begin{bmatrix} e_{ac}^Y \\ e_{bc}^Y \\ e_{ca}^Y \\ e_{cb}^Y \\ -V_d \\ \cdots \\ e_{ca}^\Delta \\ e_{bc}^\Delta \\ e_{ca}^\Delta \\ -e_{bc}^\Delta \\ e_{ca}^\Delta + e_{bc}^\Delta + e_{ca}^\Delta \end{bmatrix} = \begin{bmatrix} \mathbf{V}_m^Y \\ \cdots \\ \mathbf{V}_m^\Delta \end{bmatrix}, \quad \mathbf{I}_m = \begin{bmatrix} i_a^Y \\ i_b^Y \\ i_c^Y \\ i_d^Y \\ I_d \\ \cdots \\ i_a^\Delta \\ i_b^\Delta \\ i_c^\Delta \\ i_d^\Delta \\ i_f^\Delta \end{bmatrix} = \begin{bmatrix} \mathbf{I}_m^Y \\ \cdots \\ \mathbf{I}_m^\Delta \end{bmatrix} \tag{4.3}$$

where $e_{ac} = e_a - e_c$ and V_d and I_d are the dc voltage and current at the converter terminal respectively.

The form of Eqs. 4.2 and 4.3 is chosen in such a way so as to facilitate the simulation of both 6-pulse and 12-pulse converters. For a 6-pulse converter Eqs. 4.2 and 4.3 simply reduce to

$$\mathbf{Z}_m = \mathbf{Z}_m^Y$$

$$\mathbf{V}_m = \mathbf{V}_m^Y$$

$$\mathbf{I}_m = \mathbf{I}_m^Y$$

Note, however, that Eq. 4.1 is for the condition when all the valves are conducting. During normal operation of the converter, a smaller number of valves are conducting. The nonconducting valves, represented by open circuits, must somehow be eliminated from the above equation. The converter model can be viewed as a sequence of network topologies. The network topology changes at the instant of a valve turning ON or OFF. Using Kron's reduction, Eq. 4.1 can be reduced to a set which is valid for a particular circuit topology. This is accomplished by defining the incidence matrix, $\mathbf{C}_n$, which relates the independent currents $\mathbf{I}_m$ in the original circuit to the currents $\mathbf{I}_n$ in the reduced model.

$$\mathbf{I}_m = \mathbf{C}_n \mathbf{I}_n \tag{4.4}$$

Once the incidence matrix is defined for a particular circuit topology, the remaining parameters can be determined as follows

substituting 4.4 into 4.1,

$$\mathbf{V}_m = \mathbf{Z}_m \mathbf{C}_n \mathbf{I}_n$$

multiplying both sides by $\mathbf{C}_n^t$

$$\mathbf{C}_n^t \mathbf{V}_m = \mathbf{C}_n^t \mathbf{Z}_m \mathbf{C}_n \mathbf{I}_n$$

Defining

$$\mathbf{V}_n = \mathbf{C}_n^t \mathbf{V}_m$$

and

$$\mathbf{Z}_n = \mathbf{C}_n^t \, \mathbf{Z}_m \, \mathbf{C}_n$$

the final set of equations representing the reduced model for a particular circuit topology becomes

$$\mathbf{V}_n = \mathbf{Z}_n \, \mathbf{I}_n$$

To solve this equation numerically using the trapezoidal rule of integration, it is first rewritten into its differential form, that is

$$\mathbf{V}_n = (\mathbf{R}_n + p\mathbf{L}_n) \, \mathbf{I}_n$$

and then rearranged

$$p\mathbf{I}_n = \mathbf{L}_n^{-1} (\mathbf{V}_n - \mathbf{R}_n \, \mathbf{I}_n) \qquad (4.5)$$

where $p=d/dt$ and $\mathbf{R}_n$ and $\mathbf{L}_n$ are the resistance and inductance matrices in the reduced set. The inductance matrix $\mathbf{L}_n$ in Eq. 4.5 is a square matrix and can be easily inverted. Equation 4.5 is solved for the independent currents $\mathbf{I}_n$ from which the mesh currents $\mathbf{I}_m$ are calculated using Eq. 4.4. The valve currents and the transformer primary currents can then be written in terms of mesh currents $\mathbf{I}_m$.

Clearly, the efficiency of the method depends on the the approach used to generate the incidence matrix $\mathbf{C}_n$ [8]. In the next section, it is shown that $\mathbf{C}_n$ can be generated in a logical manner for any given circuit topology.

4.3 Generation of the incidence matrix

Figure 4.2 shows the mesh diagram for a 12-pulse bridge. If all the valves were conducting, there would be ten links corresponding to ten mesh currents. During normal operation only 2 or 3 valves are conducting in each bridge; therefore, only a small number of links and branches will remain in the circuit. The dimension of the incidence matrix is 10 x n for a 12-pulse bridge and 5 x n for a 6-pulse bridge where n is the number of remaining links in the circuit of Fig. 4.2. By considering all possible conduction patterns, a logic statement can be derived for each link which is equal to "1" if a particular link exists in the reduced circuit and is equal to "0" otherwise. When all the existing links are determined, a check is made to see whether the valves selected as tree branches in the original tree (i.e. valves 3,6 in each bridge) in Fig. 4.2 are still conducting. If either one of these valves has turned off, a new tree branch must be selected and the appropriate elements in matrix $\mathbf{C}_n$ must be modified as explained in Appendix C.

4.4 Calculation of the valve voltages

The voltages across the non-conducting valves must be calculated at each instant of time to determine their firing (ON/OFF) state for the next time step. Once the incidence matrix $\mathbf{C}_n$ has been generated, the independent currents $\mathbf{I}_m$ and the voltages $\mathbf{V}_m$ are updated using the most recent values of $\mathbf{I}_n$ and $\mathbf{V}_n$. A modified form of Eq. 4.1 which includes valve voltages in the loop equations is used to determine the valve voltages.

$$\mathbf{V}_x = \mathbf{V}_m - \mathbf{Z}_m \mathbf{I}_m \tag{4.6}$$

where

$$\mathbf{V}_x = \begin{bmatrix} v_1^Y - v_3^Y \\ v_2^Y - v_3^Y \\ v_4^Y - v_6^Y \\ v_5^Y - v_6^Y \\ v_3^Y + v_6^Y \\ \cdots \\ v_1^\Delta - v_3^\Delta \\ v_2^\Delta - v_3^\Delta \\ v_4^\Delta - v_6^\Delta \\ v_5^\Delta - v_6^\Delta \\ 0 \end{bmatrix} + \begin{bmatrix} 0 \\ 0 \\ 0 \\ 0 \\ v_3^\Delta + v_6^\Delta \\ \cdots \\ 0 \\ 0 \\ 0 \\ 0 \\ 0 \end{bmatrix} = \begin{bmatrix} \mathbf{V}_x^Y \\ \cdots \\ \mathbf{V}_x^\Delta \end{bmatrix} + \mathbf{V}_x^c \qquad (4.7)$$

and v_j^Y and v_j^Δ are the voltages across the jth valve in the upper and lower bridges respectively. For a 6-pulse bridge, the vector $\mathbf{V}_x$ reduces to $\mathbf{V}_x^Y$, that is $\mathbf{V}_x = \mathbf{V}_x^Y$. If the voltages v_3^Y, v_6^Y, v_3^Δ and v_6^Δ in Eq. 4.7 were all zero, all other voltages could be directly calculated from Eq. 4.6. In general the vector $\mathbf{V}_x$ is related to the valve voltages by the matrix D.

$$\mathbf{V}_x = \mathbf{D}\,\mathbf{V}_v \qquad (4.8)$$

where

$$\mathbf{V}_v = [v_1^Y, \ldots, v_6^Y \mid v_1^\Delta, \ldots, v_6^\Delta]^t \quad , \quad \mathbf{D} = \begin{bmatrix} \mathbf{D}^Y & 0 \\ 0 & \mathbf{D}^\Delta \end{bmatrix}$$

and

$$\mathbf{D}^Y = \begin{bmatrix} 1 & 0 & -1 & 0 & 0 & 0 \\ 0 & 1 & -1 & 0 & 0 & 0 \\ 0 & 0 & 0 & 1 & 0 & -1 \\ 0 & 0 & 0 & 0 & 1 & -1 \\ 0 & 0 & 1 & 0 & 0 & 1 \end{bmatrix} \quad , \quad \mathbf{D}^\Delta = \begin{bmatrix} 0 & 0 & 1 & 0 & 0 & 1 \\ 1 & 0 & -1 & 0 & 0 & 0 \\ 0 & 1 & -1 & 0 & 0 & 0 \\ 0 & 0 & 0 & 1 & 0 & -1 \\ 0 & 0 & 0 & 0 & 1 & -1 \end{bmatrix}$$

Similarly, $\mathbf{D}$ is $\mathbf{D}^Y$ for a 6-pulse bridge. Since the voltage across the conducting valves is zero, the columns corresponding to these valves in $\mathbf{D}$ are eliminated. After similar elimination of the rows corresponding to the existing links in the

reduced model, the matrix $\mathbf{D}$ is reduced to a square matrix $\mathbf{D}_n$. The unknown valve voltages are then calculated from the reduced form of Eq. 4.8 given by

$$\mathbf{V}_{vn} = \mathbf{D}_n^{-1} \mathbf{V}_{xn}$$

4.5 Voltage and current transformation matrices

The voltages e_{ac}^{Y}, e_{ca}^{Δ},.... in $\mathbf{V}_m$ are the line-to-line ac voltages on the secondary side of the transformer. In the Y-Y connected bridge the secondary phase voltages are related to the primary voltages by the transformer tap ratio. Because of the $1/\sqrt{3}$ factor inherent in the Y-Δ connection, the tap ratio is increased by a factor of $\sqrt{3}$ for the Y-Δ transformer so that the peak ac voltage applied across the lower and upper bridges is of the same amplitude. The transformation matrix $\mathbf{T}_v$ relates the secondary voltages $\mathbf{V}_m$ to the primary voltages.

$$\mathbf{V}_m = \mathbf{T}_v \mathbf{V}_p$$

where $\mathbf{V}_p = [v_{ap} \;\; v_{bp} \;\; v_{cp}]^t$ is the vector representing the primary ac voltages and

$$\mathbf{T}_v = t_i \begin{bmatrix} 1 & 0 & -1 \\ 0 & 1 & -1 \\ -1 & 0 & 1 \\ 0 & -1 & 1 \\ 0 & 0 & 0 \\ \cdots & \cdots & \cdots \\ 0 & 0 & -\sqrt{3} \\ 0 & \sqrt{3} & 0 \\ 0 & 0 & \sqrt{3} \\ 0 & -\sqrt{3} & 0 \\ \sqrt{3} & \sqrt{3} & \sqrt{3} \end{bmatrix} = \begin{bmatrix} \mathbf{T}_v^Y \\ \cdots \\ \mathbf{T}_v^\Delta \end{bmatrix}$$

When writing the equations for the ac side of the system, the transformer secondary currents should be referred to the primary side. By inspection of Fig. 4.2, the secondary currents are calculated from the mesh currents using the following relations.

$$i_{as}^Y = i_a^Y - i_c^Y$$

$$i_{bs}^Y = i_b^Y - i_d^Y$$

$$i_{cs}^Y = i_c^Y + i_d^Y - i_a^Y - i_d^Y$$

$$i_{ba}^\Delta = i_a^\Delta - i_c^\Delta + i_f^\Delta$$

$$i_{cb}^\Delta = i_a^\Delta + i_b^\Delta - i_c^\Delta - i_d^\Delta + i_f^\Delta$$

$$i_{ac}^\Delta = i_f^\Delta$$

where i_{as}^Y and i_{ba}^Δ are the a-phase transformer secondary currents.

The primary currents are related to the secondary currents by the transformer tap ratios.

$$\mathbf{I}_p = t_i \mathbf{I}_s^Y + \sqrt{3}\, t_i \mathbf{I}_s^\Delta$$

where

$$\mathbf{I}_p = \begin{bmatrix} i_{ap} \\ i_{bp} \\ i_{cp} \end{bmatrix} \quad , \quad \mathbf{I}_s^Y = \begin{bmatrix} i_{as}^Y \\ i_{bs}^Y \\ i_{cs}^Y \end{bmatrix} \quad , \quad \mathbf{I}_s^\Delta = \begin{bmatrix} i_{ba}^\Delta \\ i_{cb}^\Delta \\ i_{ac}^\Delta \end{bmatrix}$$

expressing $\mathbf{I}_s^Y$ and $\mathbf{I}_s^\Delta$ in terms of the mesh currents $\mathbf{I}_m$, the transformation matrix which relates the primary ac currents directly to the converter mesh currents is given by

$$\mathbf{I}_p = t_i \left[\begin{array}{ccccc|ccccc} 1 & 0 & -1 & 0 & 0 & \sqrt{3} & 0 & -\sqrt{3} & 0 & \sqrt{3} \\ 0 & 1 & 0 & -1 & 0 & \sqrt{3} & \sqrt{3} & -\sqrt{3} & -\sqrt{3} & \sqrt{3} \\ -1 & -1 & 1 & 1 & 0 & 0 & 0 & 0 & 0 & \sqrt{3} \end{array}\right] \mathbf{I}_m = \left[\mathbf{T}_i^Y \mid \mathbf{T}_i^\Delta\right] \begin{bmatrix} \mathbf{I}_m^Y \\ \cdots \\ \mathbf{I}_m^\Delta \end{bmatrix}$$

4.6 Representation of the ac system and the harmonic filters

The ac system is represented by an equivalent voltage source in series with an equivalent reactance. Obviously, a full representation of the entire ac system including a detailed simulation of ac generators will result in a more accurate and realistic response of the system under transients, but the requirements on computer time and storage would be prohibitive. The use of a Thevenin equivalent is better suited to the detailed of the dc simulation. The Thevenin equivalent circuit can be updated at arbitrary intervals for a realistic representation of the ac system.

In an HVDC system, both the rectifier and the inverter are connected to the ac system through tap changing transformers. A number of harmonic shunt filters are usually placed on the ac side at both ends of the line. The filters are usually in the form of series RLC circuits tuned to eliminate the 5th,

7th, 11th, 13th harmonic in a 6-pulse bridge and 11th and 13th harmonics in a 12-pulse bridge. A damped high-pass filter is also added for higher harmonics. These filters serve a twofold purpose; that of reducing harmonics in voltages and currents, and of supplying reactive power. The reactive power supplied by the filters is generally not sufficient to fully compensate the reactive power drawn by the converter; hence additional capacitor banks are usually installed.

Although the ac shunt filters are treated as static elements in a simplified model, their effect on the harmonics and the dynamic response of the ac system cannot be neglected in a detailed analysis. Complete representation of the filters is however very costly from a computational point of view as they add considerably to the number of differential equations to be solved during the simulation. Depending on the nature of the study and the disturbance under consideration, full representation of the filters at all dc terminals may not be necessary. For most studies, a complete representation of the filters at those dc terminals which are electrically near and are thus more affected by the disturbance under study may be sufficient.

The differential equations representing the ac side are given below. In the following, $p=d/dt$ and the subscript j refers to the harmonic number of the filter. For convenience, equations for only one phase of the ac system are given.

$$pi_{ac} = \left(\frac{1}{l_{th}}\right)\left(e_{th} - r_{th}i_{th} - v_{ap}\right)$$

$$pv_{ap} = \left(\frac{1}{c_c}\right)\left[i_{ac} - \sum_{j=5,7,11,13} i_{fj} - i_{ap} - i_{hp} - \left(\frac{1}{r_{hp}}\right)\left(v_{ap} - v_{hp}\right)\right]$$

$$pi_{fj} = \left(\frac{1}{l_j}\right)(v_{ap} - v_{cj} - r_j\, i_{fj})$$

$$pv_{cj} = \left(\frac{1}{c_j}\right) i_{fj} \qquad j = 5,7,11,13$$

$$pi_{hp} = \left(\frac{1}{c_j}\right)(v_{ap} - v_{hp})$$

$$pv_{hp} = \left(\frac{1}{c_{hp}}\right) i_{hp} + \left(\frac{1}{r_{hp}c_{hp}}\right)(v_{ap} - v_{hp})$$

Where,

i_{ac} : ac phase current

v_{ap} : ac phase voltage at the converter bus

e_{th} : ac system Thevenin phase voltage

r_{th}, l_{th} : Thevenin resistance and inductance

i_{fj} : harmonic filter currents

v_{cj} : harmonic filter capacitor voltage

r_j, l_j, c_j : filter resistance, inductance and capacitance

i_{hp} : high-pass filter current

v_{hp} : high-pass filter capacitor voltage

r_{hp}, l_{hp}, c_{hp} : high-pass filter resistance, inductance and capacitance

4.7 Simulation algorithm

The differential equations describing the ac system, harmonic filters and reactive compensation, dc converter and dc lines are all assembled and put into the form $\dot{\mathbf{X}} = \mathbf{A}\,\mathbf{X} + \mathbf{B}\,\mathbf{U}$. The complete set of differential equations is then solved using the trapezoidal rule of integration. The vector $\mathbf{X}$ contains ac phase currents and voltages, reactive compensator and filter currents and voltages, converter currents $\mathbf{I}_n$ as well as dc line variables.

Every time the converter network topology changes, the converter equations 4.1 should be updated to a new reduced set given by Eq. 4.5. To do this, a new incidence matrix should first be generated from the knowledge of the valves conduction state. The matrices $\mathbf{R}_n$ and $\mathbf{L}_n$ and the vector $\mathbf{V}_n$ are then calculated form $\mathbf{Z}_m$ and $\mathbf{V}_m$ respectively using the new incidence matrix.

If a change in the conduction state of any of the valves from the previous time step had been detected, the currents $\mathbf{I}_n$ in the new reduced set must be properly initialized before the integration process starts. The mesh currents $\mathbf{I}_m$ and subsequently the valve currents are updated. The secondary voltages $\mathbf{V}_m$ are also updated using the most recent values of the primary voltages just obtained from the solution of differential equations $\dot{\mathbf{X}}$. The valve voltages are then calculated using the updated values of $\mathbf{V}_m$ and $\mathbf{I}_m$.

Before the conduction state of the valves for the next time step can be determined, the status of the control pulses for each valve should be known; for a valve to turn ON its control gate must first be pulsed . Therefore, depending on the converter type (rectifier or inverter), appropriate control subroutines are called at this point. Once the conduction state of valves is updated, the program moves to the next time step where a new incidence matrix is

generated if there is change in the conduction state of the valves. A simplified flowchart of the program is shown in Fig. 4.3.

4.8 Simulation of the dc control system

The converter valves are equipped with control gates by which their firing can be controlled. A valve will fire only when the anode-to-cathode voltage across its terminals is positive and a control pulse exists at its control gate. Different types of controls can be implemented by controlling the firing delay of the valves. For example, if it is desired to control the current in a rectifier, the current is measured and compared with its set value. If the current exceeds the set value, it is reduced by increasing the ignition delay of the valves and hence reducing the dc voltage which in turn causes the current to drop. Conversely, the current can be increased by reducing the delay time in valve ignitions.

The two common types of grid control schemes are the "individual phase" and the "equidistant pulses" firing schemes. With the individual phase firing scheme, a saw-tooth voltage is compared with a control voltage V_c that is generated by a current regulator or an extinction angle controller. The starting point of the saw-tooth voltage corresponds to the zero crossing of the commutation voltage. As shown in Fig. 4.4, a firing pulse of 120 degrees duration is generated when the saw-tooth voltage crosses the control voltage, V_c. Although this method provides satisfactory results with converters connected to strong ac systems, it has been found to be not suitable for converters operating onto a weak ac connection because of harmonic instability arising from the magnification of ac harmonics additional to 5th, 7th, etc. [26]. An improved method of grid control is to use a control system in which firing pulses are timed by a phase-locked oscillator. This method, usually referred to

as the equidistant pulses firing scheme, has been developed and expanded upon by several authors [27-29]. Although the problem of harmonic instability with individual phase control on HVDC systems which are connected to weak ac systems can be overcome by designing appropriate active filters in the control loop, methods using the voltage controlled oscillator (VCO) have proven to be more reliable; as a result, the individual phase firing scheme is gradually being abandoned.

The VCO is a voltage to frequency converter that converts an input dc voltage into a train of pulses whose frequency is proportional to the input dc voltage. Since the firing instants are no longer derived from the zero crossings of the commutation voltage, in steady state, the pulses are fired at equal distances. The input dc voltage to the VCO could be the error in the current from the current regulator or the error in the angle from the extinction angle controller. A change in the input dc voltage changes directly the frequency of the output pulses, hence the name pulse frequency control (PFC) systems.

The VCO can be modified in such a way that the phase of the pulses rather than their frequency is proportional to the input control voltage. This type of control system is then called a pulse phase control (PPC) system. Due to proportional characteristic of the PPC as opposed to integral characteristic of the PFC systems, the implementation of the constant firing angle control in PPC systems becomes trivial by simply applying a constant input voltage. Both control systems are however suitable for the purposes of controlling the current or the angle of the converters in HVDC systems.

4.8.1 Simulation of the current regulator

The block diagram for the current regulator is shown in Fig. 4.5. The measured current is compared with the current setting and the error is fed to the VCO after being amplified. The VCO produces control pulses which are applied to a ring counter. The ring counter is made up of shift registers. Each time a pulse arrives at the input of the ring counter, the contents of the counter are moved by one position. During steady state operation, the control voltage applied to the VCO is zero and the VCO is adjusted to generate control pulses which are 60 degrees apart for 6-pulse operation and 30 degrees for the 12-pulse operation. This ensures that the duration of the pulses applied to the valves are 120 degrees. If there is a change in the control voltage due to the deviation of the current from its set value, the frequency of the oscillator changes accordingly until the control voltage returns to zero where again the pulses are generated at 30 degrees intervals (for 12-pulse operation) shown in Fig. 4.6.

To implement the constant firing angle control α_{min}, it is only necessary to delay the arrival of the control pulse at the shift register until the commutation voltage has reached a predefined positive value. During a transient, if the ac voltage at the rectifier side is not high enough to maintain the current control, the control is automatically shifted to the Constant Ignition Angle control where the pulses are generated with a delay corresponding to α_{min} from the actual zero crossings of the ac voltages.

4.8.2 CEA control for inverters

There are two types of extinction angle controls. One is of the feedback type in which the extinction angle is measured and then control applied to correct it, and the other is the prediction type which predicts the angle from the voltage and current conditions. The prediction type has the advantage of keeping the voltage-time area after commutation larger than a certain minimum value whereas with the feedback type extinction angle control, it is necessary to wait for a change in the extinction angle from the disturbance before any action is taken by the controller to restore the angle. Past studies have indicated that using prediction type control leads to more desirable results under transient conditions where ac commutation voltages are highly distorted. To increase the precision of the operation, the prediction type controller can be accompanied by a feedback loop which measures the error in the extinction angle and feeds it back to the controller.

Most of the original methods using prediction type used one of the commutation voltages directly or differentiated. A method based on the integration of the commutation voltages was later developed [30]. In this method each valve is controlled separately and a fresh computation of the correct firing angle is performed every cycle. Integration of the commutation voltages reduces its harmonic distortion and is thus particularly helpful when the commutation voltages are highly distorted as in the case when the converter is connected to a weak ac bus.

Under steady-state and assuming sinusoidal waveforms, the equation which defines the commutation process is given by

$$\sqrt{3}e_m\cos\beta - \sqrt{3}e_m\cos\gamma + k\, I_d = 0 \qquad (4.9)$$

where,

e_m : ac phase voltage (0-p)

β : angle of advance (i.e. $\beta = \gamma + u$)

γ : extinction angle

u : commutation angle

k : constant proportional to the commutation reactance

I_d : converter dc current

The first two terms in Eq. 4.9 can be thought of as voltage-time areas under angles β and γ. The third term $k\, I_d$ must then correspond to the commutation angle "u".

The point that the valve has to be fired in order to guarantee an extinction angle of γ is determined by the following relation.

$$\sqrt{3}\, e_m \cos\omega t - \sqrt{3}\, e_m \cos\gamma + k\, I_d = 0 \qquad (4.10)$$

Here, the time reference is taken at zero angle of delay. Equation 4.10 is satisfied at $\omega t = \alpha = \pi - \beta$, the angle of firing.

The first two terms are generated by integrating the commutating voltage from $-\pi + \gamma$ to the present instant as shown in Fig. 4.7.

$$A = \int_{-\pi+\gamma}^{\omega t} \sqrt{3}e_m \sin\omega t\, dt = \sqrt{3}e_m\cos\omega t - \sqrt{3}e_m\cos\gamma$$

Therefore if a dc voltage of $k I_d$ is added, the output of the integrator Eq. 4.10 will be satisfied at the time this negative signal crosses zero.

The basic idea presented above can be expanded to make it possible for the inverter to operate at greater angles of advance, β . This is done by adding an extra term to Eq. 4.10.

$$\sqrt{3}\, e_m \cos\omega t - \sqrt{3}\, e_m \cos\gamma + k\, I_d + V_{cc} = 0 \qquad (4.11)$$

When the control voltage V_{cc} is zero, the operation is on CEA control. The greater the signal V_{cc}, the greater is the angle of advance β. Current regulation at the inverter side can thus be accommodated by defining the appropriate control voltage V_{cc} as the error signal from a summer which compares the current with its set value. The error signal is amplified only when I_d is less than the current setting and is set to zero when it is greater to ensure inverter operation on CEA control.

4.9 Numerical examples

To demonstrate the capabilities of the detailed simulation program, three examples were chosen. In the first example, the rectifier quantities for a 12-pulse converter operation with complete filter representation are given. The second example demonstrates the response of a dc link to a commutation failure on the inverter side. Finally, in the third example, the ac/dc system response to a 25% drop in the ac voltage on the rectifier side of a multiterminal dc system are presented.

The simulated system was a dc link (Fig. 4.8) consisting of 12-pulse converters. The ac harmonic filters tuned to eliminate 11th and 13th harmonics were fully represented. High-pass filters to damp higher harmonics

were also included. Dc lines were represented by their equivalent pi models. Several pi sections can be simulated if desired. Figures 4.9-11 show the rectifier side quantities.

Steady-state values of the dc voltages and control angles can be checked using the following procedure. For this example, the dc line resistance was set to $R_l = 10\Omega$. The rest of the system parameters necessary for steady-state calculations are given in Table 4.1.

Table 4.1 System parameters for the dc link

	RECTIFIER	INVERTER
e_{th} (KV)	55.0	50.0
X_l (Ω)	7.54	7.54
I_{do} (KA)	1.00	0.90
α_{min} , γ_{min}(DEGS)	7.00	18.00
t	1.00	1.00

In this example the ac voltage were chosen such that the inverter station operated as a voltage-controlling station while operating with minimum angle of margin (γ_{min}). The rectifier station operating on current control regulated the line current to $I_{do} = 1.0$ KA . The dc voltage at the inverter terminals is given by

$$| V_{d2} | = \frac{3\, n_b \sqrt{3}}{\pi} e_m \cos(\gamma_{min}) - \frac{3\, n_b X_l}{\pi} I_{do} \qquad (4.12)$$

where n_b is the number of 6-pulse bridges in the converter ($n_b = 2$ for 12–pulse converter). The dc voltage at the rectifier side is

$$V_{d1} = | V_{d2} | + R_l I_{do}$$

The operating firing angle at the rectifier station is then calculated from the following relation

$$\alpha = \cos^{-1}\left(\frac{V_{d1} + \frac{3\, n_b X_l}{\pi} I_{do}}{\frac{3\, n_b \sqrt{3}}{\pi} e_{m1}} \right) \qquad (4.13)$$

The voltage e_{m1} in above is the zero-to-peak secondary voltage. Using the parameters given in Table 4.1, the following approximate results are obtained.

$$| V_{d2} | = 142.90 \text{ (KV)}$$

$$V_{d1} = 152.90 \text{ (KV)}$$

$$\alpha = 23.13 \text{ (DEGS)}$$

4.9.1 Simulation of a commutation failure

A common inverter maloperation is a commutation failure. It is usually caused by a combination of low ac voltage (perhaps due to an ac fault), high direct current and/or late arrival of the control pulse. It is identifiable by the extension of the commutation period from one valve to another beyond the point where the commutation voltage reverses.

To study the effect of the commutation failure on the system parameters, the arrival of the control pulse to valve 1 was delayed for 15°. In this example, the minimum extinction angle was set to 18° and the commutation angle (u) was found from the simulation to be approximately 25°. As observed in Fig. 4.12d, the failure to commutate from valve 1 to valve 2 caused the inverter current to rise to about 1.4 KA. The additional current came from the discharge of the dc line capacitance. During this fault, the rectifier current was not affected as much as the inverter current.

Figure 4.12e shows that the dc voltage across the upper bridge. Since the commutation failure was programmed to occur in the upper bridge, the voltage across this bridge drops to zero indicating an unusual sequence of valve firing. The total dc voltage across the converter however drops to half of its normal value. The second drop in dc voltage magnitude in Fig 4.12b is due to the action of the inverter current regulator. Since the down swing in the dc current exceeded the current margin (100 A), the inverter current regulator was automatically activated. For a short period, the inverter operated at a larger extinction angle than the preset minimum value. This resulted in a temporary drop in the dc voltage magnitude as observed in Fig 4.12b.

4.9.2 Simulation of a multiterminal dc system

A parallel-connected, radial multiterminal dc system consisting of a 12-pulse rectifier and two 12-pulse inverter stations was considered. The primary controls consisting of the current regulator and firing angle controller were simulated in detail at all terminals. The upper and lower limits on control angle were incorporated in the control simulation.

The widely used current margin method of control was assumed; as such the converter current orders were coordinated to establish a 10% current margin between the rectifier current setting and the sum of inverter current settings. With this method of control, under normal steady-state conditions, one of the converters usually an inverter operates as a voltage-controlling terminal while all other terminals operate on current and power control.

In this example, inverter 2, was the voltage-controlling terminal primarily due to its lower ac voltage. The type of fault simulated was that of a 3-phase 25% drop in the ac voltage at the rectifier station for a period of 5 cycles. During the fault, due to the depressed ac voltage at the rectifier terminal, its control automatically shifted to minimum firing angle control mode and the current control was lost. The controls at inverter 2 switched over to current control due to a lower dc voltage profile set by the rectifier station. As a result, the rectifier became the voltage-controlling terminal absorbing the current margin. Figures 4.13-15 show that once the fault was cleared, the system returned smoothly and swiftly to its normal operating state.

Using the system parameters given in Table 4.2, the steady-state values of the dc voltages and control angles can be calculated using the same relation between ac and dc quantities as given in Eq. 4.12.

Table 4.2 Three-terminal dc system parameters

	RECTIFIER 1	INVERTER 2	INVERTER 3
e_{th} (KV)	62.5	55.0	57.5
X_l (Ω)	7.54	7.54	7.54
I_{do} (KA)	1.85	1.00	0.75
α_{min} , γ_{min}(DEGS)	7.00	18.00	18.00
t	1.00	1.00	1.00

The line resistances between the dc terminals and a midpoint neutral bus connecting the three dc terminals were $R_{l1} = 5\Omega$, $R_{l2} = 3\Omega$ and $R_{l3} = 3\Omega$ respectively. In this example, inverter 2 was controlling the voltage by operating on it CEA control while rectifier 1 and inverter 3 operated on their current controls and regulated the currents at their terminals to the current orders given in Table 4.2. The inverter 2 voltage can be calculated using Eq. 4.12 from which all other voltages are calculated. The voltages and currents at all terminals are given by

$$V_{d1} = 169.74 \text{ (KV)} \qquad I_{d1} = 1.85 \text{ (KA)}$$
$$|V_{d2}| = 157.19 \text{ (KV)} \qquad I_{d2} = 1.10 \text{ (KA)}$$
$$|V_{d3}| = 158.24 \text{ (KV)} \qquad I_{d3} = 0.75 \text{ (KA)}$$

The control angle at the rectifier station can be calculated using Eq. 4.13. The extinction angle at the inverter 3 is calculated using a similar relation given by

$$\gamma = \cos^{-1}\left[\frac{|V_{d3}| + \frac{3\,n_b\,X_{l3}}{\pi} I_{do3}}{\frac{3\,n_b\,\sqrt{3}}{\pi} e_{m3}}\right] \tag{4.14}$$

$$\alpha_1 = 18.2 \text{ (DEGS)}$$
$$\gamma_3 = 27.3 \text{ (DEGS)}$$

During the fault, the rectifier operated at its constant ignition control ($\alpha = \alpha_{min}$) and controlled the voltage. Both inverters operated on their current controls. The average value of all dc voltages and currents during the fault are given by

$$V_{d1} = 130.75 \text{ (KV)} \qquad I_{d1} = 1.75 \text{ (KA)}$$
$$|V_{d2}| = 119.00 \text{ (KV)} \qquad I_{d2} = 1.00 \text{ (KA)}$$
$$|V_{d3}| = 119.75 \text{ (KV)} \qquad I_{d3} = 0.75 \text{ (KA)}$$

The extinction angles at inverters 2 and 3 are computed using Eq. 4.14 and are given by

$$\gamma_2 = 42.8 \text{ (DEGS)}$$
$$\gamma_3 = 46.6 \text{ (DEGS)}$$

4.10 Conclusion

In this chapter, an algorithm for detailed simulation of the dc system was presented. The simulation results on sample two-terminal and three-terminal demonstrated various capabilities of the algorithm. The simulation results showed agreement with calculations using approximate relations of the average-valued (simplified) HVDC models.

The results have indicated that the occurrence of the commutation failures lead to abnormal dc voltage and currents at the converter terminal. Studying the impact of commutation failure on system operation is particularly important with weak ac system connections. In such cases, the increased sensitivity of converter ac voltage to disturbances results in distorted voltages which often lead to commutation failures. In practice, upon the detection of a commutation failure, some control action, such as advancing the firing of the valves, is taken to avoid cascade commutation failures.

The results on rectifier side fault demonstrated the capability of the program to handle mode shifts. Upon the removal of the fault, the system returned smoothly to its normal operating state.

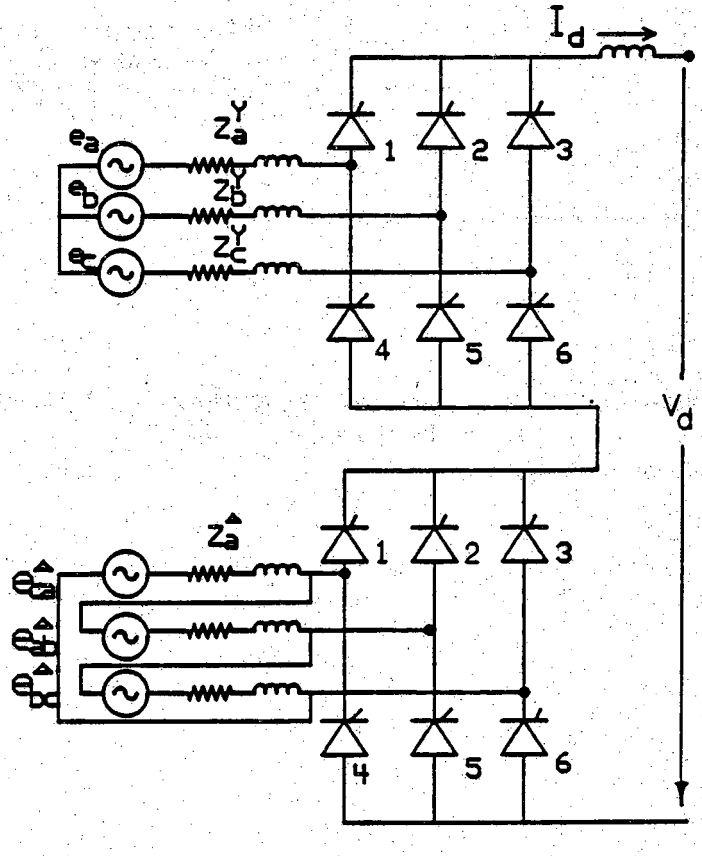

Figure 4.1 12-pulse converter with ac side quantities referred to the transformer secondary

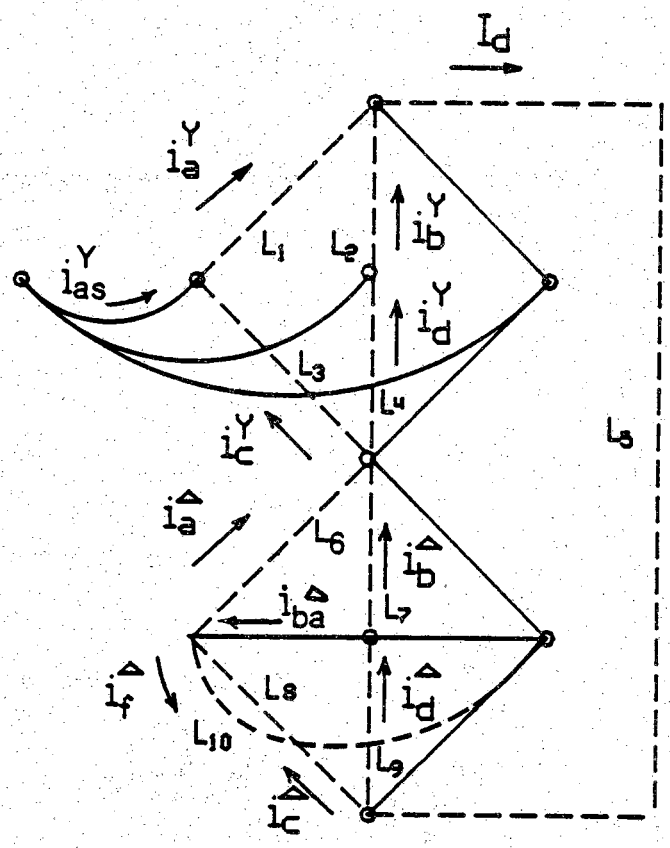

Figure 4.2 Mesh diagram for a 12-pulse converter

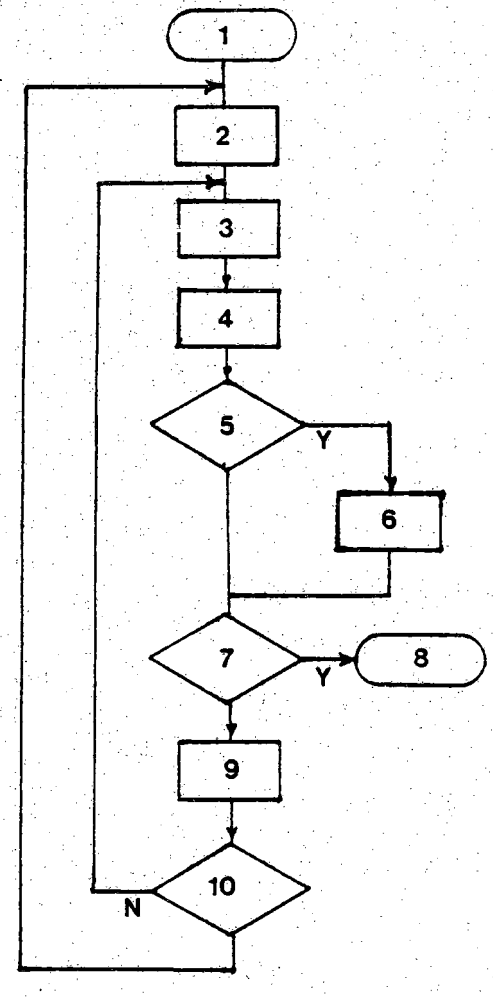

1. start
2. Generate the incidence matrix, C_n.
3. Solve the complete set of differential equations $\dot{X}$. Calculate thyristor voltages and currents.
4. Check the status of the grid pulses.
5. Any thyristor firing or extinction detected.
6. If the switching occurs between the time steps, interpolate the state variables back to the switching instant.
7. End of study ?
8. Exit
9. Advance the time, $t = t + \Delta t$
10. Any change in the conduction state of the thyristors ?

Figure 4.3 Detailed simulation program

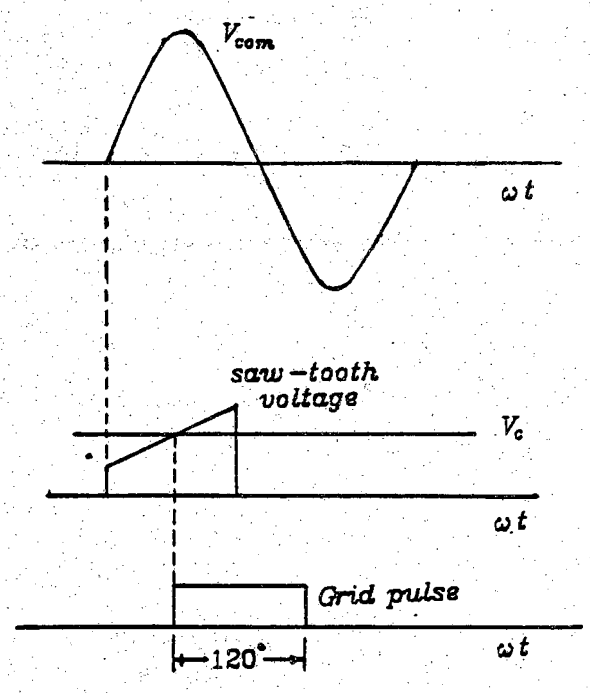

Figure 4.4 Individual phase control

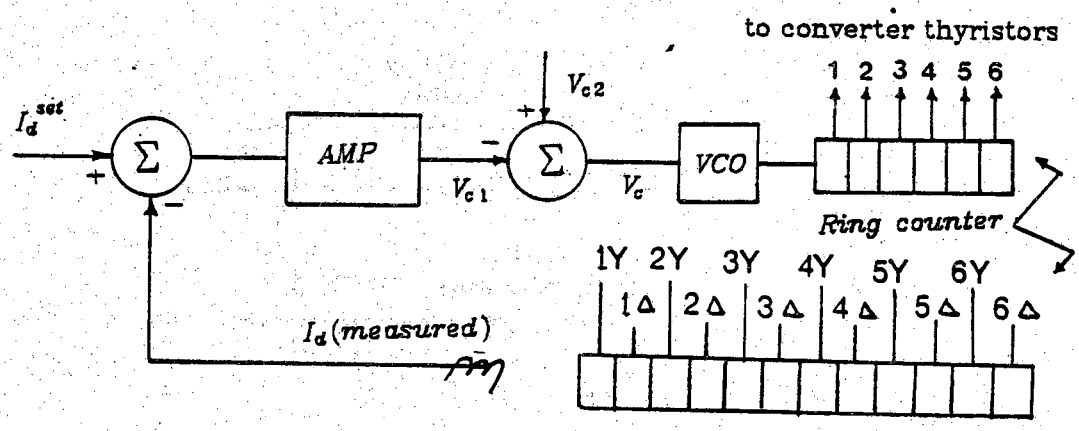

Figure 4.5 Block diagram of the current regulator

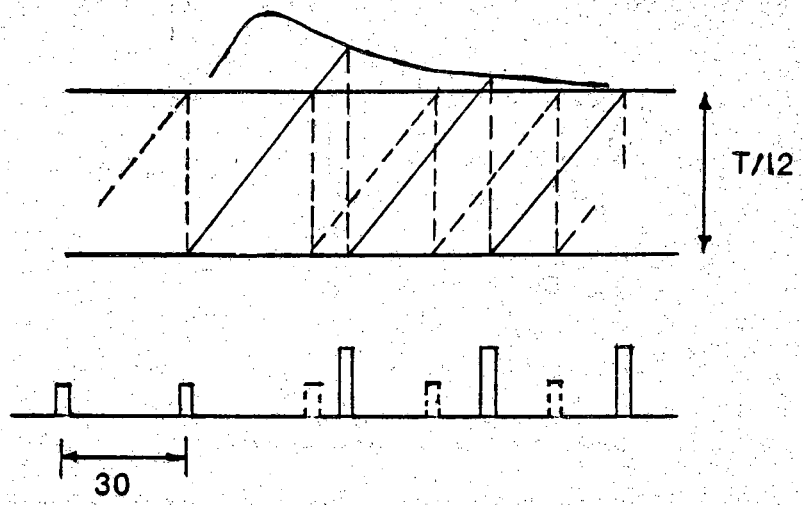

Figure 4.6 Generation of the control pulses by VCO

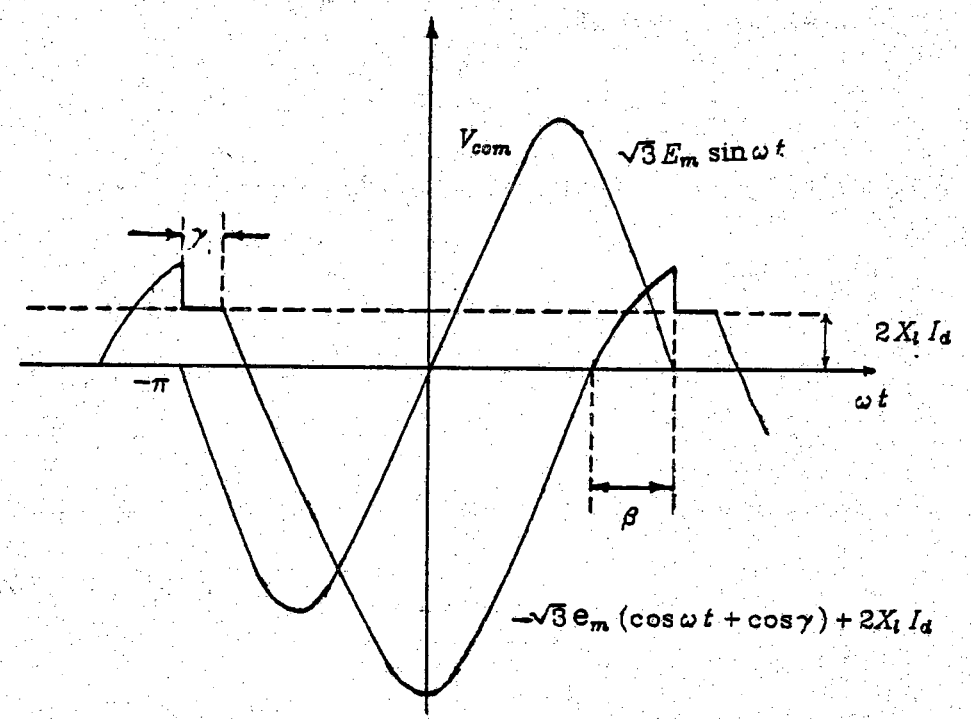

Figure 4.7 Integration of the commutation voltage for CEA control

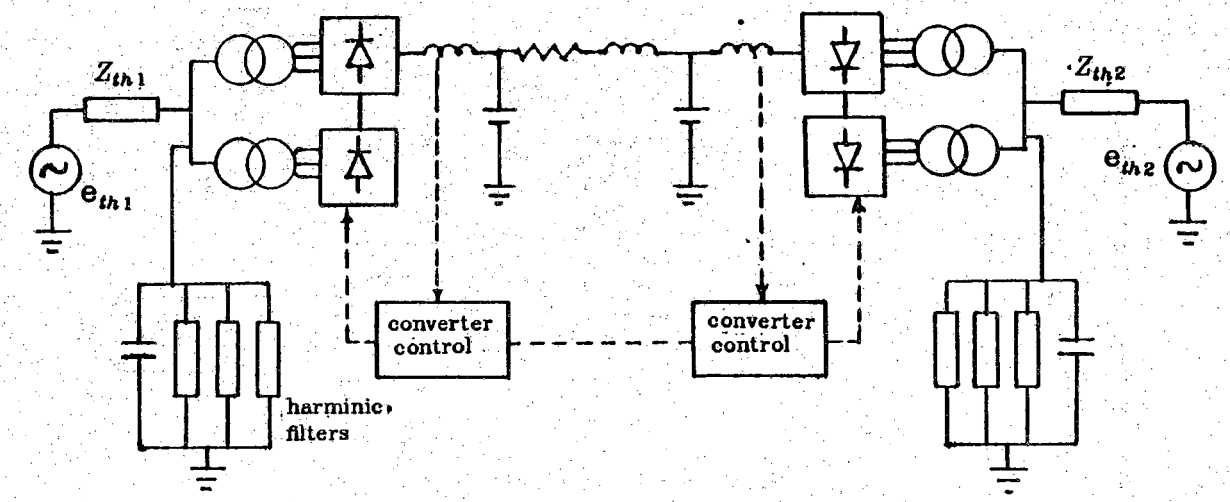

Figure 4.8 Detailed model of a dc link

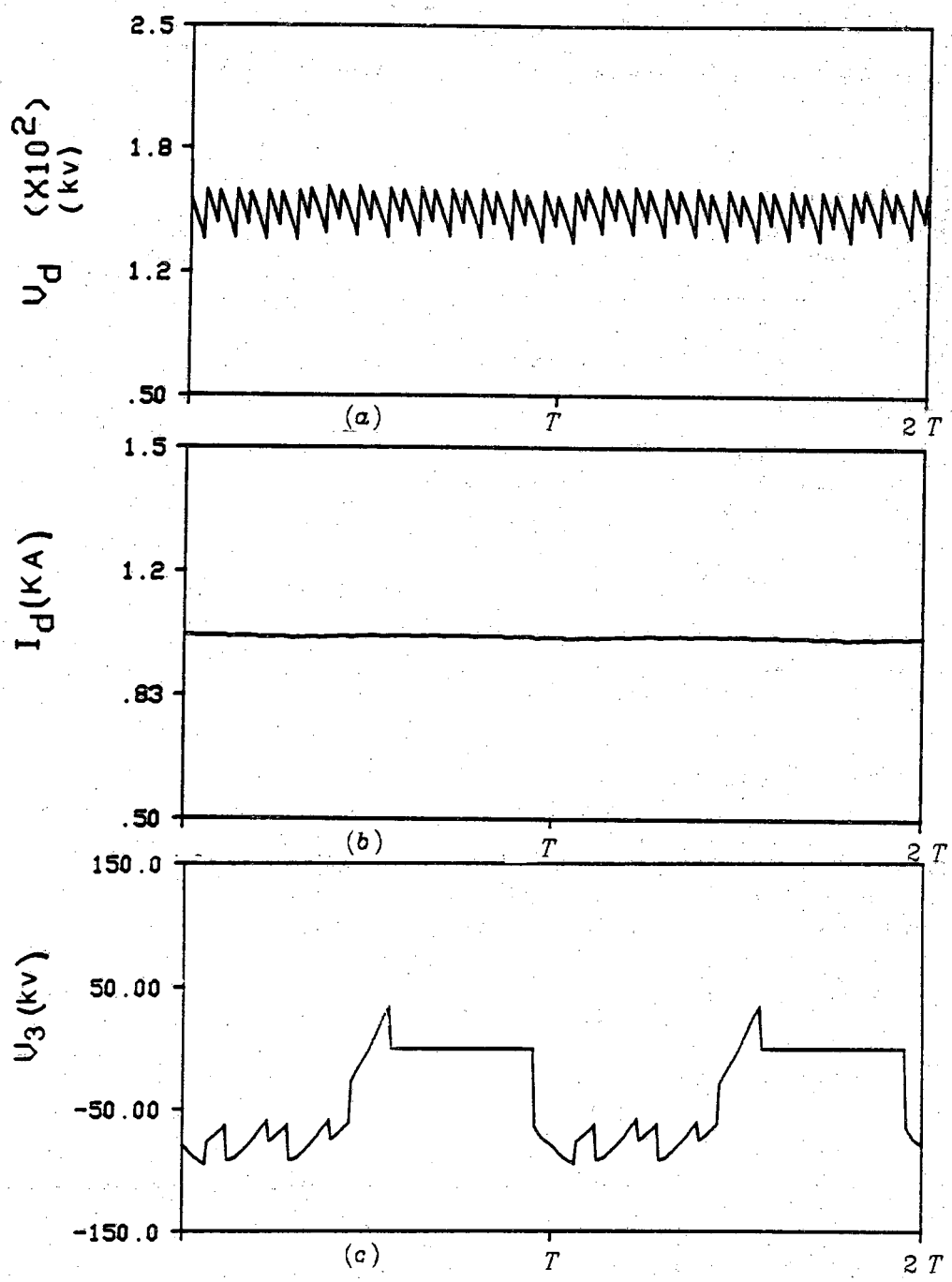

Figure 4.9 Normal 12-pulse rectifier operation: (a) DC voltage; (b) DC current; (c) Voltage across valve 3; (d) Y-Y bridge primary current; (e) Y-Δ bridge primary current; (f) Total primary current (g) Current through 11th harmonic filter; (h) Current through 13th harmonic filter; (i) Current through high pass filter

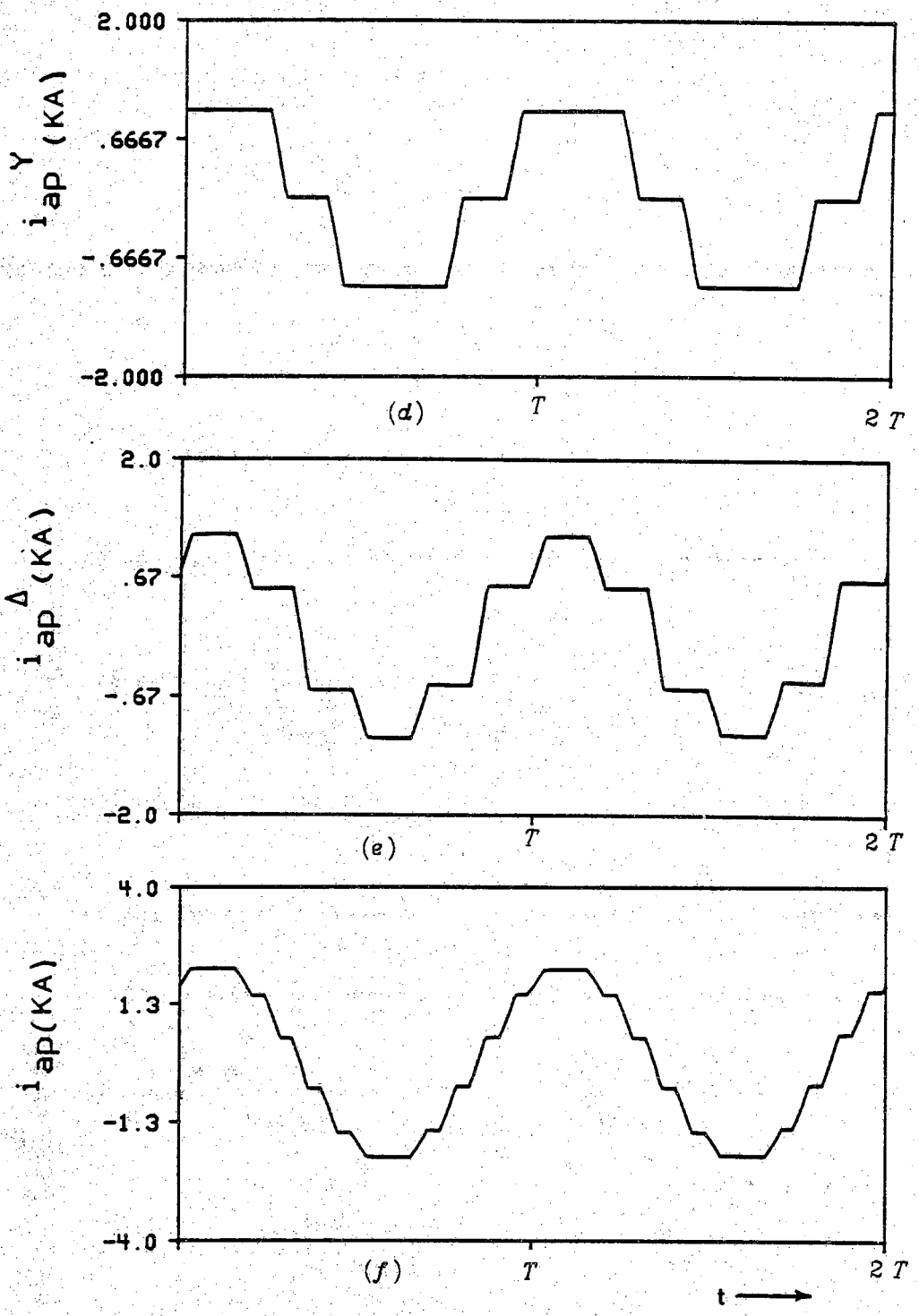

Figure 4.9 continued

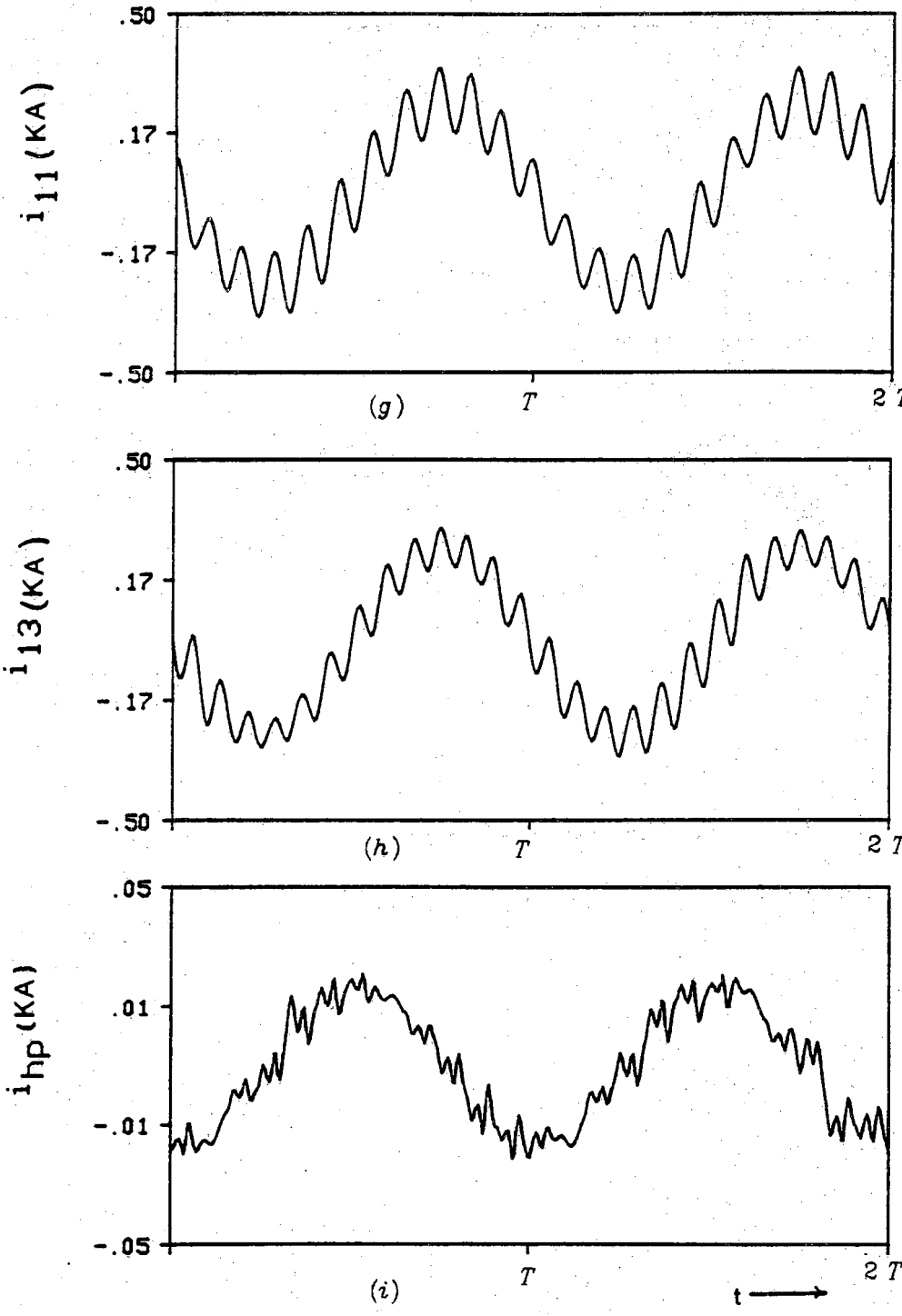

Figure 4.9 continued

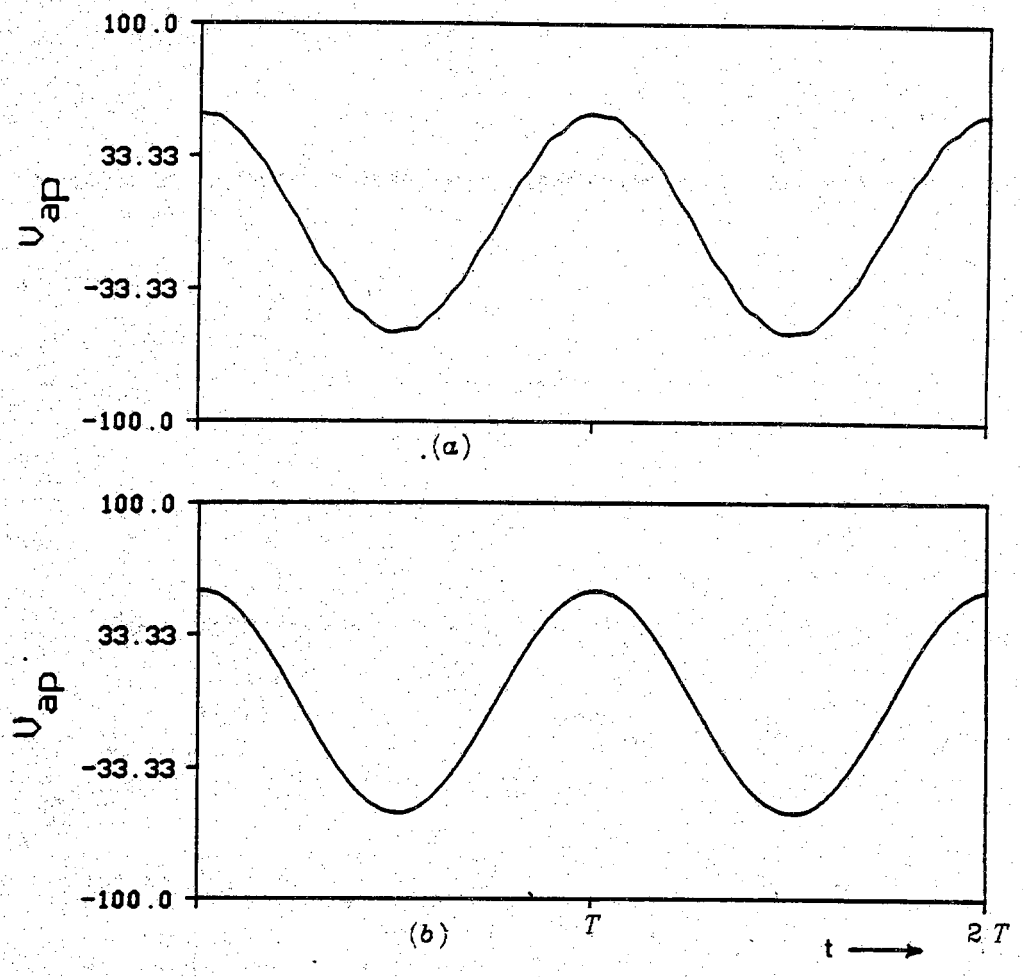

Figure 4.10 AC phase voltage: (a) Filters switched out;
(b) With filters

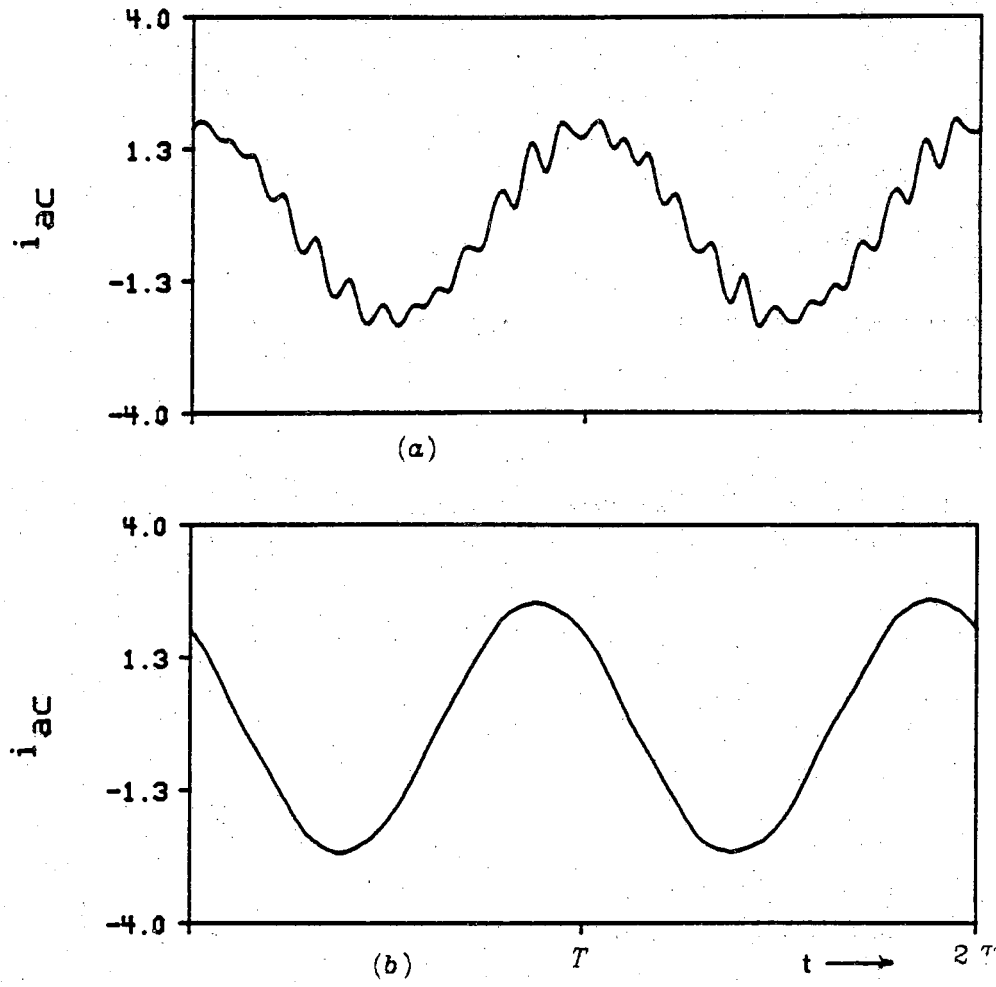

Figure 4.11 AC phase current: (a) Filters switched out
(b) With filters

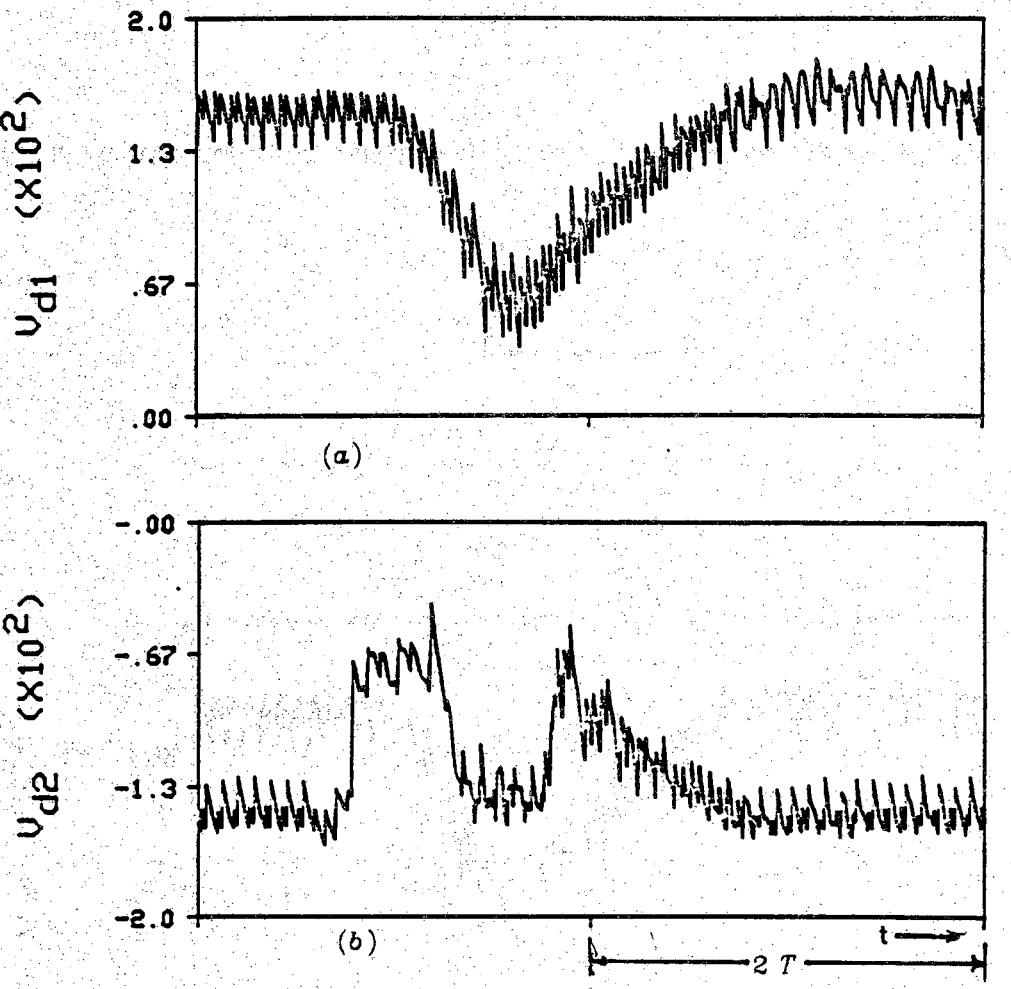

Figure 4.12 Commutation failure: (a) Rectifier dc voltage; (b) Inverter dc voltage; (c) Rectifier dc current; (d) Inverter dc current (e) DC voltage across Y-Y bridge; (f) Primary currents

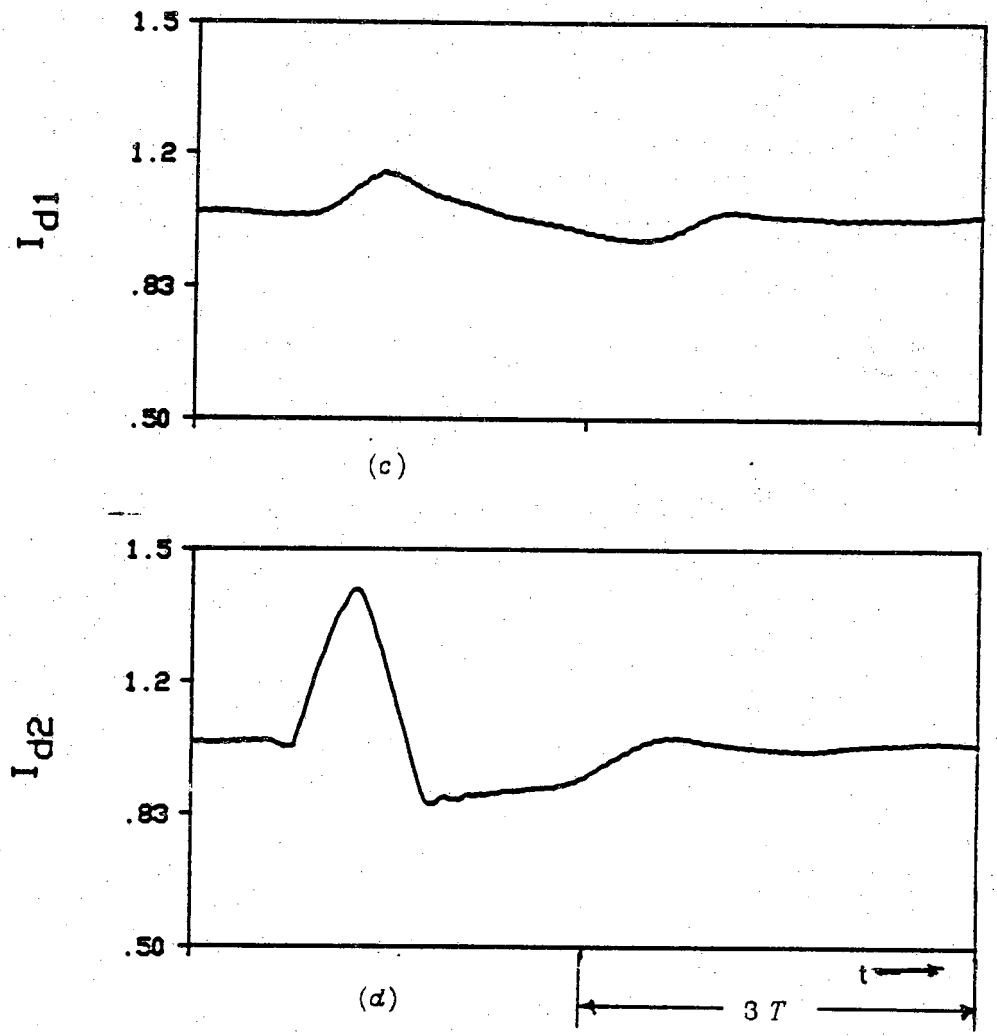

Figure 4.12 continued

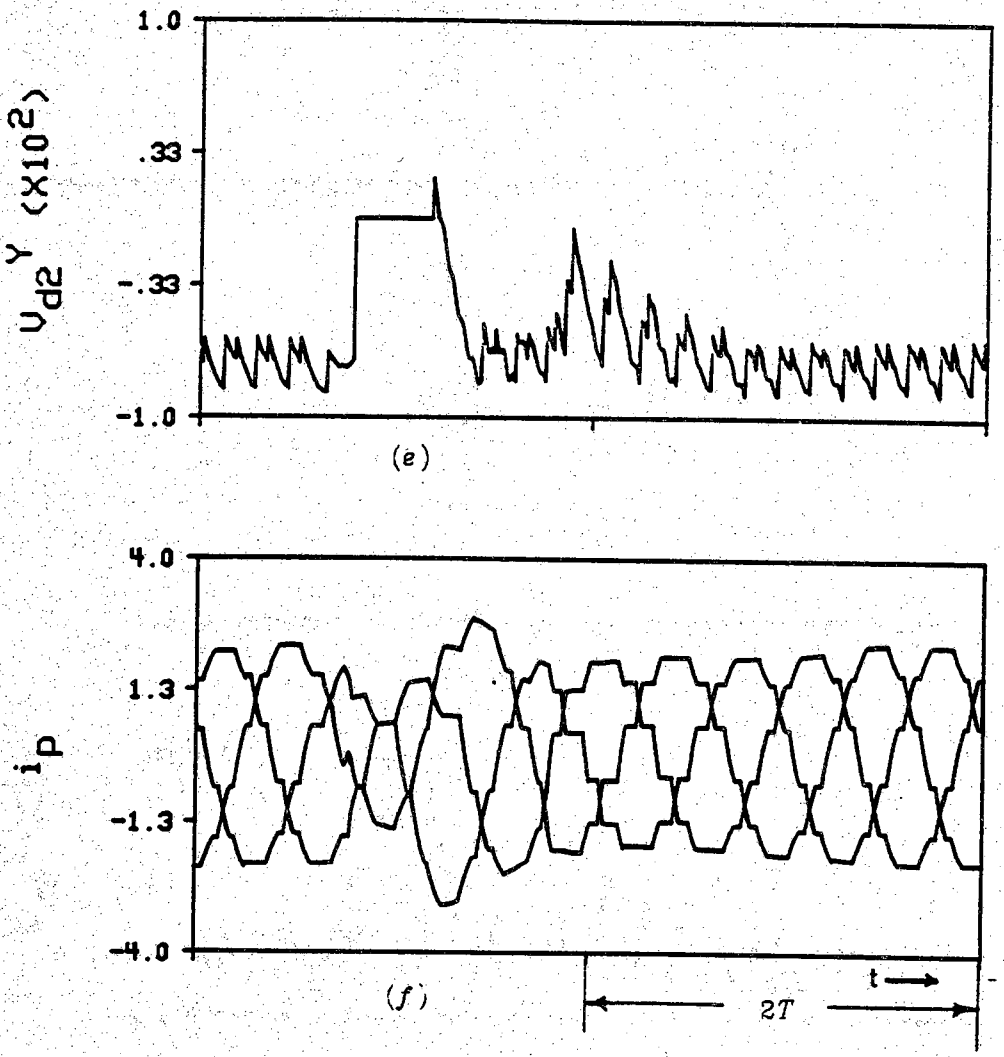

Figure 4.12 continued

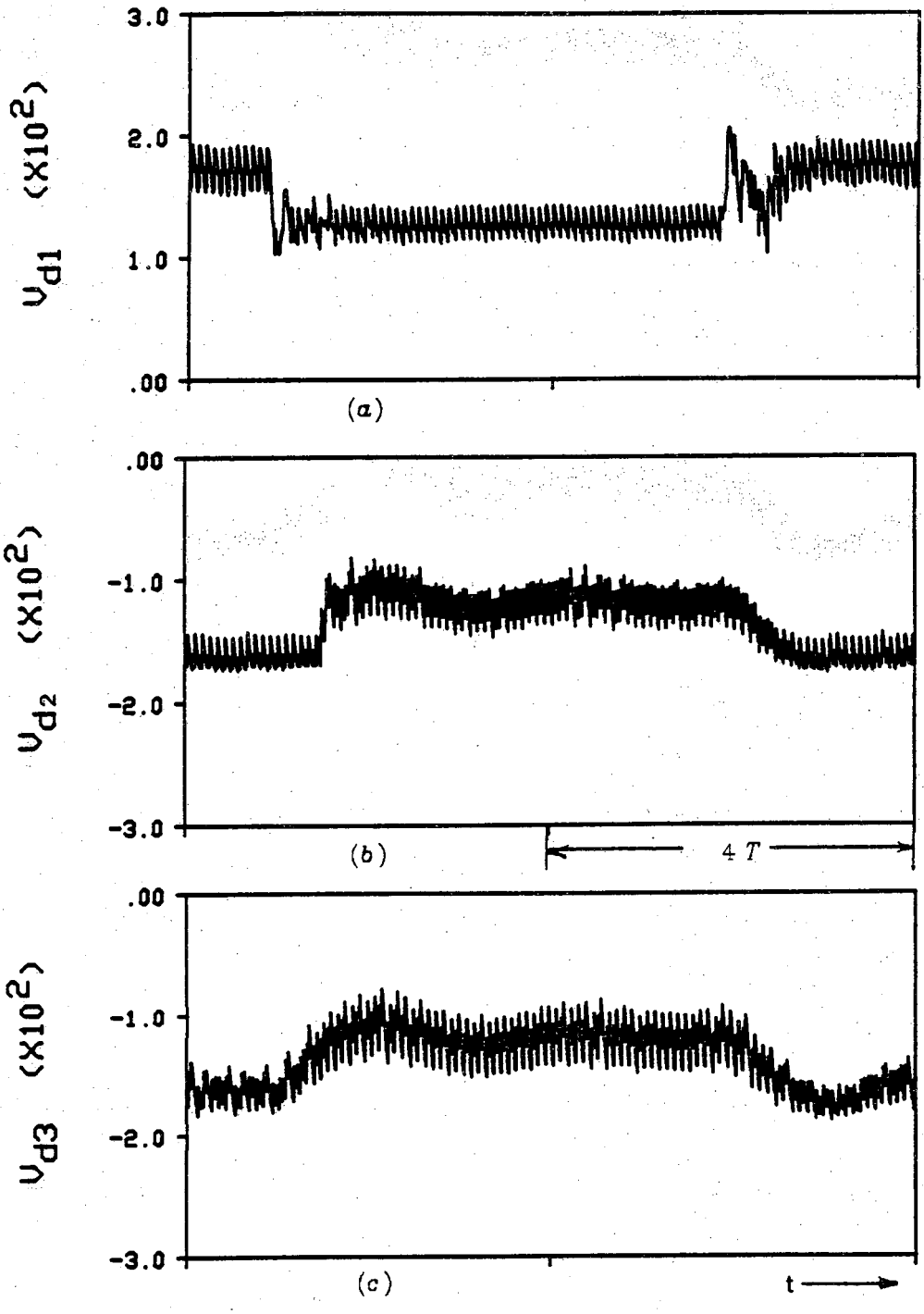

Figure 4.13 Rectifier side fault: (a-c) DC voltages
(d-f) DC currents

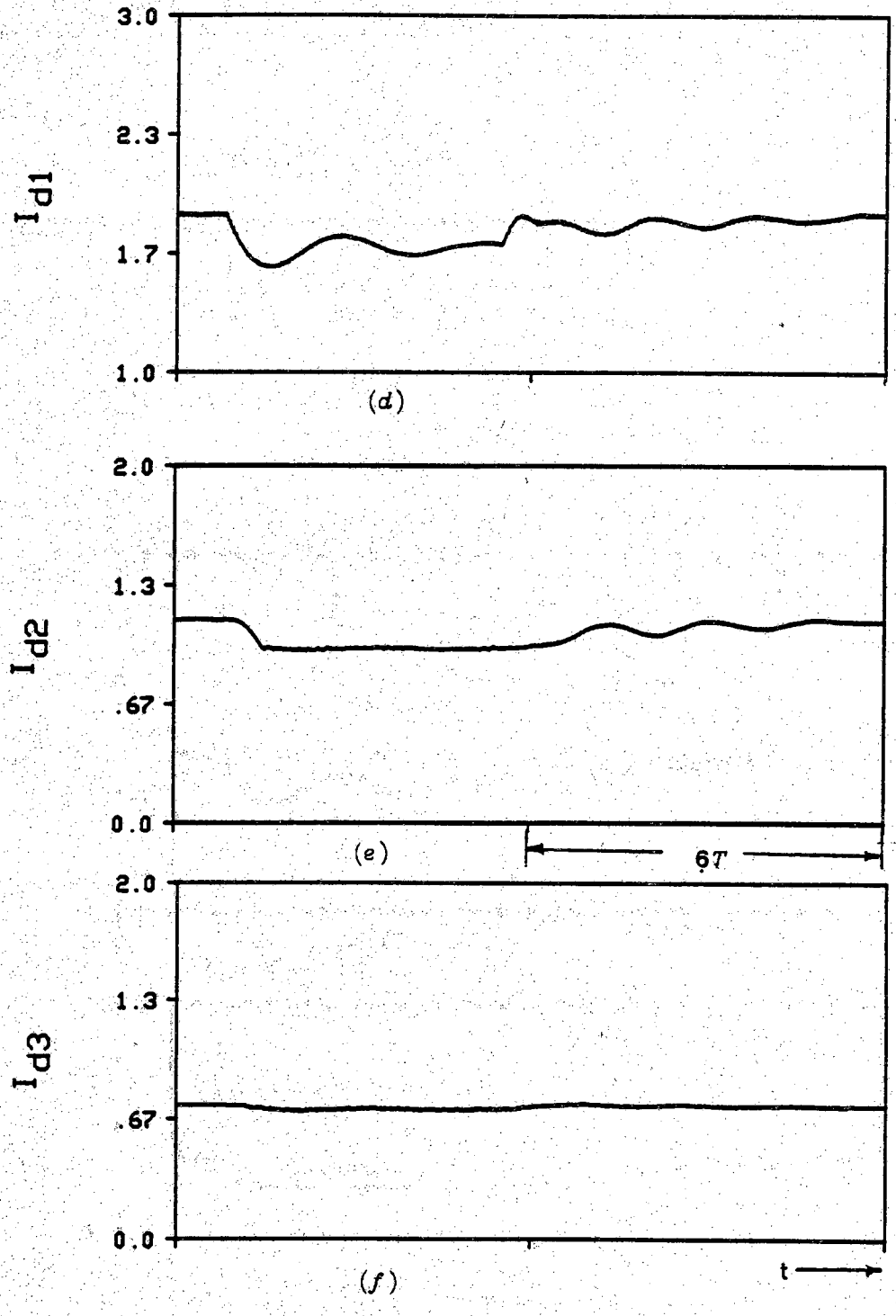

Figure 4.13 continued

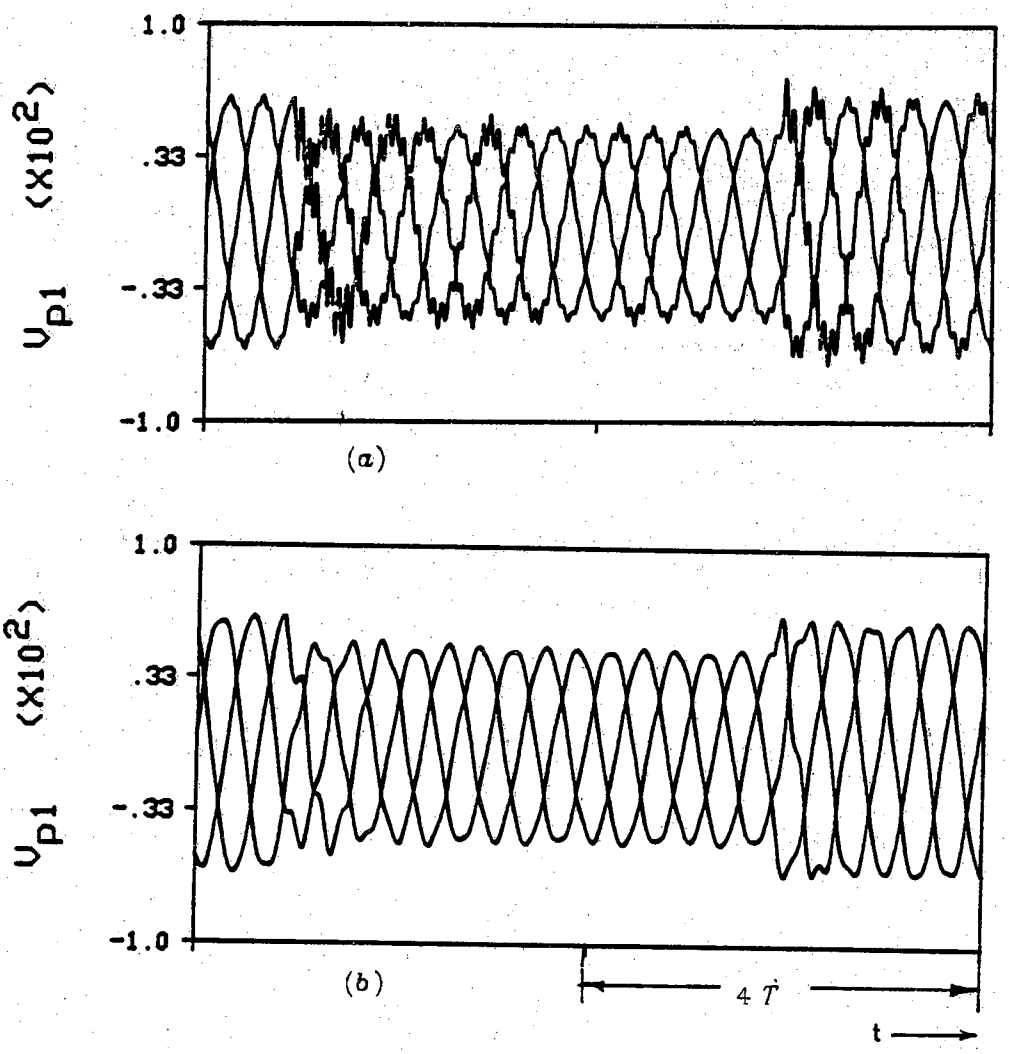

Figure 4.14 Rectifier side ac voltages: (a) Filters switched out (b) With filters

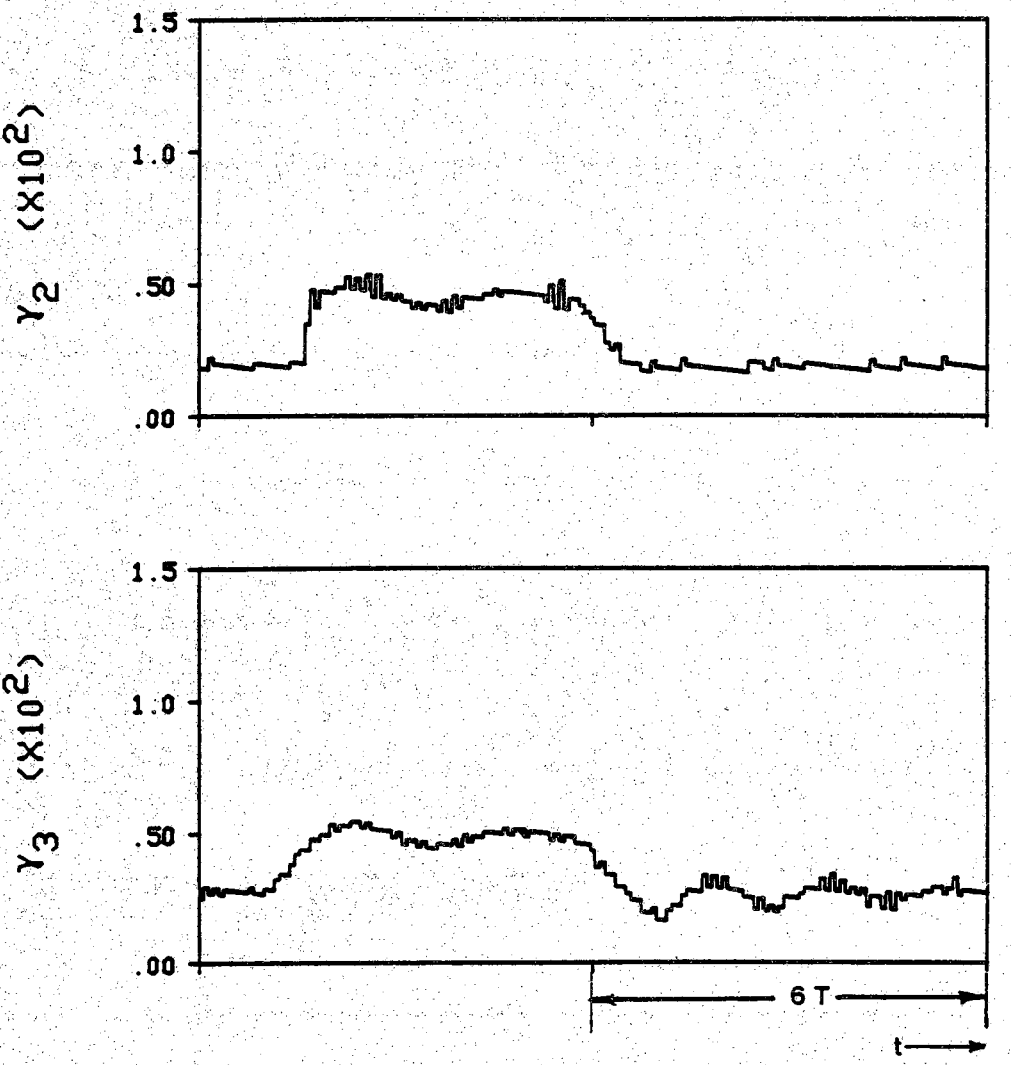

Figure 4.15 Extinction angles during the ac system fault at the rectifier side

CHAPTER 5

COORDINATING THE DC POWER INJECTIONS OF A MULTITERMINAL HVDC SYSTEM TO EFFECT DYNAMIC NETWORK FLOW CONTROL IN THE AC NETWORK

In an integrated ac-dc power system, the power injections of the dc network can be coordinated to effect, within limits, the desired ac power flow distribution in the ac network. In this chapter the feasibility of coordinating the dc injections of a multiterminal HVDC system to dynamically control the power flows of a select group of ac lines is examined. Potential applications of the method are to steer and to regulate the power flows of a select group of ac lines, and also to damp the power oscillations in these ac lines. The effectiveness of the proposed dynamic flow controller is demonstrated by numerical examples illustrating steering, regulating and damping control action.

5.1 Introduction

Besides being efficient in their primary function as bulk power transfer transmission, dc systems offer controllability that can be used for a variety of purposes, such as power modulation to enhance the damping and dynamic stability of the ac system [31-34], and reactive power control [5,35]. As more dc terminals, in the form of links or multiterminal systems, come into operation, the opportunity for coordinating the dc powers of these terminals to control the power flow in the ac network increases. Traditionally, desired changes in the power flow within the ac network are obtained by rescheduling generations and adjusting phase-shifting transformers. Such traditional methods, however, are much slower acting than that possible with dc control. Besides, higher production cost results when the rescheduled generations depart from the optimal dispatch solution. A better alternative is to first utilize whatever leftover terminal capacity of the dc system to alleviate power flow and voltage violations before resorting to generation shifting.

Changing the dc power injections have a similar effect on the ac network flows as changing the generations. A multiterminal HVDC system usually operates with one of the terminals, the voltage-controlling terminal, acting as a slack terminal [36]; as a result the slack terminal's power is determined indirectly by the controls of the other terminals and the dc network losses. With negligible energy storage capability in the dc network, changing the dc power of one converter in response to a local ac disturbance would inevitably transfer the effect of the disturbance, through the dc network, to that part of the ac system to which the voltage-controlling terminal is connected. Whether it be rearranging the distribution of ac power flows or providing damping to

the ac system, coordination of the dc injections is necessary to achieve the desired local effect at acceptable cost on a system-wide basis.

Coordinating the dc power injections of a multiterminal dc system to control real and reactive ac power flows for steady-state operation has been demonstrated in [1,2]. The effectiveness of steady-state power flow control depends on the extent of the ac-dc network interconnection, available control effort, and the transfer impedances between converter buses and ac lines whose power are to be controlled.

The ability to control the ac line flows dynamically can be used to facilitate operation of the integrated ac-dc power system in several ways. Potential applications of the dynamic control of ac network flows using a multiterminal HVDC system are steering and regulating the power flows in a select group of ac lines and damping the power oscillations in these lines. The effectiveness of the dynamic network flow controller applied to steering and regulating the power flows, and to damping the power oscillations in ac lines is demonstrated by numerical examples using a transient simulation program.

5.2 Problem formulation

An essential requirement of on-line dynamic control procedures is computation speed. And one key factor to faster computation is to keep the computational burden to a minimum. Often this calls for some degree of simplification to the problem description. In this study of the dynamic network flow control problem, the fast electrical transients of the network elements are ignored, as in standard transient stability studies, only the slower electrical power oscillations caused by the electromechanical oscillations of

machines are considered.

The objective of the on-line dynamic network flow controller is to provide the converter controls with the required changes in the dc power orders that will bring about the desired ac line flows in a select group of ac lines.

Let P^k_{aci} and P^k_{dcj} be the instantaneous values, at the k th sampling instant, of the real power flow in the ith ac line and the dc power injection of the jth dc terminal, respectively. If the desired power flow of the ith ac line is P^s_{aci}, the desired change in the power flow of the ith ac line, x^s_i, will be $P^s_{aci} - P^k_{aci}$. Changing the dc power injections into the ac network will alter the distribution of power flows within that ac network. Let $x_i = P_{aci} - P^k_{aci}$ be the change in the power flow in the ith ac line corresponding to a change in dc power at the jth terminal given by $u_j = P_{dcj} - P^k_{dcj}$.

Naturally, it is desirable to achieve the desired ac line flows with as small a change in dc power injections as possible. Hence, the problem of finding the required changes in dc powers is formulated as that of finding the minimum of the objective function

$$f = \sum_{i=1}^{n} \sigma_i (x_i - x_i^s)^2 + \sum_{j=1}^{m} \alpha_j u_j^2 \qquad (5.1)$$

where σ_i's and α_j's are weighting factors, and m and n are the number of dc terminals and the number of ac lines in the select group, respectively.

In terms of the ac network distribution factors g_{ij}'s, the ac network constraint equations relating the changes in power flows of the n ac lines to the changes in power transfers of the dc network are

$$x_i = \sum_{j=1}^{m} g_{ij}u_j, \qquad i=1,\ldots,n \tag{5.2}$$

In general, m and n are not equal, therefore, the u_j's cannot be obtained simply by setting x_i's to the desired values of x_i^s's in Eq. (5.2).

The dc network constraint on the changes in dc power powers, u_j's, is basically one of power balance - that is the net injected power into the dc network should be equal to the dc system losses. Ignoring terminal losses and also the second order terms of u_j's, the change in the dc network losses owing to the changes in dc power transfers can be expressed in terms of the corresponding B coefficients of the dc network. Such a refinement in the control formulation has been shown to be unnecessary [2]. Furthermore, with the control computations repeated at short time intervals, the change in dc network losses from one computation to the next due to changes in the dc power transfers can be neglected. Thus

$$\sum_{j=1}^{m} u_j = 0 \tag{5.3}$$

The change in power of the slack terminal (say, u_m) being dependent on those of the other terminals can be eliminated from Eqs. (5.1) and (5.2), yielding

$$f = \sum_{i=1}^{n} \sigma_i(x_i - x_i^s)^2 + \sum_{j=1}^{m-1} \alpha_j u_j^2 + \alpha_m \left[\sum_{j=1}^{m-1} u_j\right]^2 \tag{5.4}$$

$$x_i = \sum_{j=1}^{m-1} (g_{ij} - g_{im})u_j \qquad i=1,\ldots,n \tag{5.5}$$

The solution to the above constrained problem is obtained by minimizing the unconstrained Lagrangian function [2]

$$L = \sum_{i=1}^{n} \sigma_i(x_i - x_i^s)^2 + \sum_{j=1}^{m-1} \alpha_j u_j^2 + \alpha_m \left[\sum_{j=1}^{m-1} u_j\right]^2 + \sum_{i=1}^{n} \lambda_i \left[x_i - \sum_{j=1}^{m-1} (g_{ij} - g_{im})u_j\right] \tag{5.6}$$

where λ_i's are the Lagrangian multipliers.

The necessary conditions for a minimum are:

$$\frac{dL}{dx_i} = 2\sigma_i(x_i - x_i^s) + \lambda_i = 0, \quad i=1,\ldots,n \tag{5.7}$$

$$\frac{dL}{du_j} = 2\alpha_j u_j + 2\alpha_m \sum_{l=1}^{m-1} u_l - \sum_{i=1}^{n} \lambda_i(g_{ij} - g_{im}) = 0,$$

$$j=1,\ldots,(m-1) \tag{5.8}$$

$$\frac{dL}{d\lambda_i} = x_i - \sum_{j=1}^{m-1} (g_{ij} - g_{im})u_j = 0, \quad i=1,\ldots,n \tag{5.9}$$

Eliminating the λ_i's and x_i's, the required u_j's are given by the matrix equation

$$(\mathbf{A} + \mathbf{H}^t \mathbf{S} \mathbf{H})\, \mathbf{U} = \mathbf{H}^t \mathbf{S} \mathbf{X}^s \tag{5.10}$$

where the superscript t denotes the transpose of the vector or matrix.

$$\mathbf{A} = \begin{bmatrix} \alpha_1 + \alpha_m & \alpha_m & \cdots & \alpha_m \\ & \alpha_2 + \alpha_m & \cdots & \alpha_m \\ & & & \\ & & & \alpha_{m-1} + \alpha_m \end{bmatrix}$$

$$\mathbf{H}^t = \begin{bmatrix} g_{11} - g_{1m} & g_{21} - g_{2m} & \cdots & g_{n1} - g_{nm} \\ g_{12} - g_{1m} & g_{22} - g_{2m} & & \\ \cdot & & & \\ \cdot & & & \\ \cdot & & & \\ g_{1(m-1)} - g_{1m} & & & g_{n(m-1)} - g_{nm} \end{bmatrix}$$

$$\mathbf{S} = \text{diag}\,[\sigma_1, \sigma_2, \ldots, \sigma_n]$$

$\mathbf{U}$ is the m-1 vector, $(u_1, u_2, \ldots, u_{m-1})^t$

$\mathbf{X}^s$ is the n vector, $(x_1^s, x_2^s, \ldots, x_n^s)^t$

5.3 Control implementation

The information exchange among the various controllers and the ac-dc power system for implementing the network flow control is shown in Fig. 5.1. In this study, the response of the ac-dc power system to the changes in the power orders of the dc system is determined by an ac-dc transient stability program. Changes in the control mode of the multiterminal dc system are properly accounted for in the transient simulation [37]. The network flow controller samples the values of key ac lines flows and dc powers at the rate of 60 Hz and uses them to compute the required changes in the dc power orders according to the specified control function. The required changes in the dc powers as determined by the network flow controller are then used to update the dc power orders of the converters. At the next sampling interval, the above procedure is repeated over again.

5.4 Examples

The following studies are based on the test system shown in Fig. 5.2. The ac system was adapted from a nine-bus system given in [25]; parameters of the ac-dc test system are given in Appendix D.

5.4.1 Damping of power oscillations

A disturbance to the ac-dc system was created by simulating a temporary fault on bus 5 for 8 cycles. The power flows P_{78}, P_{45} and P_{46} during and after the fault, with no damping control applied to the dc system, are shown in Fig. 5.3. The fault caused a shift in the operating mode of the dc system, with inverter 2 losing the voltage control function to inverter 3 temporarily. With no damping control, the dc powers remained essentially constant after the fault. The power oscillations in the same three lines with damping control, shown here in Fig. 5.4, are less oscillatory than the case with no damping control applied. The result obtained with 3 cycles of communication and computation delay in the control loop is similar to that obtained with no delay, except for the slight delay in the response that can be observed by comparing Fig. 5.5 with Fig. 5.4. The available control effort for damping purposes from a converter may be limited by the device rating, this can be taken into consideration by limiting the change in its dc power. Figure 5.6 shows the response obtained with a power rating of 1.0 pu applied to converter 2. The technique for implementing the limit on the change in dc powers is the same as that described in [2]. Although the damping action was not as good as the case without the limit, it is still noticeably better than that obtained without damping control.

If the values of P^s_{aci} at the kth instant cannot be prespecified, they can be determined by a moving average computation, such as

$$P^s_{aci} = \sum_{j=k-np}^{k} P^j_{aci}$$

where np is the number of past sampling points used in the weighted average of P_{aci}. Figure 5.7 shows the controlled response with 3 cycles delay in the control loop and the desired values of power flows, P^s_{aci}'s, determined by the moving averages of measured power flows using a np of 20.

5.4.2 Steering and regulating line powers

In practice, steering could be used to relieve an overloaded line or to improve the steady-state stability margin of the ac system. For purposes of illustration, a change in operating state of the system was introduced by dropping the real and reactive components of the load on ac bus 6 by 30%. Figure 5.8 shows the steering of the power flow P_{78} back to its previous level by ramping the desired value, P^s_{ac1}, of that line over a 10 cycle duration after the initial transient power swing has settled. Following the steering operation, the power flow P_{78} was arbitrarily regulated at its predisturbance level. Raising the power flow P_{78} after the load at ac bus 6 has been lowered caused more of the generated power from unit 3 to flow clockwise, increasing the power flow through the ac line between buses 4 and 5. Should this increase in the power flow P_{45} be also of concern, simultaneous control of the power flows P_{78} and P_{45} can be applied. Figure 5.9 shows the response with simultaneous control of P_{78} and P_{45} by the network flow controller, in this case both line flows were steered toward and regulated arbitrarily at their previous levels.

With communication and computation delays in the control loop, compensation for these delays was required to stablize the regulating action. Using a lead compensator for the 3 cycle delay, the result for simultaneous control of P_{45} and P_{78} is shown in Fig. 5.10.

5.5 Discussion

An alternative formulation of the above minimization problem is:

minimize

$$f = \sum_{i=1}^{n} \sigma_i \left| x_i - x_i^s \right| + \sum_{j=1}^{m} \alpha_j \left| u_j \right| \tag{5.11}$$

subject to the network constraints of Eqs. (5.2) and (5.3) and the limits on the converter capacity

$$P_{dcj}^{k} - P_{dcj}^{min} \leq u_j \leq P_{dcj}^{max} - P_{dcj}^{k} \tag{5.12}$$

The absolute condition on the physical variables in the objective function can be handled by either introducing decision variables or program logic. This formulation has advantages of being able to enforce limits of converter capacity directly within the solution procedure and the use of a standard LP package. However, the performance of the LP formulation in cases calling for simultaneous control of two or more lines is not as predictable as the quadratic formulation in regard to the choice of the weighting factors in the objective function.

5.6 Conclusion

The numerical examples have shown that with proper coordination the dc injections of a multiterminal HVDC system can be used to steer and to regulate the power flows of a select group of ac lines, and to damp the power oscillations in these lines. In this study, the same algorithm has been applied to provide damping, steering or regulating action by modifying the weighting factors and the compensator. Perhaps, an optimized version, dedicated to perform a specific task, may be more preferable in practice.

The results presented in this chapter motivate further research on dynamic network flow control using dc systems; in particular, developing a systematic control design methodology that can take into account the changes in condition of the ac system.

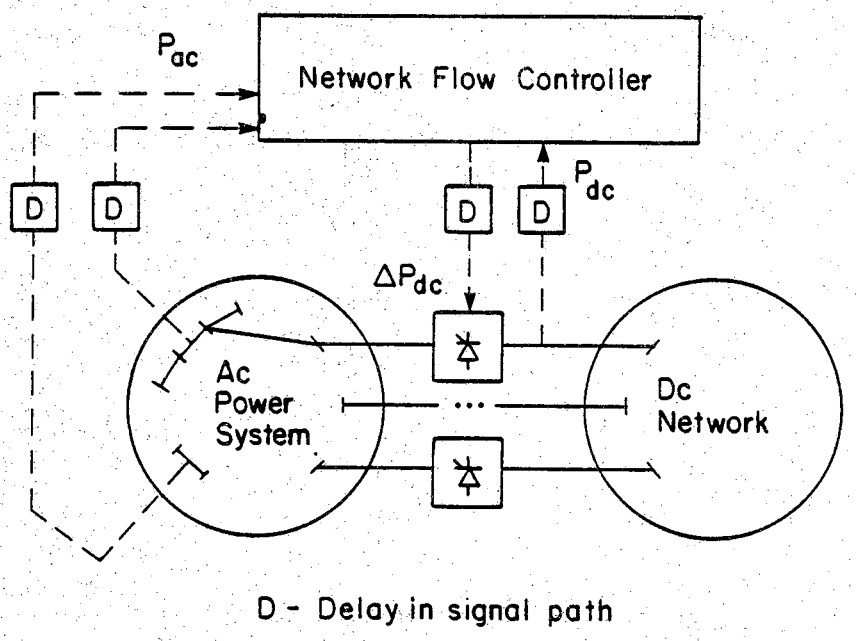

Figure 5.1 AC network flow control

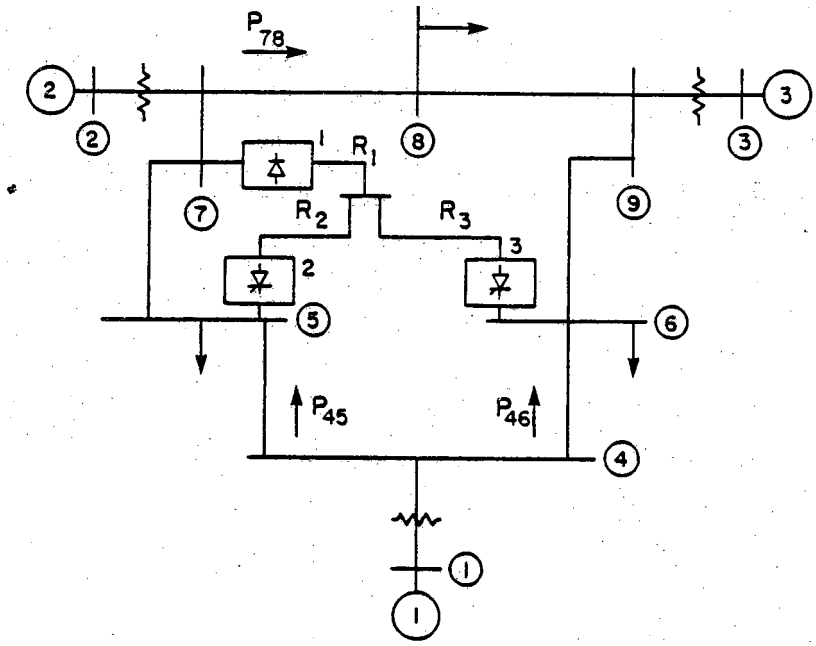

Figure 5.2 Sample 3-terminal, 3-machine system

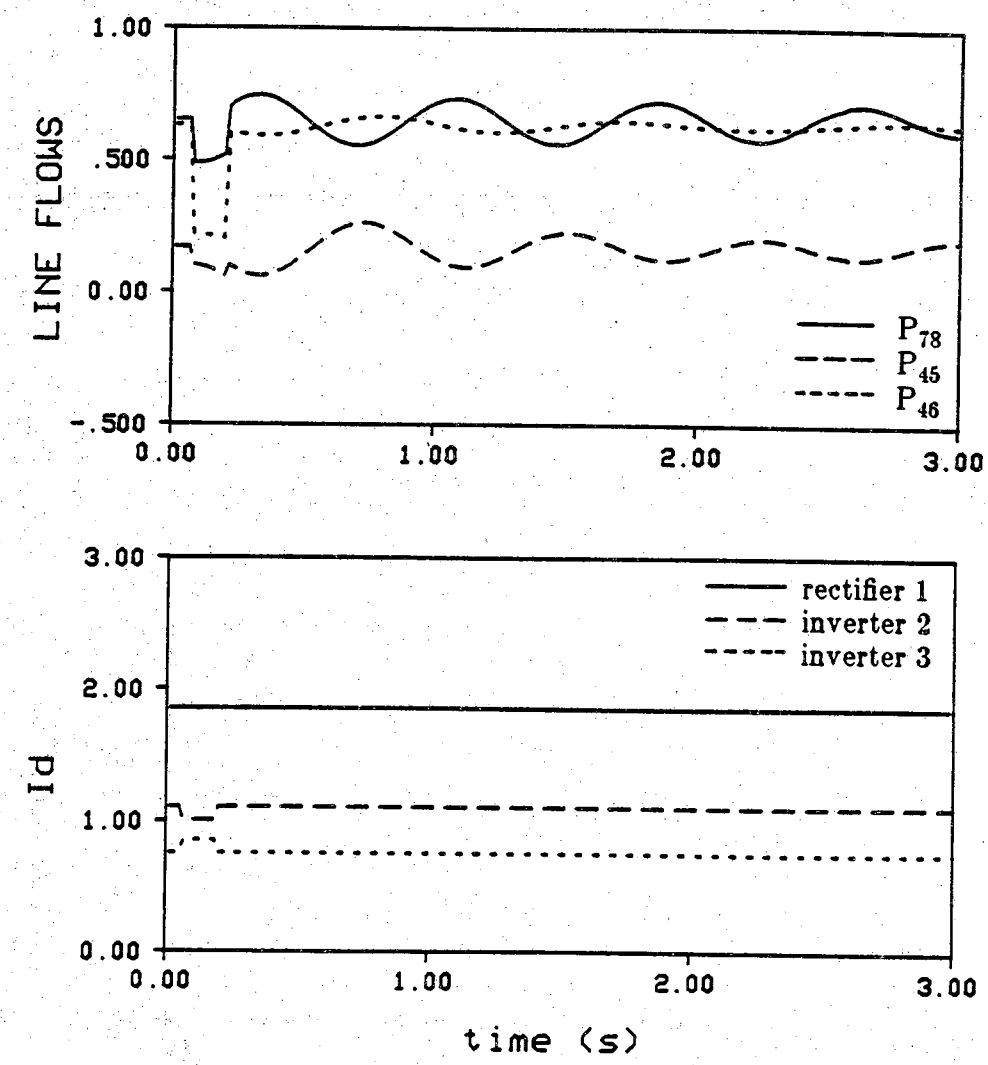

Figure 5.3 Response of system without damping control

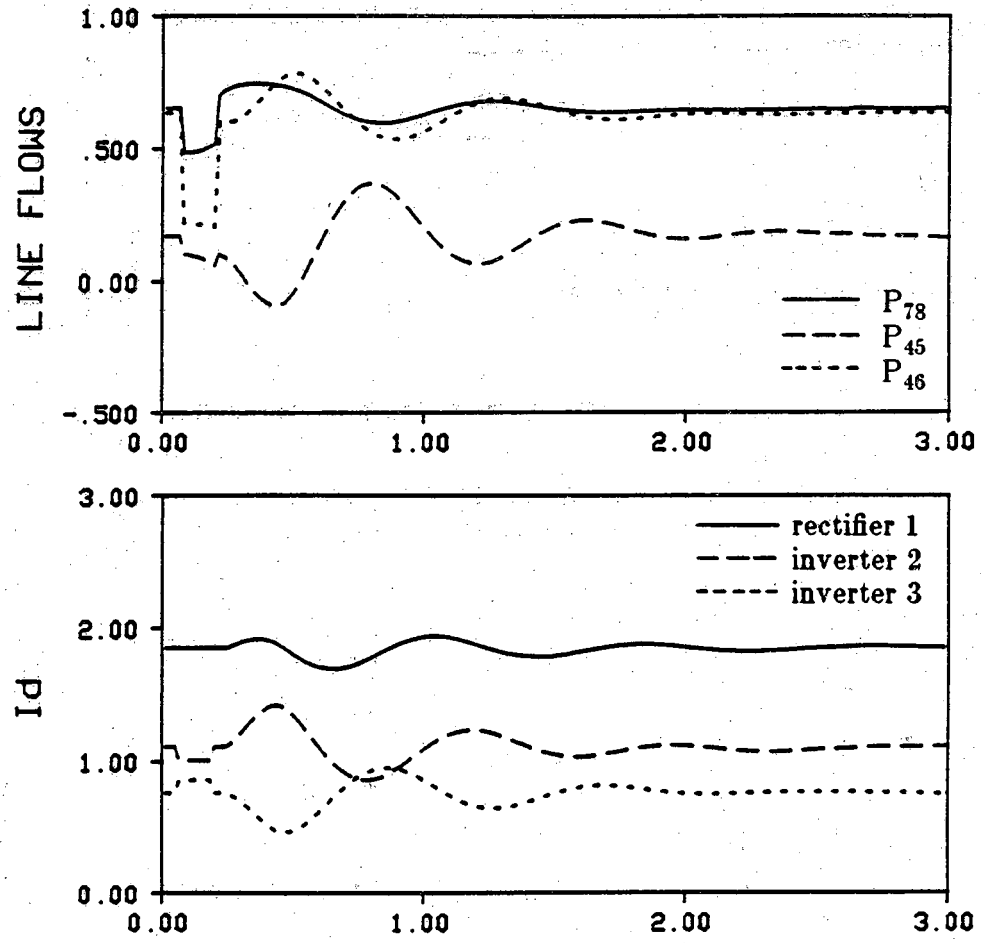

Figure 5.4 Damping applied to line flows P_{78}, P_{45} and P_{46} with no control delay

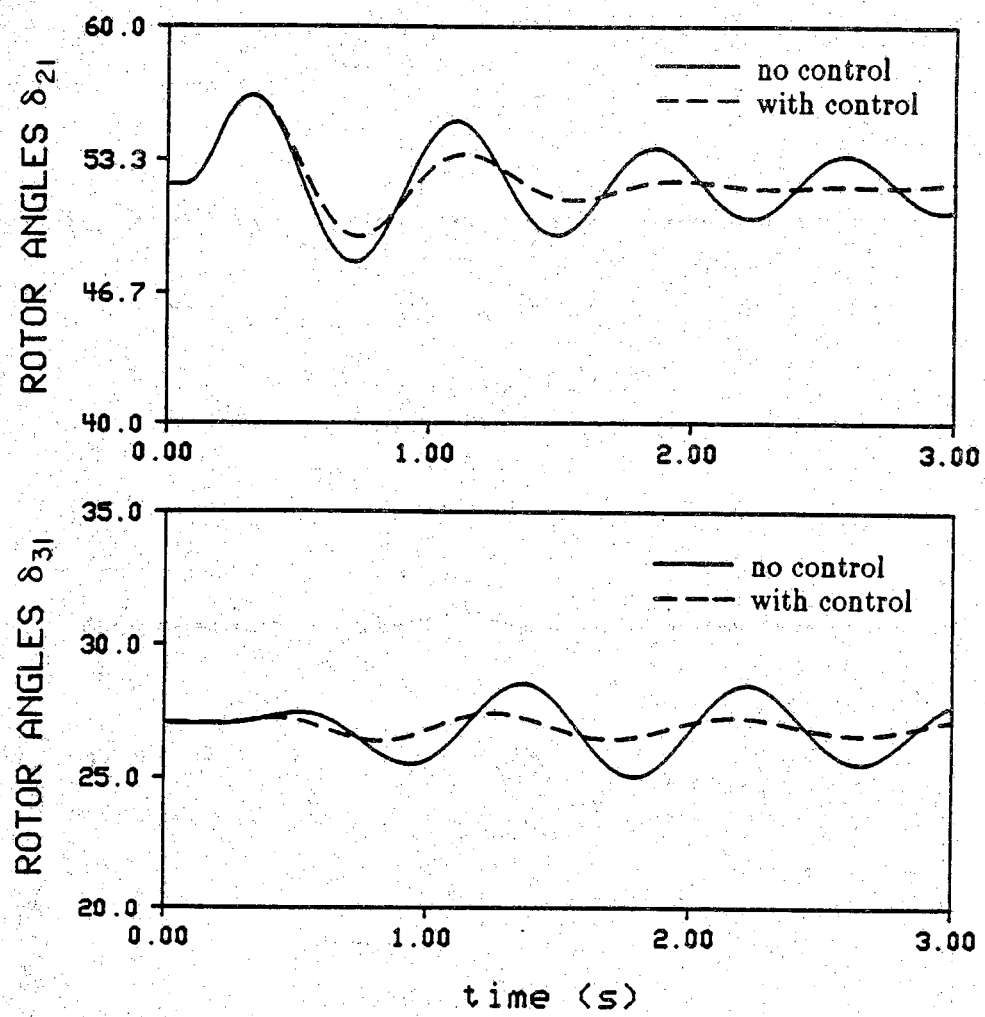

Figure 5.4 Continued

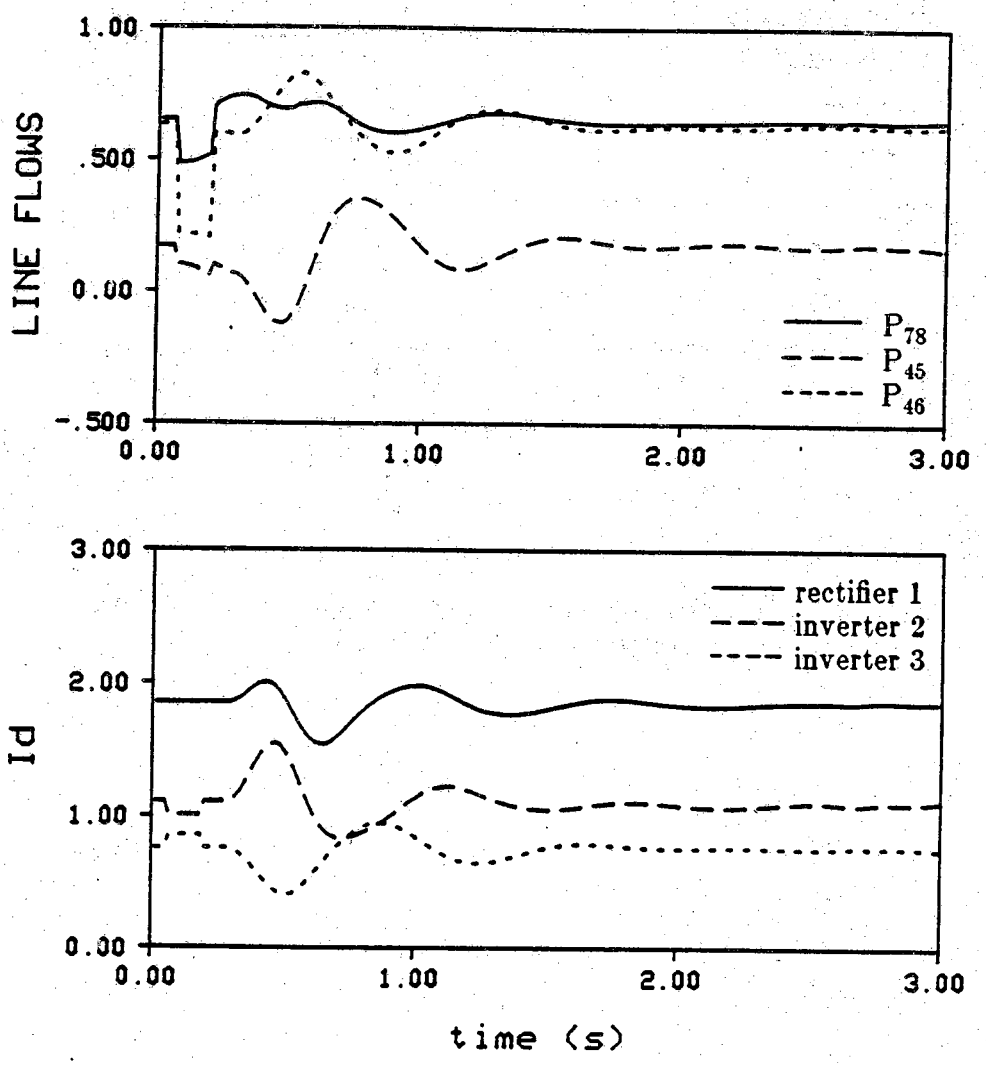

Figure 5.5 Damping applied to line flows P_{78}, P_{45} and P_{46} with 3 cycles of control delay

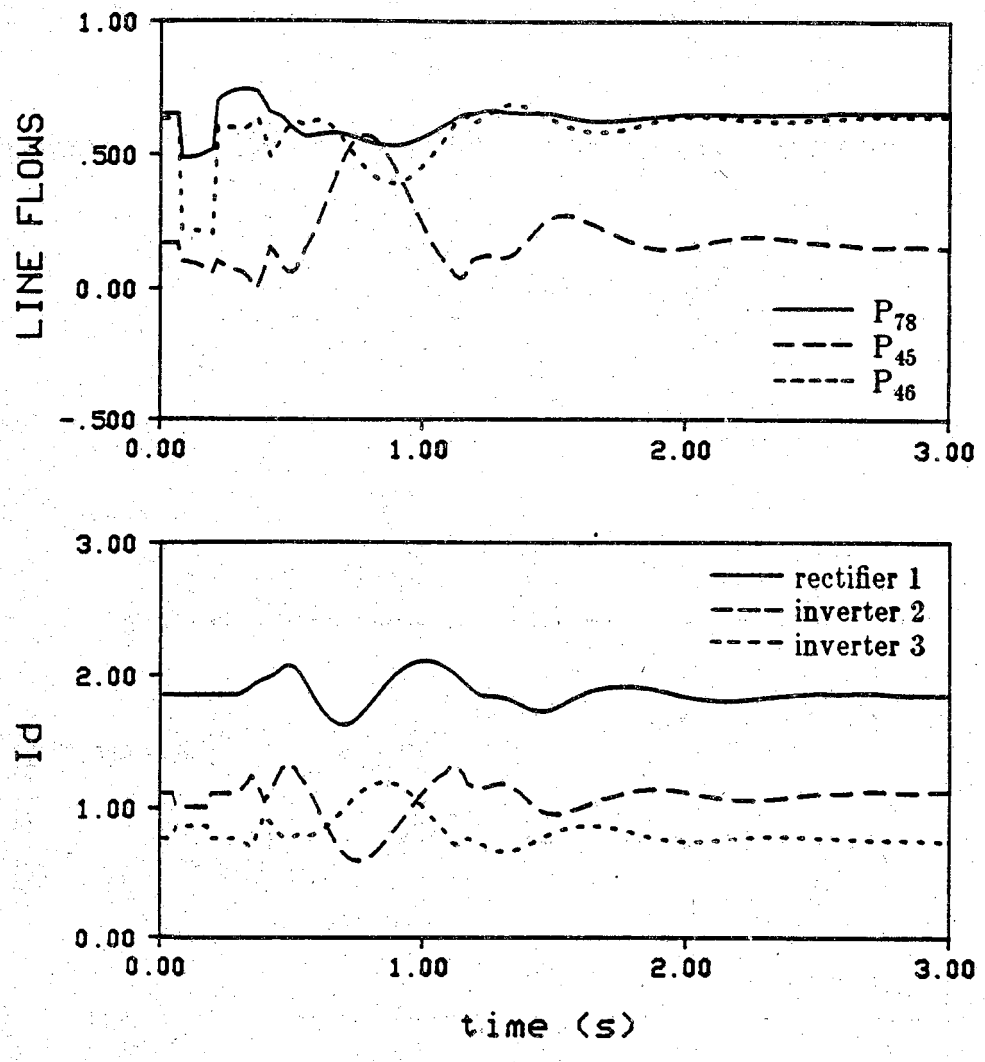

Figure 5.6 Damping applied to line flows P_{78}, P_{45} and P_{46} with 3 cycles of control delay and limit on converter 2

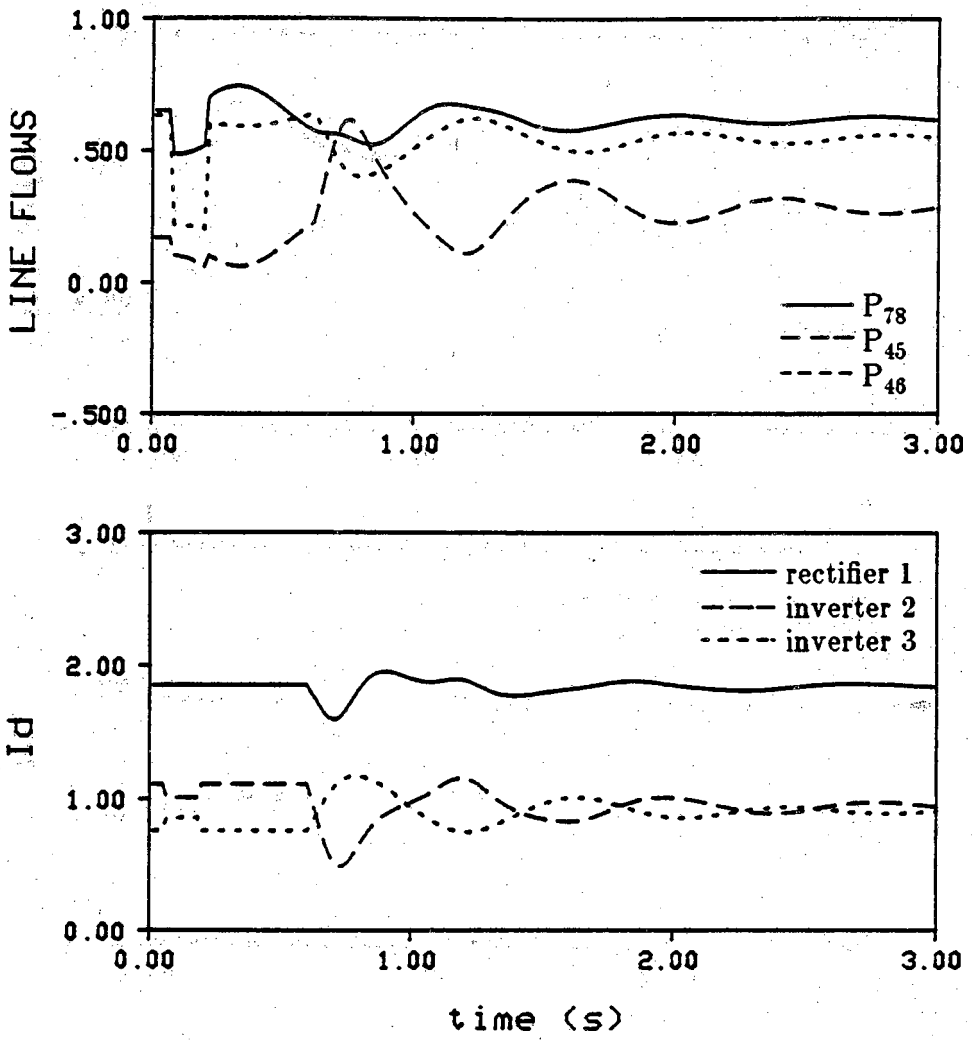

Figure 5.7 Damping applied to line flows P_{78}, P_{45} and P_{46} with 3 cycles of control delay and moving averages

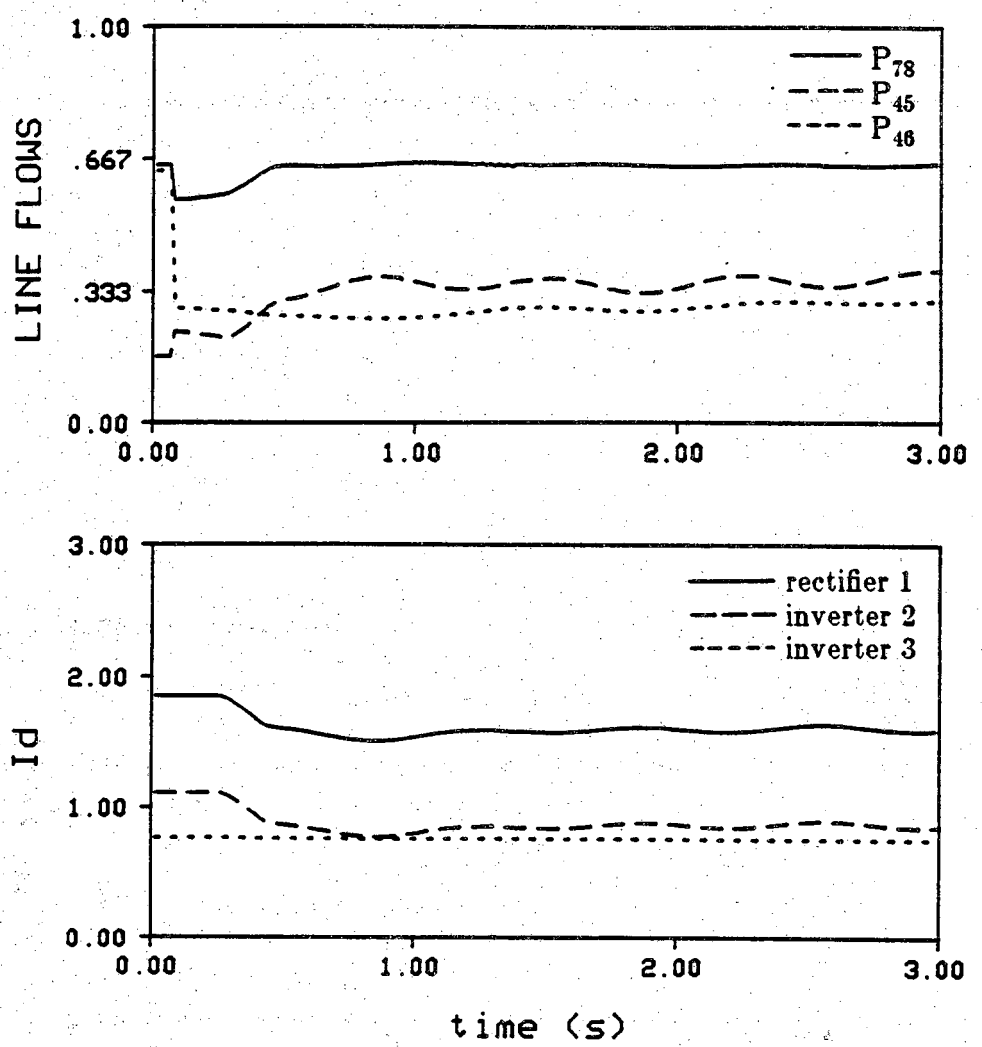

Figure 5.8 Steering and regulating P_{78} with no control delay

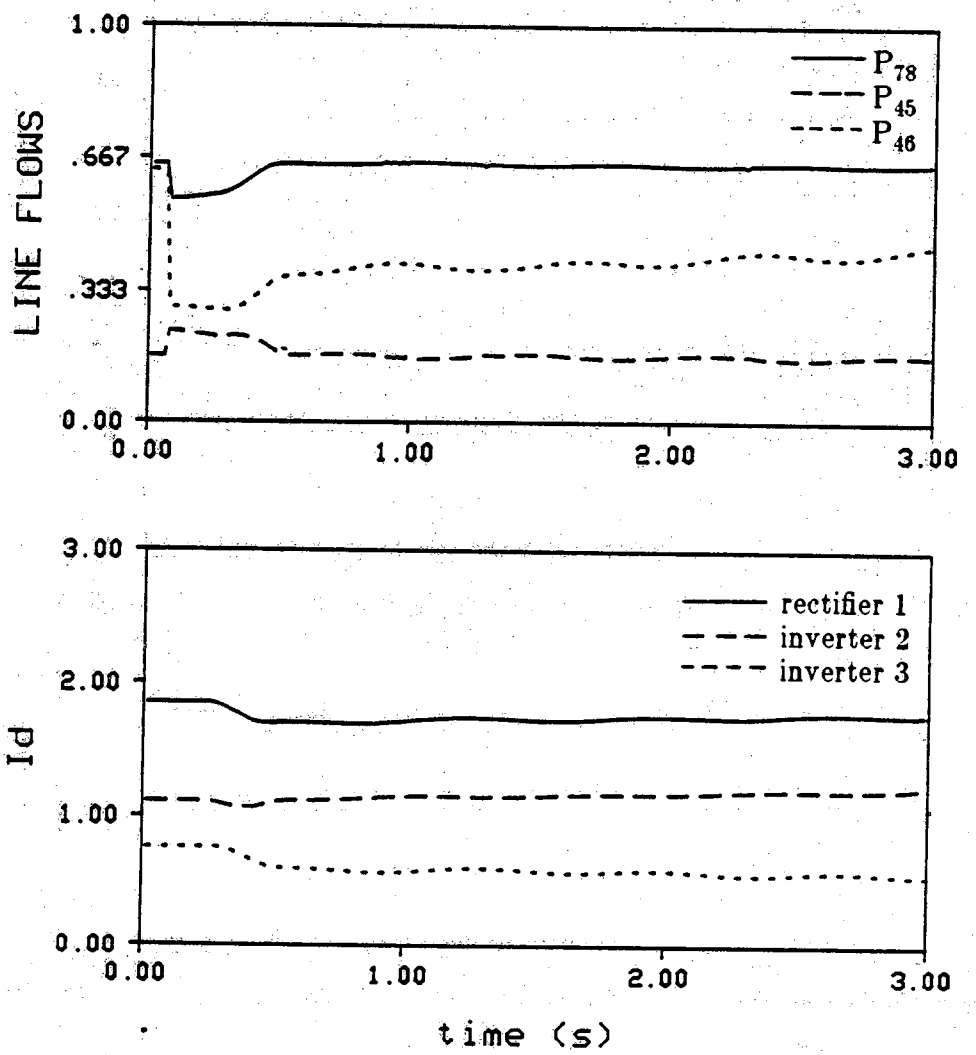

Figure 5.9 Steering and regulating P_{78} and P_{45} with no control delay

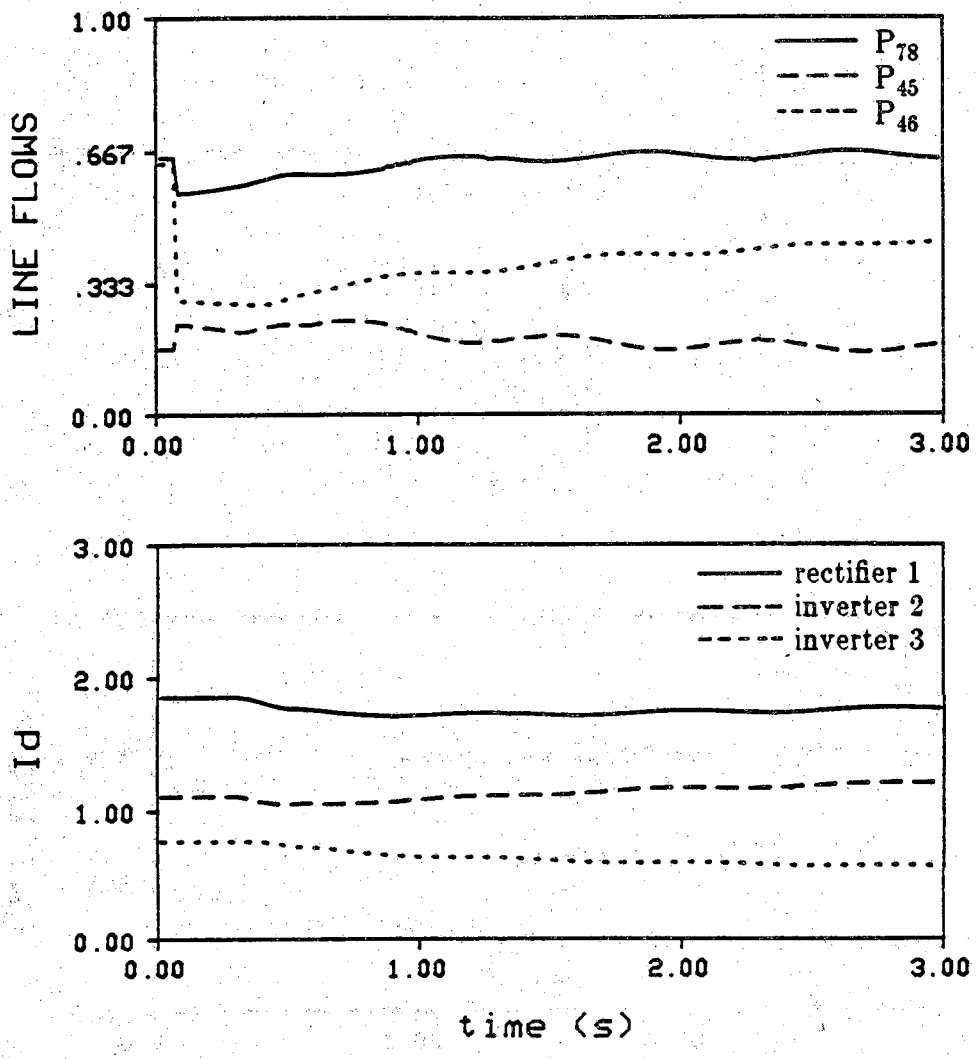

Figure 5.10 Steering and regulating P_{78} and P_{45} with 3 cycles of control delay and compensation

CHAPTER 6
CONCLUSIONS AND RECOMMENDATIONS

6.1 Conclusions

In the planning and design of a HVDC system, a large number of system studies are conducted to evaluate the performance of the ac/dc system under all probable conditions. Such studies are also conducted when comparing various options, for example, comparing the ac alternative to the dc case. Similar analytical tools, using perhaps more sophisticated or detail modeling are necessary for operational considerations to study the system response and stability under balanced and unbalanced conditions.

The main objective of this research has been to develop an on-line ac power flow controller using the dc injections of a multiterminal HVDC system. However, dynamic simulation programs are needed to evaluate the dynamic performance of the controller. The development of these simulations led to new formulation and simulation techniques described in chapters 3 and 4.

In chapter 3 of this report, a new algorithm for representing multiterminal dc systems in transient stability programs has been set forth. With the dynamics of the dc network and controls neglected, a systematic method to determine the control mode of operation during transients is required, as a change in the control mode of operation of the dc system might occur during faults or other disturbances in the ac system. Existing methods use a selection

logic approach which may have to cycle through all probable operating modes of the multiterminal dc system for the correct mode of operation. The proposed method which utilizes a Linear Programming formulation, determines the mode of operation and the dc network solution of a general multiterminal dc system simultaneously. The constraints in the LP formulation automatically ensure that the solution obtained is feasible. It is therefore computationally more efficient than previous methods. Furthermore, nonlinear control characteristics can be handled by the new method. Such control characteristics are simulated by modifying appropriate limits of these constraints in an iterative loop around the main LP calculation. The numerical examples , presented in chapter 3 illustrating various features of the proposed ac/dc transient stability algorithm confirmed the versatility of the new method.

Detailed representations of the dc converter and its controls are necessary to study harmonic and unbalanced fault problems and also in dynamic simulation studies where the disturbance is so severe and close to the converter that the probability of commutation failures is high. Such detailed representations provide much more insight into the interaction of the dc system controls with the ac system than similar studies with simpler representations. The development of a digital simulation program using detailed representations of the converter and its controls is presented in Chapter 4. The algorithm, based on tensor techniques is computationally more efficient and also more versatile than those based on other approaches. For example, the algorithm has the inherent capability of handling unusual converter valve conduction topologies in a systematic manner. Tests of the algorithm conducted on sample two-terminal and three-terminal dc systems demonstrated the working of the algorithm. Steady-state values of these results have been verified by

calculations using established equations. Results on sample systems are included in Chapter 4 to illustrate the capability of the algorithm in simulating the ac/dc system response to faults and also the condition of commutation failure.

Finally, the feasibility of coordinating the dc injections of a multiterminal dc system to dynamically control the power flows of selected ac lines is demonstrated by examples showing the successful application of such a controller to steering, regulating and damping of the power flows in the ac network.

The above functions are accomplished with the same coordinated control algorithm using different compensators for each function. It is observed that the control performance obtained is sensitive to the transfer characteristics of the ac network to the dc injections. Although changes in the ac network can be accounted for by modifying the compensators, such modifications will have to be done on-line on a continual basis.

6.2 Recommendations

It has been demonstrated, through this research work, that dynamic network flow control using the dc injections of a multiterminal dc system is feasible. Because of the sensitivity of the control performance to ac network condition, it is recommended that further work be carried out to develop an adaptive on-line network flow controller. This would require developing a method to identify the ac network state and characterizing this state in the form that can be used to design the compensator. Also the steering and regulating control action would require a sound decision making process, based on security enhancement or economic operation criteria, to better define the

purpose of such controller.

Presently, there is considerable interest to add small dc taps on existing dc links to supply way-side loads. Since such taps are likely to be connected to weak ac busses, the development of control to satisfactorily operate these taps will be of much interest. In this regard, the detailed simulation program developed in this report will be a useful simulation tool for evaluating the dynamic performance of new dc controls.

LIST OF REFERENCES

LIST OF REFERENCES

[1] G. Opoku and C. M. Ong, "Coordination of Reactive Power Sources to Correct Bus Voltage Violations in an AC-DC System," IEEE Trans. Power Apparatus & Systems, Vol. PAS-103, pp. 1128-1134, June 1984.

[2] C. M. Ong and H. Fudeh, "AC Power Flow Control with a Multiterminal DC System," IEEE Trans. Power Apparatus & Systems, Vol. 100, pp. 4687-4691, November 1981.

[3] C.M. Ong and A. Hamzei-Nejad, "A General-Purpose Multiterminal DC Load-Flow," IEEE Trans. Power Apparatus & Systems, Vol. 100, No. 7, pp. 3166-3174, July 1981

[4] H. Fudeh and C. M. Ong "A Simple and Efficient AC-DC Load-Flow Method for Multiterminal DC Systems," IEEE Trans. Power Apparatus & Systems, Vol. 100, pp. 4389-4396, November 1981.

[5] J. Milias-Argitis, G. Giannakopoulos, G. Galanos, "Dynamic Simulation for Multiterminal HVDC Systems," IEEE Trans. Power Apparatus & Systems, Vol. PAS-97, pp.587-593, March/April 1978.

[6] K.R. Padiyar, Sachchidanand, "Digital Simulation of Multiterminal HVDC Systems Using a Novel Converter Model", presented at the IEEE PES 1982 Summer Meeting.

[7] S. Williams and I. R. Smith, "Fast Digital Computation of 3-phase Thyristor Bridge Circuits", Proc. IEE, Vol. 120, No. 7 1973.

[8] J. Milias-Argitis, G. Galanos, "Dynamic simulation of HVDC Transmission Systems," IEEE Transactions on Power Apparatus and Systems, Vol. PAS-92 No. 8, pp. 2056-2065, May/June 1976.

[9] G.D. Breuer, J.F. Luini, and C. C. Young, "Studies of Large AC/DC Systems on the Digital Computer," IEEE Transactions on Power Apparatus and Systems, Vol. PAS-85, pp. 1107-1116, Nov, 1966.

[10] J.F.Clifford, and A.H. Schmidt, Jr., " Digital Simulation of a DC Transmission System and its Control," ibid,. PAS-89, pp. 97-105, Jan. 1970.

[11] N. Sato, N.V. Dravid, S.M. Chan, A.L. Burns and J.J. Vithayathil, "Multiterminal HVDC System Representation in a Transient Stability Program," presented at the IEEE PES Winter Meeting, New York, NY, Feb. 1980.

[12] J. Arrillaga and I.M. Elamin, "Transient Stability Performance of a 3-machine System Including an HVDC Link", Proc. IEE, v. 123, No. 11, November 1976, pp. 1239-44.

[13] G.K. Carter, C.E. Grund, H.H. Happ and R.V. Pohl, "The Dynamics of AC/DC Systems with Controlled Multiterminal HVDC Transmission," IEEE Transactions on Power Apparatus and Systems, Vol. PAS-96, no. 2, March/April 1977.

[14] M.D. Heffernan, K.S. Turner, J. Arrillaga and C.P. Arnold, "Computation of AC/DC Disturbances- Part I. Interactive Coordination of the Generator and Converter Transient Models," Trans. IEEE, paper 81 WM 059-5, Winter Power Meeting, Atlanta, Feb. 1981.

[15] K.S Turner, M.D. Heffernan, C.P. Arnold and J. Arrillaga, "Computation of AC/DC Disturbances- Part II. Derivation of Power Frequency Variables from Converter Transient Response," Trans. IEEE, paper 81 WM 060-3, Winter Power Meeting, Atlanta, Feb. 1981.

[16] K.S. Turner, M.D. Heffernan, C.P. Arnold and J. Arrillaga, "Computation of AC/DC Disturbances- Part III. Transient Stability Assessment," Trans. IEEE, paper 81 WM 061-1, Winter Power Meeting, Atlanta, Feb. 1981.

[17] IEEE Committee Report by the Working Group on Dynamic Performance and Modeling of Dc System, "Functional Model of Two-terminal HVDC Systems for Transient and Steady-state Stability, ", IEEE/PES 1983 Summer Meeting, Paper No. 83 SM 464-5. July 1983.

[18] G. K. Carter, C. E. Grund, H. H. Happ and R. V. Pohl, " The Dynamics of AC-DC Systems with Controlled Multiterminal HVDC Transmission," IEEE Trans. Power Apparatus and Systems, Vol. PAS 96, No.2, March/April 1977, pp. 402 - 413.

[19] U. Lamm, E Uhlmann and P. Danfors, "Some Aspects of Tapping of HVDC Transmission Systems," Direct Current, May 1963, pp. 124 -129.

[20] R. Foerst, G. Heyner, K.W. Kanngiesser, and H. Waldman, "Multiterminal Operation of HVDC Converter Stations," IEEE Transactions on Power Apparatus and Systems, Vol. PAS-88, No.7, July 1969.

[21] J. Reeve " Multiterminal HVDC Power Systems," IEEE Trans. Power Apparatus and Systems, Vol. PAS 99, No.2, March/April 1980, pp. 729

[22] F. Nozari, C. E. Grund and R. L. Hauth, "Current Order Coordination in Multiterminal DC Systems," IEEE Trans. Power Apparatus & Systems, Vol. PAS 100, No.11, Nov. 1981, pp. 4629-4636.

[23] T. Sakurai, K. Goto, S. Irokawa, K. Imai and T. Sakai, "A New Control Method for Multiterminal HVDC Transmission Without Fast Communication Systems, Vol. PAS 102, No.5, May 1983, pp. 1140-1150.

[24] Ebasco Services Inc., "Methodology for Integration of HVDC Links in Large AC Systems - Phase I: Reference Manual, Final Report, EPRI EL 3004, March 1983.

[25] P. M. Anderson and A. A. Fouad, Power System Control and Stability, Volume 1, The Iowa State University Press, USA, 1977.

[26] J.D. Ainsworth, "Harmonic Instability Between Controlled Static Converters and AC Networks," Proc. IEE, Vol. 114, pp. 949-957, July 1967.

[27] J.D. Ainsworth, "The Phase-Locked Oscillator: A New Control System for Controlled Static Converters," IEEE Trans. Power Apparatus and Systems, Vol. PAS-87, pp. 859-865, March 1968.

[28] A. Ekstrom, "A Refined HVDC Control System," ibid,. PAS-89, No. 5/6, May/June 1970.

[29] E. Rumpf, S. Ranade, "Comparison of Suitable Control Systems for HVDC Stations Connected to Weak AC Systems, Part I: New Control Systems," IEEE Summer Meeting and International Symposium on High Power Testing, Portland, Ore., July 1971.

[30] N.G. Hingorani and P. Chadwick, "A New Constant Extinction Angle Control for AC/DC/AC Static Converters," IEEE Transactions on Power Apparatus and Systems, Vol. 87, pp. 866-872, March 1968. Disc. p.872.

[31] E. Uhlmann, "Stabilization of an Ac Link by a Parallel DC Link," Direct Current, pp. 89-94, August 1964.

[32] R. L. Cresap, D. N. Scott, W. A. Mittelstadt and C. W. Taylor, "Operating Experience with Modulation of the Pacific HVDC Intertie," IEEE Trans. Power Apparatus & Systems, Vol. PAS-97, No. 4, pp. 1053-1059, July/August 1978.

[33] R. J. Piwko and E. V. Larsen, "HVDC System Control for Damping of Subsynchronous Oscillations," IEEE Trans. Power Apparatus &

Systems, Vol. PAS-101, No. 7, pp. 2203-2211, July 1982.

[34] C. E. Grund, R. V. Pohl and J. Reeve, "Control Design of an Active and Reactive Power HVDC Modulation System with Kalman Filtering," IEEE Trans. Power Apparatus & Systems, Vol. PAS-101, No. 10, pp. 4100-4111, Oct. 1982.

[35] D. O'Kelly, "Voltage Control for an HVDC Converter," IEE Proceedings, Vol. 131, Pt. C, No. 1, Jan. 1984, pp. 5 - 15.

[36] K. W. Kanngeisser, J. P. Bowles, J. Reeve, E. Rumpf, "HVDC Multiterminal System," CIGRE Report 14-08, 1974.

[37] C. M. Ong and A. Hamzei-Nejad, "Digital Simulation of Multiterminal HVDC Systems for Transient Stability Studies Using a Simplified DC System Representation," IEEE Paper 84SM588-0, PES Summer Meeting, Seattle, July 15 -20, 1984.

APPENDICES

Appendix A

Parameters of the dc system

Commutation resistances

$$R_{c1} = R_{c2} = 0.0247 \text{ pu}, R_{c3} = 0.0157 \text{ pu}.$$

DC line resistances

$$R_1 = 0.0150 \text{ pu}, R_2 = 0.0312 \text{ pu}, R_3 = 0.319 \text{ pu}$$

Table A-1 VDCOL characteristics

Rectifier 1	OG = 0.30	GF = 0.15	OE = 1.85	ED = 0.50
Inverter 2	OT = 0.0	TQ = 0.25	OP = 1.00	PN = 0.50
Inverter 3	OT = 0.0	TQ = 0.25	OP = 0.75	PN = 0.50

(Coordinates as labeled in Fig. 3.2)

Appendix B

Mesh impedance matrices for 6-pulse and 12-pulse converters

The mesh equations for a Y-Y bridge are arranged such that the impedance matrix $\mathbf{Z}_m^Y$, is symmetric. The non-zero elements for the upper triangle of this matrix are given below.

$$Z_{11}^Y = Z_a^Y + Z_c^Y + Z_3 + Z_1$$
$$Z_{12}^Y = Z_3 + Z_c^Y$$
$$Z_{13}^Y = -Z_a^Y - Z_c^Y$$
$$Z_{14}^Y = -Z_c^Y$$
$$Z_{15}^Y = Z_3$$
$$Z_{22}^Y = Z_b^Y + Z_c^Y + Z_2 + Z_3$$
$$Z_{23}^Y = -Z_c^Y$$
$$Z_{24}^Y = -Z_b^Y - Z_c^Y$$
$$Z_{25}^Y = -Z_3$$

$$Z_{33}^Y = Z_a^Y + Z_c^Y + Z_4 + Z_6$$
$$Z_{34}^Y = Z_c^Y + Z_6$$
$$Z_{35}^Y = -Z_6$$
$$Z_{44}^Y = Z_b^Y + Z_c^Y + Z_5 + Z_6$$
$$Z_{45}^Y = -Z_6$$
$$Z_{55}^Y = Z_3 + Z_6 + Z_d$$

Where,

Z_a^Y, Z_b^Y, Z_c^Y : converter transformer phase reactances

$Z_1, \ldots, Z_6$: conducting impedances of the thyristors

Z_d : impedance of the smoothing reactor

For a 12-pulse converter, the impedance matrix corresponding to the Y-Δ bridge is appended to the matrix given above as explained in chapter 4. The

nonzero elements of this matrix and the coupling matrix $\mathbf{Z}_c$ are given below.

$$Z_{11}^{\Delta} = Z_1 + Z_3$$
$$Z_{12}^{\Delta} = Z_3$$
$$Z_{15}^{\Delta} = -Z_c^{\Delta}$$
$$Z_{21}^{\Delta} = Z_b^{\Delta} + Z_3$$
$$Z_{22}^{\Delta} = Z_b^{\Delta} + Z_2 + Z_3$$
$$Z_{23}^{\Delta} = -Z_b^{\Delta}$$
$$Z_{24}^{\Delta} = -Z_b^{\Delta}$$
$$Z_{25}^{\Delta} = Z_b^{\Delta}$$
$$Z_{33}^{\Delta} = Z_4 + Z_6$$
$$Z_{34}^{\Delta} = Z_6$$
$$Z_{35}^{\Delta} = Z_c^{\Delta}$$
$$Z_{41}^{\Delta} = -Z_b^{\Delta}$$
$$Z_{42}^{\Delta} = -Z_b^{\Delta}$$
$$Z_{43}^{\Delta} = Z_b^{\Delta} + Z_6$$
$$Z_{44}^{\Delta} = Z_b^{\Delta} + Z_5 + Z_6$$
$$Z_{45}^{\Delta} = -Z_b^{\Delta}$$
$$Z_{51}^{\Delta} = Z_a^{\Delta} + Z_b^{\Delta}$$
$$Z_{52}^{\Delta} = Z_b^{\Delta}$$
$$Z_{53}^{\Delta} = -Z_a^{\Delta} - Z_b^{\Delta}$$
$$Z_{54}^{\Delta} = -Z_b^{\Delta}$$
$$Z_{55}^{\Delta} = Z_a^{\Delta} + Z_b^{\Delta} + Z_c^{\Delta}$$

where Z_a^{Δ} , Z_b^{Δ} and Z_c^{Δ} are transformer reactances for the Y-Δ bridge. The nonzero elements of the coupling matrix are as follows:

$$Z_c^{51} = -Z_3$$
$$Z_c^{52} = -Z_3$$
$$Z_c^{53} = -Z_6$$
$$Z_c^{54} = -Z_6$$

Note that when the thyristor conducting impedances are neglected, this matrix is zero and the matrices Z_m^Y and Z_m^{Δ} are greatly simplified.

Appendix C

Generation of the incidence matrix, C_n

The mesh diagram for a 12-pulse bridge is shown in Fig. 4.2. The tree shown by bold lines was arbitrarily selected. The circuit can be fully represented by ten mesh currents corresponding to ten links in Fig 4.2. For a 6-pulse bridge, this number is reduced to 5. The logic variable L_i corresponding to link "i" is equal to "1" when the link exists in the reduced set and is "0" when it is eliminated from the circuit. Similarly, the logic variable x_i is defined to be equal to 1 when a thyristor is conducting and zero when it is off. Using Boolean algebra, an expression can be derived for each link by considering different conduction patterns in the bridge. Therefore,

L_1 exists when $x_1^Y x_3^Y + x_1^Y x_2^Y = 1$

similarly, L_2 to L_{10} are defined by

$$L_2 = x_2^Y x_3^Y$$

$$L_3 = x_4^Y x_6^Y + x_4^Y x_5^Y$$

$$L_4 = x_5^Y x_6^Y$$

$$L_5 = x_1^Y + x_2^Y + x_3^Y$$

$$L_6 = x_1^\Delta x_3^\Delta + x_1^\Delta x_2^\Delta$$

$$L_7 = x_2^\Delta x_3^\Delta$$

$$L_8 = x_4^\Delta x_6^\Delta + x_4^\Delta x_5^\Delta$$

$$L_9 = x_5^\Delta + x_6^\Delta$$

$$L_{10} = 1$$

Note that link 10 will always exist in the reduced model. To generate $\mathbf{C}_n$, starting with a 10x10 identity matrix, the columns corresponding to the non-existing links are eliminated first. Since the tree selected in the Fig. 4.2 contains four branches that correspond to four conducting valves, if in a particular circuit topology, either one of these valves in not conducting, it cannot remain a branch and thus a new tree branch should be selected.

For example, if conductor 3 is not conducting, either links 1 or 2 should become a tree branch. A simple mesh analysis shows that if L_1 becomes a branch , then element c_{15} in $\mathbf{C}_n$ should be changed to 1. and if L_2 becomes a branch, then element c_{25} in $\mathbf{C}_n$ should be set to 1 and c_{21} to -1 if column 1 exists.

The matrix $\mathbf{C}_n$ can thus be fully constructed by applying the same argument to all four valve groups of a 12-pulse bridge. In accordance with other parts of the algorithm, the matrix $\mathbf{C}_n$ is defined by

$$\begin{bmatrix} \mathbf{C}_n^Y & 0 \\ \mathbf{C}_n^c & \mathbf{C}_n^\Delta \end{bmatrix}$$

where $\mathbf{C}_n^c$ is the coupling matrix and $\mathbf{C}_n = \mathbf{C}_n^Y$ for the 6-pulse bridge.

Appendix D

Parameters of the ac-dc system

Commutation resistances

$R_{c1} = R_{c2} = 0.0548$pu, $R_{c3} = 0.0315$pu.

DC line resistances

R_1=0.0150pu, R_2=0.0312pu, R_3=0.319pu

GENERATORS

	UNIT 1	UNIT 2	UNIT 3
x_d	0.146	0.590	0.673
x_q	0.096	0.582	0.664
x'_d	0.061	0.096	0.139
x'_q	0.097	0.334	0.394
T'_{do}	8.69	6.00	5.14
T'_{qo}	-	1.50	1.50
S_{base}	100	100	100
H	23.64	9.92	9.60